Numerical Investigation of the Edge Profile in Hot-Rolling

by

John Veale
BSc Eng (Civil)

A thesis submitted in partial fulfilment of the requirements for the degree of Master of Science in Engineering.

Centre for Research into Computational and Applied Mechanics
University of Cape Town

October 1992

ACKNOWLEDGMENTS

I wish to express my appreciation to the following people and organizations:

- My supervisors, Doctor CD Mercer and Professor JB Martin for their help and guidance with this thesis.
- Hulett Aluminium Limited for providing information and for supporting this work financially.
- The Foundation for Research and Development for financial assistance.

ABSTRACT

During the hot-rolling of aluminium ingot into sheet, the material elongates in the rolling direction as it is reduced vertically. The spread which occurs in the lateral direction during the multiple pass schedules used in industry is minimal. However, the deformation on these edges is important. During the initial passes a concave profile develops — the material near the surfaces spreads outward while the material at the centre moves inward.

The concave profile can lead to defects in the final product; these are the 'roll over' of material from the edges to the top and bottom surfaces, the fold over of material in the centre of the edge, and the formation of vertical edge cracks. To remove these the edges are trimmed at the end of the process. Research work in this area was motivated by the possibility of identifying means of reducing the amount of material that needs to be trimmed. The objectives of this thesis are to develop techniques of simulating the rolling, and to use these to investigate the deformation mechanisms which lead to the concave edge profile.

Models of the rolling were developed using the general purpose, non-linear finite element code ABAQUS. To reproduce the edge profiles accurately requires large three-dimensional models, for which the explicit dynamic method was found to be the most suitable.

The results of the analyses were used to investigate the mechanisms which lead to the concave edge profile. In the roll-gap the work-load arches through the ingot; and for roll passes with small reductions a stress pattern occurs which leads to the concave edge profile. In this pattern the stresses of highest magnitude at the surfaces are compressive stresses in the vertical direction, while in the centre of the ingot they are orientated in the rolling direction and are tensile. Thus deformation occurs by vertical compression near the surfaces, and by stretching in the rolling direction at the centre. At the edges the material is not constrained laterally; and due to the Poisson effect, the material spreads outward near the surfaces, and moves inward at the centre.

The effect of certain variables on the edge profile were investigated with the modelling. The friction between the work-rolls and the ingot was found to have significant influence on the amount of lateral surface spread. Work hardening, strain rate and temperature effects in the material lead to variations in the yield stress through the height of the ingot. These effects were included in the modelling and were found to affect the shape of the profile, but to a lesser extent than the friction.

Contents

List of Figures

List of Tables

List of symbols

Rolling problem

δ	reduction for roll pass, mm
R	work-roll radius, m
L	length of ingot, m
W	width of ingot, m
H	height of ingot, m
p	roll pressure, MPa
f	friction stress, MPa

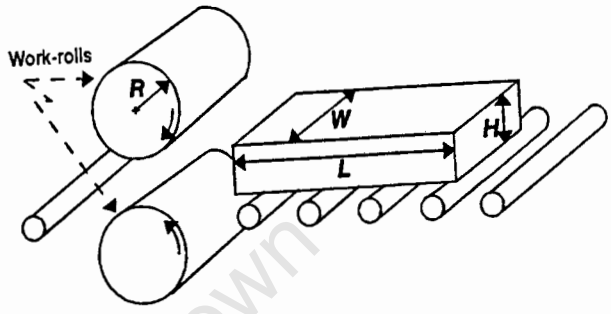

Mechanical parameters

ρ	density, g/m^3
E	Young's modulus, GPa
ν	Poisson's ratio
σ_y	uniaxial yield stress, MPa
$\bar{\sigma}$	effective stress, MPa
μ	coefficient of friction

Subscripts

0	initial conditions
1	after first roll pass

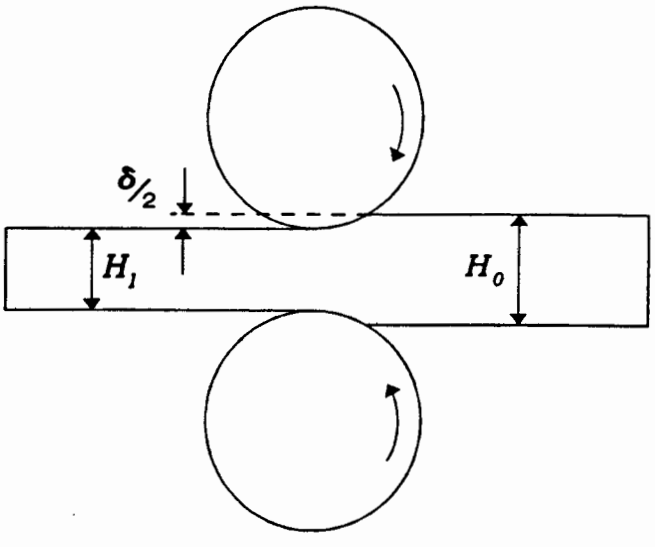

Chapter 1

Introduction

In the metal processing industry, rolling is the most commonly used deformation process. Rolling is applied in many different ways. Some processes produce products of a particular shape such as angle bar and T-sections, whilst other processes simply reduce the thickness of slabs or sheets of metal in order that they can be used for further processing.

The process investigated for this thesis is one used by Hulett Aluminium in their plant in Pietermaritzburg. This is a hot-rolling process in which aluminium alloy ingots, originally 470 mm thick, are reduced to sheets with a thickness in the region of 5 mm after multiple passes back and forth through a two-high stand of counter rotating work-rolls.

A sketch of the industrial set up is given in Figure 1.1. The ingot is run into the gap between the two rotating work-rolls, and is then driven through the gap by the friction in between it and the work-rolls. Once the whole ingot has passed through the gap, the work-rolls are repositioned to provide the correct roll-gap for the next pass and are set to rotate in the opposite direction. The ingot is again run into the roll-gap and the process is repeated. For this particular case the ingot passes through the work-rolls 21 times.

In the rolling process there are parameters which must be known, such as the force with which the work-rolls compress the ingot, and the torque which must be applied to the work-rolls by the machinery. Various methods of analysis have been developed which can predict these values. There are, however, many more variables which need to be set to obtain good quality products economically; included among these are the camber of the work-rolls, the type of lubrication, and the rolling speed. One method of optimising these is by trial and error with the actual industrial process; however it is usually more economic to model the process in some way which can predict the effect of changes in the variables. The most popular methods employed to investigate complex problems are numerical simulations which make use of the ever improving computer power available today.

In most analyses of the rolling process the problem is assumed to be a plane strain situation in the x–y plane shown in Figure 1.1. This is usually a reasonable assumption

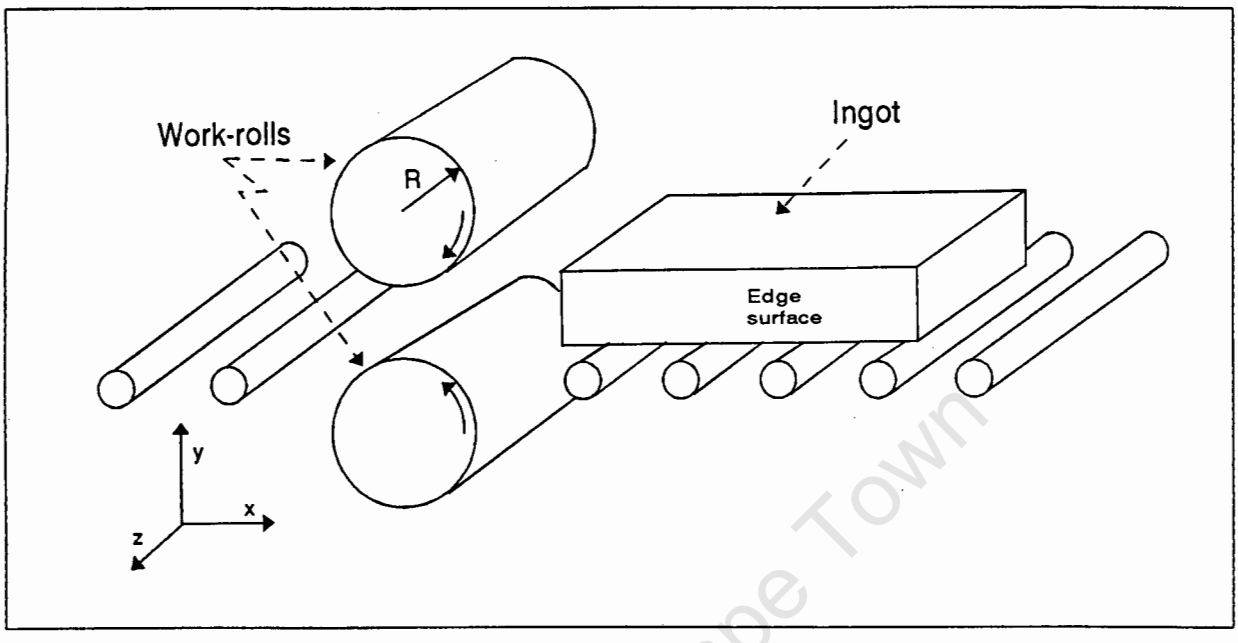

Figure 1.1: Sketch of the configuration used for hot-rolling

and important factors such as the work-roll loads and torques can be predicted with a high degree of accuracy. There are, however, some physical changes in the lateral (z) direction. The edges tend to spread — for processes with small reductions per pass a concave profile occurs, while with large reductions a convex profile occurs. Sketches of the development of the concave edge profile are given in Figure 1.2.

In the process studied here the reductions are relatively small and the concave profile develops. Due to phenomena associated with this type of profile it is necessary to trim the edges off the final product. If it were possible to reduce the amount of material that is trimmed it would increase production, and thus the topic for this thesis arose.

The objective of this thesis is to develop a means of modelling the hot-rolling process that can be used both to investigate the mechanisms which lead to a concave edge profile, and to study the effects of changes in the rolling parameters. To obtain this objective the existing theory on rolling is reviewed. There is a large amount of literature on the general rolling process and several references which look into the problem of lateral spread [1,2,3,4,5,6]. However, in only one of these is the actual shape of the edge profile studied [6].

Once an understanding of the mechanisms is developed, it can be used to identify means of reducing the amount of edge waste. One possible improvement is the identification of an optimal initial edge profile.

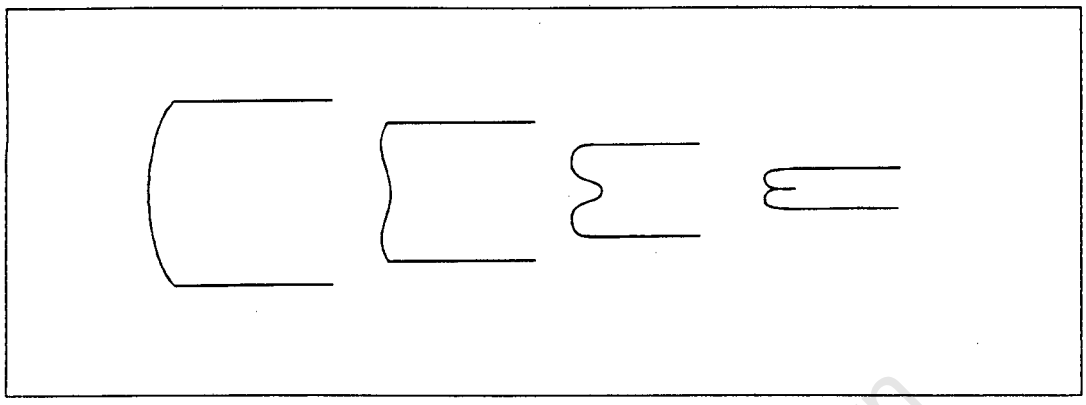

Figure 1.2: Sketch of the development of the concave edge profile

Layout of this thesis

The following two chapters contain a brief review of the existing theory in the rolling field and a more detailed review of the research into lateral effects respectively. Chapter 4 gives a brief account of the finite element method and describes how various aspects of the rolling problem are included in the modelling. The results and discussion of the important features are given in Chapter 5. Then the conclusions and scope for future work are presented in the final chapter.

Chapter 2

The Hot Rolling Process

This thesis only looks at a specific aspect of the hot-rolling process, namely the edge effects. However, the modelling required to do this must accurately reflect the entire rolling process. To achieve this, a thorough understanding of various aspects is required. Initially the traditional analytical methods of investigating the rolling problem were studied to obtain some understanding of the rolling problem. The two sections in this chapter cover the existing theory with which the rolling problem can be studied. In the first section the effects of isolated mechanisms in the rolling process are investigated through the work done in contact mechanics. The second section gives a review of the experimental work and analytical methods in the field of reduction rolling.

2.1 Investigation of the mechanics of rolling

In an attempt to understand the mechanics of the rolling problem, the theory of contact mechanics is investigated. The following discussion starts with simple contact theory and then looks at the effects of progressively complicating factors. The theory is covered in detail by Johnson [7].

Two elastic cylinders in static contact

For two cylinders in frictionless contact, as shown in Figure 2.1, Johnson uses the Hertz theory of contact to show that the pressure distribution in the contact gap is:

$$p(x) = \frac{2P}{\pi a^2}(a^2 - x^2)^{1/2}$$

where, P : the load on the rollers

a : the length of half the contact gap, and is equal to $\sqrt{\frac{4PR'}{\pi E'}}$

$$E' \quad : \quad \left(\frac{1-\nu_1^2}{E_1} + \frac{1-\nu_2^2}{E_2}\right)^{-1}$$
$$R' \quad : \quad (1/R_1 + 1/R_2)^{-1}$$

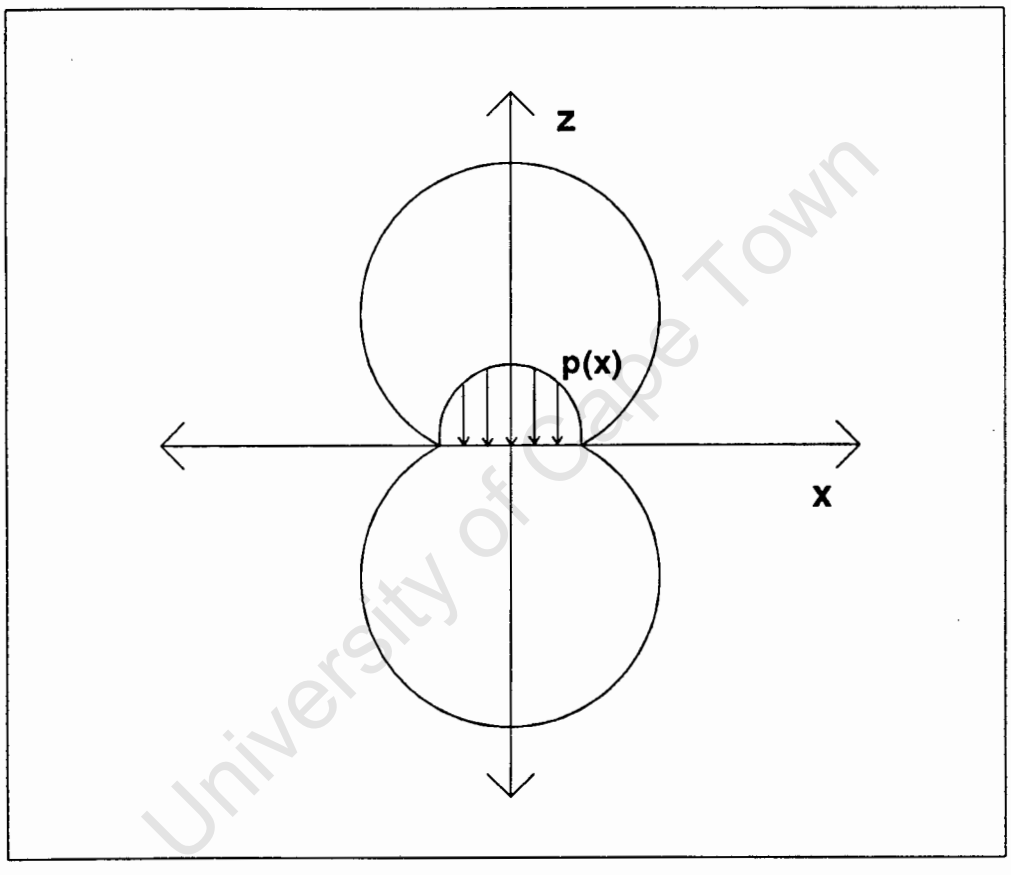

Figure 2.1: Distribution of normal stresses between elastic cylinders in static contact

Using this pressure distribution, Johnson then shows that the axial stresses along the z-axis are the following:

$$\sigma_x = -\frac{p_0}{a}\left\{(a^2+2z^2)(a^2+z^2)^{-1/2} - 2z\right\}$$

$$\sigma_z = -\frac{p_0}{a}\left(a^2+z^2\right)^{-1/2}$$

where, p_0 : maximum pressure in the centre of the contact gap

and, as these are the principal stresses, the principal shear stress along the z-axis is given by:

$$\tau_1 = -\frac{p_0}{a}\left\{z - z^2(a^2 - z^2)^{-1/2}\right\} \tag{2.1}$$

The principal shear stresses are of interest because of the simple usage with the Tresca yield criterion.[1] The Tresca maximum shear stress criterion is:

$$\max\{|\sigma_1 - \sigma_2|, |\sigma_2 - \sigma_3|, |\sigma_3 - \sigma_1|\} = 2k = \sigma_y$$

where, k : yield stress in simple shear
σ_y : yield stress in axial tension

and for the two dimensional case being studied here the yield criterion is:

$$|\sigma_1 - \sigma_2| = 2\tau_1$$

From Equation 2.1 it can be determined that the maximum value of τ_1 is $\tau_{1\ max} = 0.30p_0$ which occurs at $z = 0.78a$. Therefore first yield will occur here when $\sigma_y = 2 \times 0.30p_0$, or $p_0 = \sigma_y/0.60$. For the geometry and material properties of the hot-rolling problem being studied here, the maximum pressure would be $p_0 = 107$ MPa, the work-roll load at first yield would be 294 kN, and the length of the contact gap would be $2a = 3.38$ mm.

The stress state is obviously not an accurate description of that in rolling, as the first yield situation is at a load considerably below the rolling loads. However, there are two interesting points which are illustrated. Firstly, the point of first yield is some depth below the surface. As loads are increased this point will grow into a zone of plastic yielding, but one would still expect the largest amount of plastic work to occur in the region of the point of first yield. Secondly, the depth of the point of first yield depends on the geometry only; the point will be deeper for larger lengths of the contact gap.

Free-rolling rigid body on half-space

Due to its thickness, the ingot can initially be considered a half-space as in Figure 2.2. The case shown is for pure rolling, there are no horizontal tractive forces. The stress states shown for material in front of, underneath and behind the rollers are due to the normal stresses and deformed shape only. The material is first subjected to negative shearing, then to vertical compression, and then to positive shearing. The case for first yield is the same for free rolling as for frictionless normal contact.

[1]The Tresca yield criterion gives predictions which are very close to the von Mises yield criterion, and is used here due to its simplicity. The von Mises yield criterion will be discussed in § 4.4.

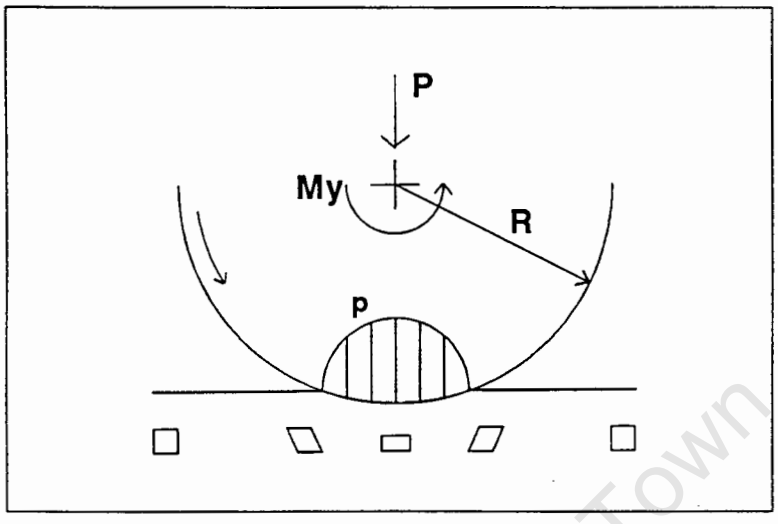

Figure 2.2: Rigid cylinder rolling on an elastic half-space

Tractive rolling with high loads

Due to the complexity of the mechanics in the hot rolling problem there is no complete analytical solution of the stress state. This is not a problem, because at the higher loads where large plastic strains occur, the elastic stresses are not important. Of importance is the region in which yielding occurs. Johnson cites the work of Mandel [8] who has developed slip line fields and hodographs for tractive rolling problems with high loading. One interesting finding of this work is that the surface of the half space is displaced permanently in the rolling direction. This is the opposite result to that of cumulative rolling contact at light loads, where the surface is displaced towards the entrance side of the contact gap.

In the rolling problem there are also no significant horizontal resultant forces acting on the work-rolls. In the roll gap, however, a resultant horizontal tractive force is required to balance the horizontal component of the normal forces in the roll gaps. The rolling problem can therefore be considered as a type of tractive rolling.

The situation is complicated further by the change in velocity of the material as its thickness is changed. To look at the rolling problem in more detail, the friction conditions in the roll-gap need to be taken into account.

Stress conditions in the roll-gap

In the study of the rolling problem the conditions in the contact gap are usually considered in two different ways. In cold-rolling, slipping friction conditions are assumed, with a

neutral point at some position in the roll gap. In hot-rolling, where there is usually no lubricant and the material is softer, the actual interface is considered to be sticking, but the tangential forces are limited by the yielding point in shear of the material.

To investigate this from the mechanics viewpoint, the case of free rolling elastic cylinders is considered. The pattern of tangential forces, or shear, in the contact gap changes with the magnitude of friction. The sketch in Figure 2.3 shows the results of a numerical analysis of rollers with dissimilar elastic properties by Bentall and Johnson [9]. The direction of tractive forces in the slipping zone A is inward on the more rigid surface. Meanwhile, the normal stress distribution is not significantly changed from the distribution predicted by the Hertz theory of contact. It can be seen that for high friction conditions sticking conditions are dominant, whereas slipping is dominant for low friction conditions, with the direction of slip changing at two points.

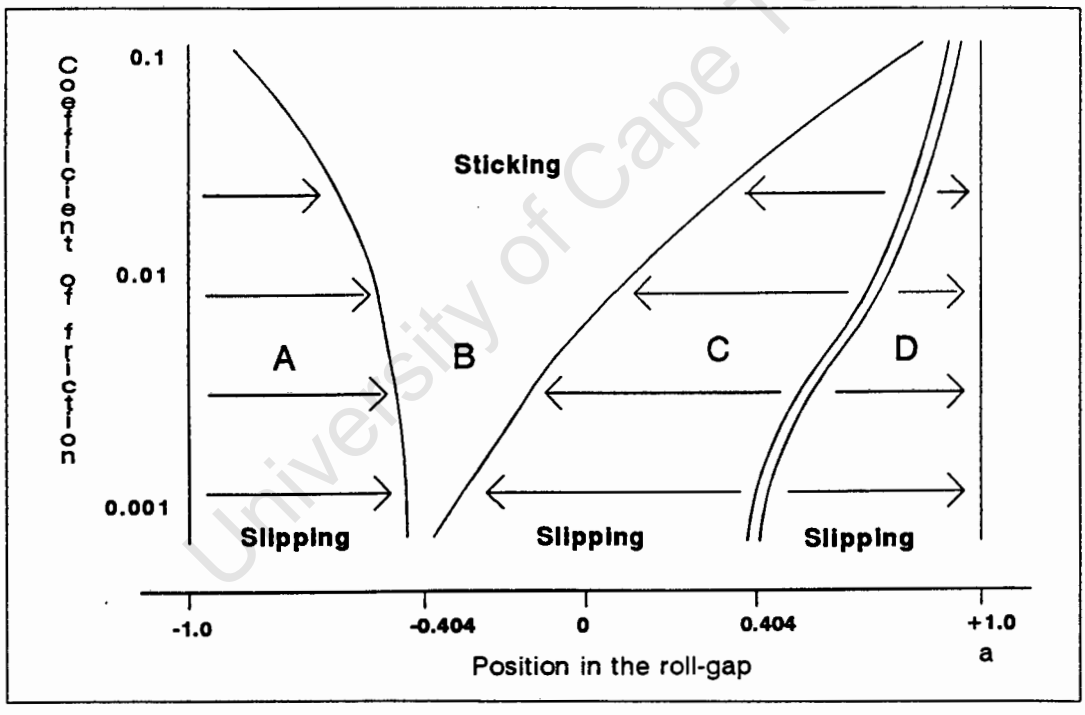

Figure 2.3: Slipping and sticking conditions along the contact gap between two free rolling elastic cylinders

In the reduction rolling case the resultant of the tangential forces must be non-zero to balance the horizontal component of the normal forces. To investigate the effect of tractive forces, the case of rolling cylinders which transmit an overall horizontal force is considered. Johnson works through the problem of elastically similar rolls and shows that there is a sticking zone at the entry side of the contact gap, and a slipping zone at the exit side.

For higher friction conditions the region of slipping shrinks, or the boundary between the two zones moves backward. Where the effects due to both dissimilar elastic properties and tractive forces are present, the tractive force effects will be the most significant.

Thus, in the rolling problem where tractive forces exist, the boundaries between the zones are also expected to move towards the back of the contact gap as friction increases.

Summary of predicted conditions

Several simple cases representative of aspects in the reduction rolling problem have been investigated here. The findings, summarised below, are useful in understanding the entire rolling process.

1. The region of highest plastic straining is expected to be below the surface, the depth of this region increasing with the size of the contact gap.
2. Material passing through the work-rolls will be subjected to shear stresses in one direction on entry into, be compressed vertically when in between, and then be subjected to shear stresses of opposite sign on exit from the work-rolls.
3. The surface of the workpiece is deformed in the rolling direction relative to the material inside the ingot.
4. For tractive rolling, there are sticking friction conditions in the entry side of the contact gap and slipping conditions at the exit side.
5. As friction is increased the boundary between sticking and slipping friction moves toward the exit side.

2.2 Development of experimental work and analytical methods

The rolling of metals has been an important industrial process for more than a century. Hartley *et al.* [10] give a detailed review of the research work done in this field. The earliest research work was reported by Hollenburg in 1883. Hollenburg investigated the flow in rolled strip by inspecting the deformation of plugs which had been placed in holes drilled into the strip. Analytical work until 1925, however, assumed that deformation was one-dimensional in the rolling problem; and horizontal stresses were ignored. In 1925 von Kármán presented his work which used a "free body equilibrium" approach and was

based on the assumption that vertical plane sections remained plane during the rolling process.[2]

In later experimental work the flow on the surface was observed by rolling billets which were marked with grooves. More detailed studies of the internal deformation were made by Orowan [11] who rolled billets made from plasticine layers of different colours.

Orowan's work brought several important points to light. The experiment with the plasticine was conducted to investigate a problem with the theory that sticking friction can occur throughout the roll-gap. Orowan presents the following question that was posed by Sir Lawrence Bragg. In the reduction rolling problem the material elongates in the rolling direction. If sticking friction does occur throughout the roll gap, how is it possible for the bottom and top surfaces to elongate? The experiment used vertical layers of laminated plasticine, rolled between wooden rollers, for which the coefficient of friction is greater than 1. The picture in Figure 2.4 shows that the surface material is severely sheared on entry into the roll gap and thereafter remains practically undeformed. The final result is that the surfaces are deformed forwards relative to the central material as predicted in § 2.1.

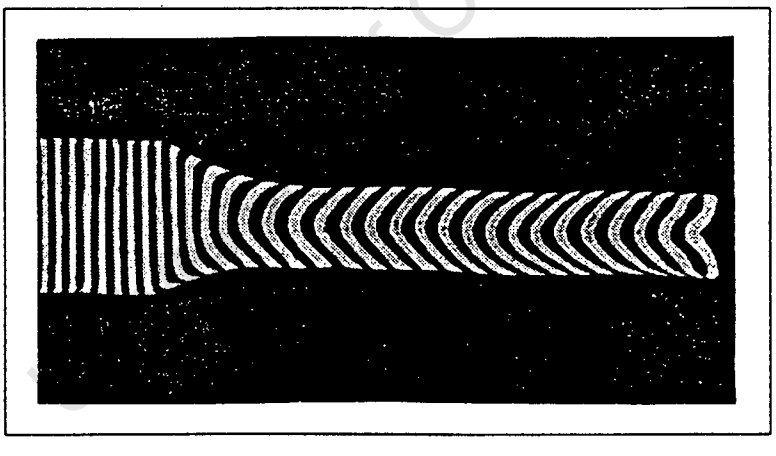

Figure 2.4: Rolling of plasticine [11]

The experiment also shows where the material is actively deforming. Orowan used Prandtl's theory for a slab of metal being deformed between two rigid platens to investigate the rolling problem. In this theory the presence of wedges of elastic material, extending from the two surfaces and meeting at a point in the centre, is explained. The presence of these wedges in the rolling gap was also found, and can be seen in Figure 2.5. These observations do not agree with the assumption of plane sections remaining plane

[2]This discussion of earlier work is based on the reference by Hartley *et al.* Citations for the above research can be found in this reference [10].

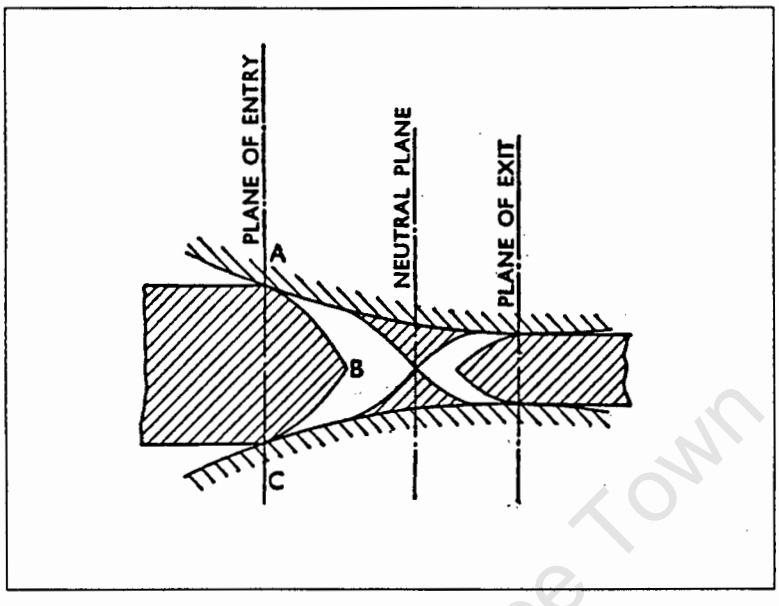

Figure 2.5: Zones of plastic and non-plastic material [11]

in the von Kármán theory. In 1943 Orowan developed a theory which takes the non-homogeneous deformation into account. This theory has been used to develop several analysis techniques.

The use of another type of analysis, the slip line field, was made possible by the better understanding of the deformation pattern in the rolling problem. This method had been used before to investigate other deformation processes, but was first applied to the rolling problem by Alexander in 1955 [12].

Slip-line fields

Slip-line fields are used to analyse problems where plastic deformation is large and elastic deformation may be neglected. The following assumptions are usually made:

1. The material is rigid-perfectly plastic.
2. Plane strain conditions exist.
3. Temperature, time, and strain rate effects on material properties can be ignored.

The body being analysed has zones, or regions, of plastically flowing material and zones of 'rigid' (elastic) material. Within the flowing zone the slip-line field represents the state

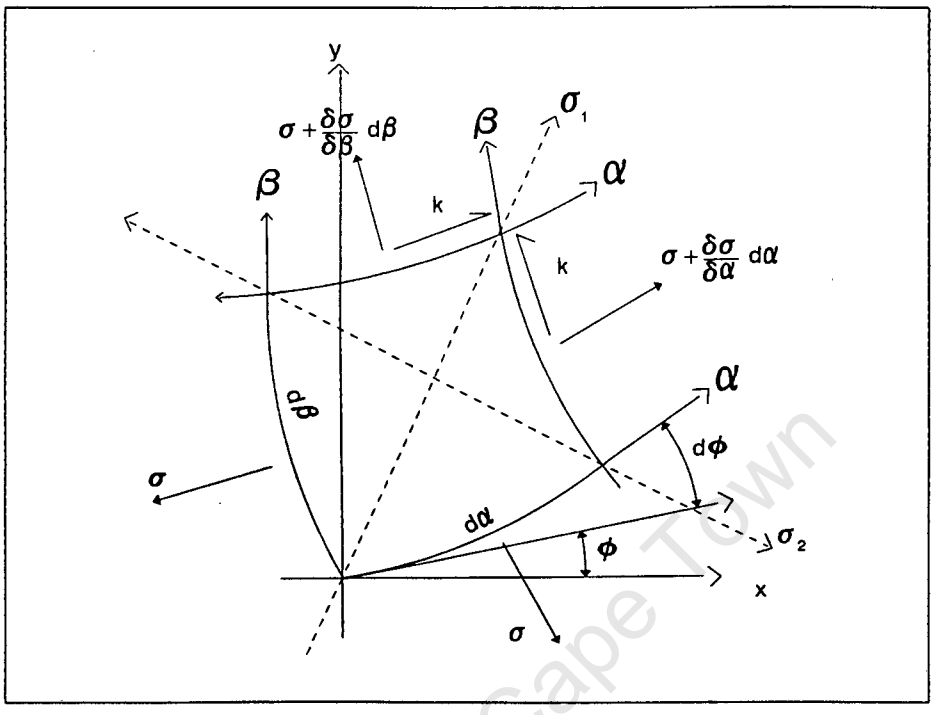

Figure 2.6: An element in a slip-line field

of stress. The slip lines occur parallel to the directions of principal shearing stress (these will be at 45 degrees to the directions of the principal stresses).

The curvilinear net consists of α-lines and β-lines which are always perpendicular to each other. The orientation of the lines and the definition of the angle, ϕ, in the figure are given by a set of conventions such as the following:

- The angle of rotation, ϕ, is positive for counterclockwise rotation from the x-axis to the α-line.
- The largest principal stress, σ_1, is orientated in the first and third quadrants of the slip line system.

The theory behind the slip line field is covered by many books on metal processing [7,13, 14,15], and so only the fundamental points are given here.

For the plane strain conditions with no elastic strains there is no Poisson's effect. Therefore the stress in the plane direction, σ_3 is equal to $\frac{1}{2}(\sigma_1 + \sigma_2)$. The maximum shear stress is therefore $(\sigma_1 - \sigma_2)$ and the Tresca yield criteria is simply:

$$(\sigma_1 - \sigma_2) = 2k \tag{2.2}$$

Substituting the value for σ_3 in the Mises yield criteria which will be given in Equation 4.4 gives:

$$\left[\frac{(\sigma_1-\sigma_2)^2+(\sigma_2-\frac{1}{2}(\sigma_1)+\sigma_2))^2+(\frac{1}{2}(\sigma_1+\sigma_2)-\sigma_1)^2}{3}\right]^{1/2}=2k$$

which simplifies to:

$$(\sigma_1-\sigma_2)=2k$$

and is the same as Equation 2.2.

The stresses for a region bounded by slip-lines are shown in Figure 2.6. The shear stresses along the slip lines are of course the yielding value, k, and the normal stress is the average of the principal stresses, $\sigma=\frac{1}{2}(\sigma_1+\sigma_2)$.

By considering the equilibrium of an element the following two conditions can be derived[3]:

1. $\sigma+2k\phi=$ constant, along an α-line
2. $\sigma-2k\phi=$ constant, along a β-line

These conditions can then be used to determine the hydrostatic pressure, σ, along a slip line if the constants are known. The constants are found from the equilibrium conditions at a boundary.

The velocity of the material in the yielding zone can be determined by the use of a hodograph, which is a vector plot of the velocities of elements of the material. The slip line solution presented by Alexander was for the hot-rolling of strip and is shown, together with the hodograph, in Figure 2.7.

Only one reference to a slip-line field solution of slab rolling was found; a reference made by Hartley *et al.* to a work in the Chinese literature [17]. This solution considers the arc of contact to be a straight line, and the arc to be completely covered by the rigid zone. Hartley *et al.* point out that the solution predicts a tensile stress at the axis of symmetry, and that this has been found to occur in practice. Under certain conditions the tension causes defects in the central region of the rolled plate.

With the advent of powerful computers, manual processes such as the slip-line field became less popular. Computer intensive numerical techniques have become the most widely used tools for researching the rolling problem analytically.

[3]The derivation of these conditions is attributed to Hencky [16].

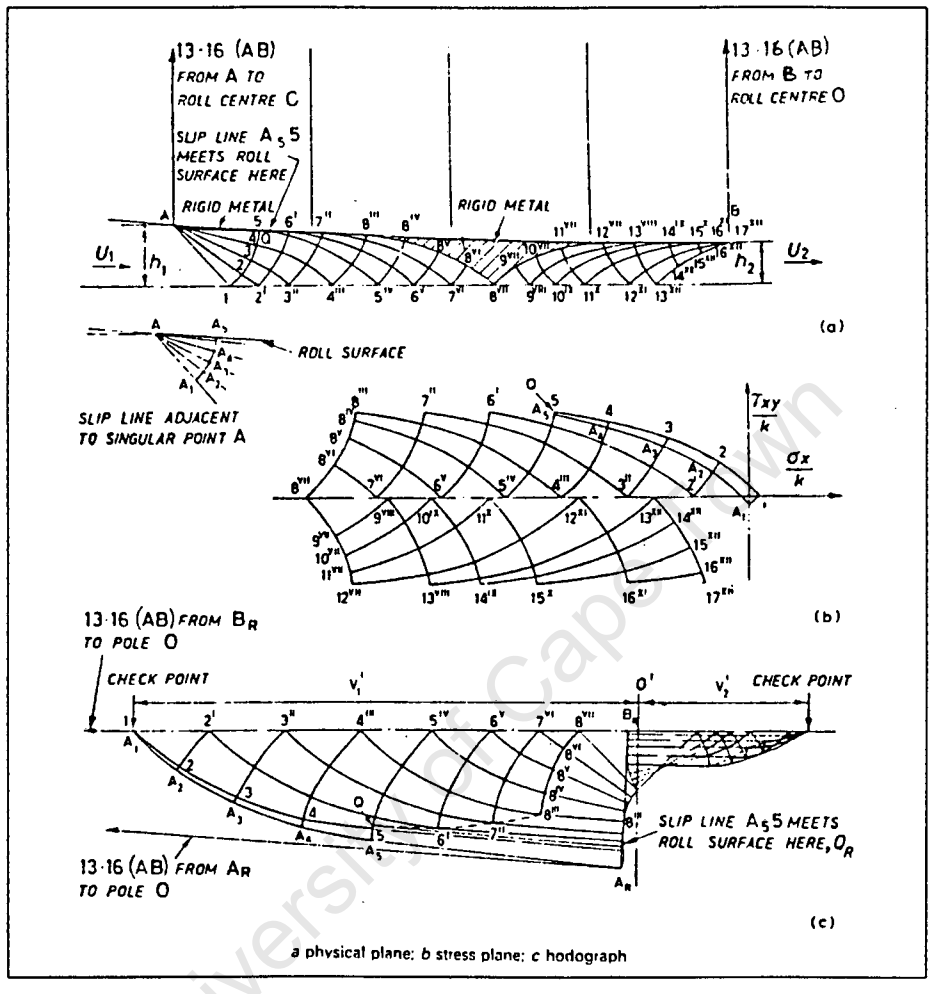

Figure 2.7: Alexander's slip-line field for the hot-rolling of strip [12]

Numerical analyses

There are several different types of numerical analysis methods. Of these, the most widely used is the finite element method. There are many advantages of this method over the traditional analytical methods. Two of these are important to this investigation. The first is that the description of the material behaviour is not restricted. Effects such as work-hardening, strain-rate dependency, and temperature dependency can and have been included in finite element modelling. The second is that it is possible to model three-dimensional problems — the only difficulty being the computational power that is required. A brief review of the finite element method will be given in § 4.1.

Chapter 3

Lateral effects

The edge profile of the AA5182 product being studied here is commonly described as 'concave' or 'double-barreled'. It is typical of rolling schedules which have smaller reductions (reduction less than 15% of the initial height for each pass). When larger reductions are performed, a convex or single barrel edge profile develops.

During the late sixties and early seventies the majority of research work into lateral effects concentrated on the magnitude of spread that occurs:

- Chitkara and Johnson, 1966 [1] rolled lead bars and investigated spread formulae proposed earlier by Wusatowski, Hill, and Sparling.
- El-Kalay and Sparling, 1968 [2] used steel bars to investigate the average spread.
- Helmi and Alexander, 1968 [3] also rolled steel to investigate spread, but investigated maximum spread.
- Beese, 1972 [4] looked at the work of the two 1968 references and did further experimental work.

The work was generally experimental and aimed at finding a means of predicting the overall spread. In rolling schedules that use the smaller reductions, the magnitude of spread is negligible (e.g. less than 1% for 10% reductions). For this reason previous research work concentrated on large reduction passes which have significantly larger amounts of spread; sometimes greater than 10% for 40% reductions.

These researchers came up with empirical formulae which could be used to predict the amount of spread. Although these formulae differ in some aspects, certain trends in factors affecting spread were identified. Three geometrical factors which lead to an increase in spread are:

1. Increase in amount of reduction (δ)

2. Decrease in shape function, defined as the initial width to workpiece-thickness ratio $(\frac{W_0}{H_0})$

3. Increase in roll diameter to workpiece-thickness ratio $(\frac{R}{H_0})$

The effects of other factors were investigated by some of the researchers. Chitkara and Johnson found that an increase in rolling speed caused the amount of spread to be decreased "slightly". EL-Kalay and Sparling concluded that "spread is not very sensitive to temperature". Different conclusions were made about the effect of friction; El-Kalay and Sparling found that a decrease in friction leads to an increase in spread, Chitkara and Johnson found the same only for slabs with width to workpiece-height ratios above 2, while Chen [18] reports Lahoti [19] to have found that increasing friction leads to a slight increase in spread.

In 1981 Sheppard and Wright [5] reported their findings from over 400 rolling tests on aluminium-alloy slabs. They confirmed the effects of the three geometrical parameters given above, and identified three non-dimensional parameters which can be used to predict the magnitude of the spread:

$$\frac{W}{\sqrt{R\delta}}, \qquad \frac{W_0}{H_0}, \qquad \frac{H_0}{R}$$

The effects of five other factors on spread were also investigated:

1. Increases in temperature were found to increase the amount of spread. Increases from 300°C to 500°C resulted in increases in spread of 20% for the M57S alloy and 30% for the 1S alloy.[1]

2. Rolling speeds were found to have negligible effect.

3. To investigate the effect of friction, lubricated and unlubricated conditions were used. Maximum spread was found to decrease for the unlubricated conditions. The decrease was small, however, when the amount of change in friction, from sticking to a coefficient of 0.05, is considered.

4. Material properties were found to have no effect. The two alloys were shown to have no significant differences in the amount of spread even though the yield stress of M57S is approximately 3 times that of 1S alloy.

5. The effect of material structure was investigated and it was found that areas of large grain size have reduced lateral deformation.

[1] In the international designation system M57S is AA5251 and 1S is AA1050A.

They conclude that spread can be predicted by formulae of the type they derived to fit their results:

$$\ln\left(\frac{W_1}{W_0}\right) = \left(0.11 + 0.032T_H - 0.01\frac{R}{H_0}\right)\left(\frac{W_0}{\sqrt{R\delta}}\right)^{-3.5}\left(\frac{W_0}{H_0}\right)\left(1.375T_H + 0.233\frac{R}{H_0} - 0.1\right)$$

where, T_H is the homologous temperature

The most likely explanation for the increased spread with higher temperatures is the lowering of the yield point. However, their finding in point 4 indicates that spread is not affected by the magnitude of the yield stress. As no other explanation for the temperature effect has been identified, the validity of point 4 appears to be questionable. Information given by Wright and Sheppard in a later paper [6] shows that the shape of the profiles for the two materials are not identical for experiments using the same parameters.

3.1 Development and shape of the edge profile

The only available literature on investigations of the profile shape are the papers by Wright and Sheppard [5], [6]. Due to the relevancy to this study, their findings and some information obtained directly from Hulett Aluminium [20] are discussed in detail here.

3.1.1 Shape of the edge profile

In their later paper Wright and Sheppard [6] discuss their study of edge profiles. They investigate the change of profile from the concave shape to the convex shape and identify a transition point between the two. The transition point is defined as a profile which has the double-barrelled deformation, but also has substantial lateral spread. The difference between the various profiles is shown in Figure 3.1 in which the deformed shapes of the edge of the billet is sketched for each type.

Wright and Sheppard cite a report by Brooks [21] which gives the following equation to identify the general profile shape:

$$\frac{2R}{h_1}\left[\arccos\left(1 - \frac{\delta}{2R}\right) + \delta\right] < 57 \text{ for double-barrelled profiles}$$

They, however, believe this equation to give incorrect predictions and give an example from their work which shows this. Using their data from experiments with two different aluminium alloys, they give the following criterion to identify the transition point:

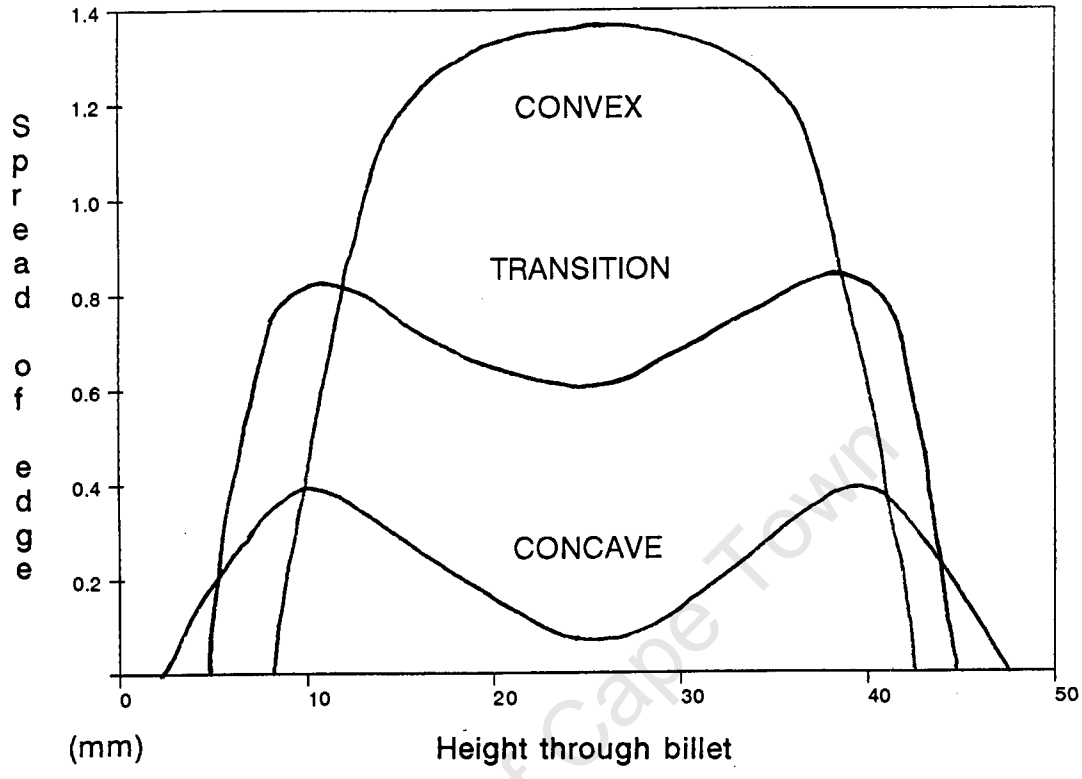

Figure 3.1: Different edge profiles

$$\frac{\sqrt{R\delta}}{H_0} = 0.82 \tag{3.1}$$

When the geometric relationship has a value below 0.82 the profile is concave, and when it has a value above 0.82 the profile is convex.

When considering the first pass of the rolling schedule being studied in this thesis, both criteria predict correctly that the profile will be concave. The Brook's criterion predicts that the transition point will occur for reductions in the region of 25% while the criterion of Wright and Sheppard predicts it to occur with reductions in the region of 35%.

3.1.2 Deformation mechanisms

In the earlier reference of Sheppard and Wright [5] the overall spread is the main area of interest. Therefore emphasis is given to rolling schedules with considerable lateral spread, which have convex edge profiles. It is in this reference that some description of the deformation process is given, and unfortunately the cases with concave profiles are ignored.

For the convex producing schedules, the spread increases as reduction increases. The increase in width occurs via two mechanisms; one is the increasing convexity of the edge profile and the other is an increase in the width of the top and bottom surfaces. Sheppard and Wright find that the rate at which the convex spread increases is less than the rate that the top and bottom surfaces grow.

The increase in width of the top and bottom surfaces is also found to occur through two different mechanisms. In one, when friction is high, the growth is due to what they have called 'side fold' — where material moves from the edges on to the top or bottom surfaces. This effect is found to account for increases in the surfaces of over 20 % for large reduction passes; for smaller reductions the effect is less (zero growth for a 10 % reduction). The other mechanism occurs when friction is lower. When experiments are performed with lubrication, the surfaces are found to grow by a larger amount, but now the growth is due to the surfaces themselves spreading outward.

Investigations at Hulett Aluminium [20] also show the effects of the 'fold over' mechanism for the type of rolling schedule being investigated in this thesis (concave producing schedule). At the end of the 21 roll passes there is an 'oxide band' on the edges of the top and bottom surfaces. This 'oxide band' consists of oxidised material from the edges which has 'folded over' on to the contact surfaces (the contact surfaces are scalped clean prior to the hot-rolling). The oxide banding is minor; between 6 and 8% of the width, and the majority of it is likely to have occurred during the final roll passes when the slab is reduced to roughly 1% of its original height.

The work of Sheppard and Wright also shows that, apart from material movements in the plane perpendicular to the rolling direction, the actual plane is deformed. This result, contrary to the assumptions of Von Kármán, is shown by marking vertical lines on the edges of ingots. The line is bent forward near the surfaces indicating that the surfaces have moved forward relative to the material in the centre of the ingot. Unfortunately this aspect is not discussed in detail, as it would give a good indication of the shear strains that had occurred.

3.1.3 Geometric shape of the edge profile

In an attempt to describe the actual profile, Wright and Sheppard tried various mathematical curves. They found that a fourth order polynomial, which has the necessary three breakpoints, gives a reasonable fit. Higher order polynomials increase the accuracy, but the accuracy with the fourth order polynomial is already in the region of the original experimental accuracy.

The polynomial below is fitted to the data by normalising the reduced thickness of the ingot and by setting the lateral spread, z, to zero at the corner where y = 0. They then perform a study of the effect of various rolling parameters on the coefficients of the polynomials.

$$z = a + by + cy^2 + dy^3 + ey^4$$

The results of this study indicate one important aspect for this investigation. One set of data is given for three successive roll passes, and the ratio between the constants is found to remain fairly constant. The rolling parameters and the coefficients for the profiles of the three passes are given in Tables 3.1 and 3.2 respectively. The fact that the ratios remain constant is important as this means that the results from analyses of a single pass will give a good indication of the profile that will develop. Data is also given for the seventh pass of another experiment which had both the same geometry and the same reduction per pass of 10%. The ratio for this is also very similar to the original ratio.

Parameter	Value	Variable	Value
Roll radius	125 mm	Material	alloy 1S
Ingot height	25 mm	Temperature	500 °C
Ingot width	37.5 mm		

Table 3.1: Parameters of Wright and Sheppard example [6]

Pass	Reduction	a	b	c	d	e
1	10 %	0.0162	3.22	-11.92	16.38	-7.92
2	10 %	-0.0021	4.87	-17.49	23.88	-11.15
3	10 %	-0.0052	6.81	-24.72	33.91	-16.03
7	10 % each	-0.0038	9.18	-30.76	45.43	-22.18

Table 3.2: Coefficients for profiles in Wright and Sheppard example [6]

3.2 Final edge profile for the hot-rolling of AA 5182 ingot

The most consecutive roll passes that Sheppard and Wright give data for is seven, during which the ingot is reduced to roughly half of its original thickness. The reductions for this schedule are in the region of the transition point ($0.71 \leq \sqrt{R\delta}/H_0 \leq 0.97$) and therefore the results give no definite indication of what happens in rolling schedules of the type being studied here, where the profile is strongly concave. The only information available comes from an internal report of Hulett Aluminium [20]. In this report a description of the edges at the end of the rolling schedule is given and a comparison is made of the

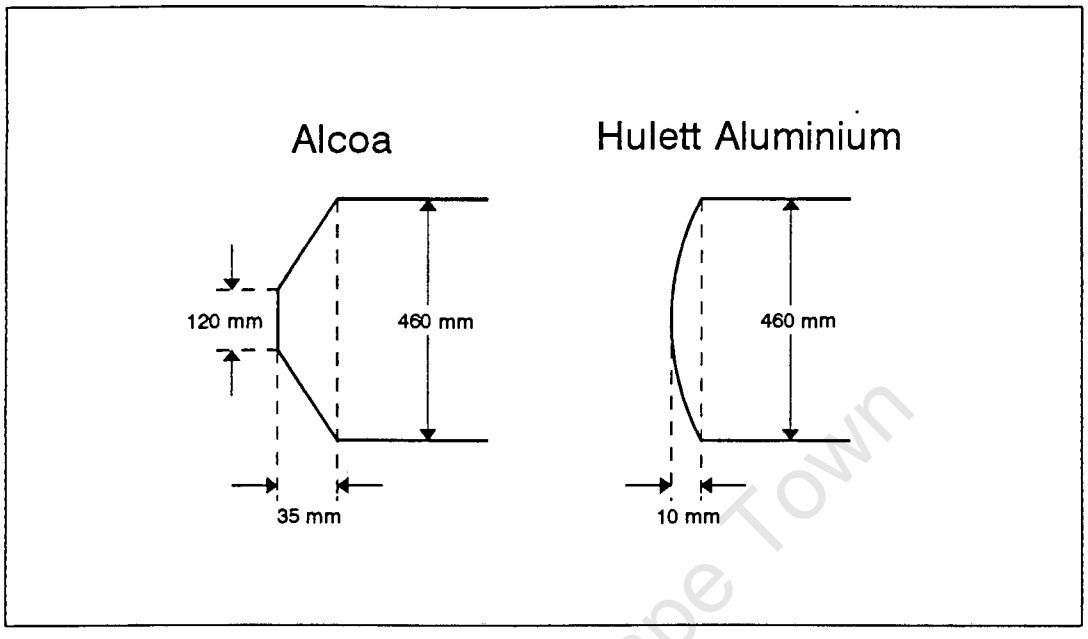

Figure 3.2: Initial edge profiles used in study at Hulett Aluminium

phenomena resulting from the rolling of ingot with two different initial edge profiles (see initial profiles in Figure 3.2).

Three phenomena are discussed. The first, oxide banding, has already been discussed above in §defmech. The second is the way the material in the centre of the edge folds in on itself. This phenomena has been named 'roll over'. The third is edge cracking, which consists of cracks which propagate from the edges in a plane perpendicular to the rolling direction. These three phenomena are sketched in Figure 3.3.

No data is available on when each of these start. The 'roll over' will commence when the actual concave profile is pressed together by the rollers. The 'oxide banding' might be due to the same process, or due to the material flowing to the surface in the 'fold over' mechanism described by Wright and Sheppard. The edge cracking phenomena is caused by the difference between the strains in the rolling direction inside the slab, and those inside the material that has bulged out at the edges. The material in the slab is forced to elongate as it is compressed between the work-rolls. The material bulging out of the edges, however, is not compressed and thus goes into tension in the rolling direction which eventually causes the edge cracks.

In the industrial process the edges of the final product are trimmed in order to remove these effects. If it were possible to reduce the maximum dimension, then waste would also be reduced.

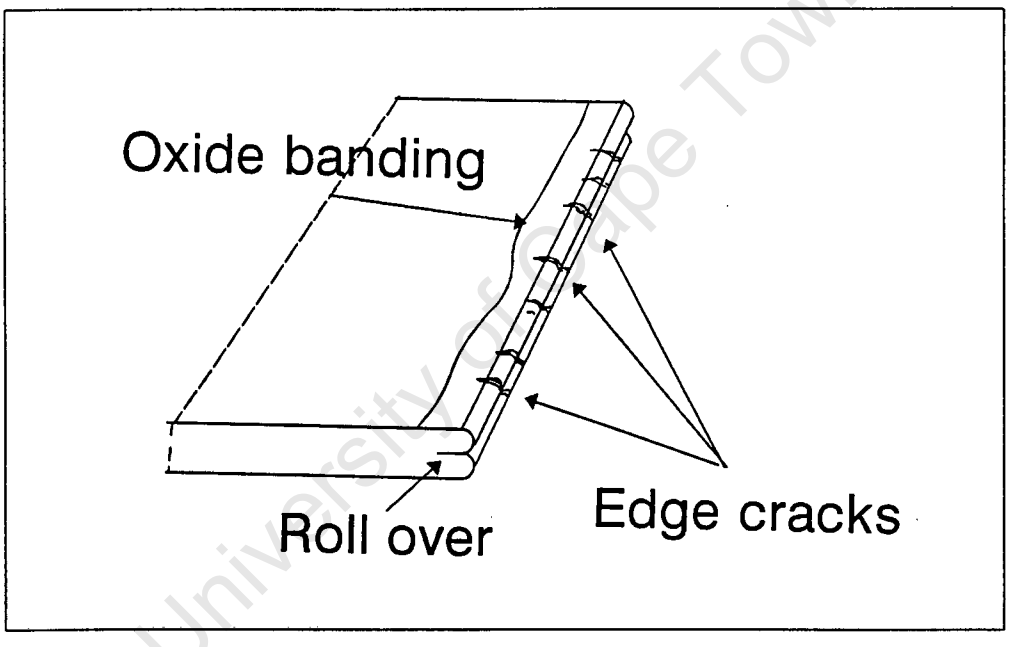

Figure 3.3: Sketch of the edge phenomena at the end of the rolling schedule

Chapter 4

Numerical Simulation of the Rolling Process

As the understanding of the rolling process developed, the analyses of the problem became more complex. Solutions to the problem, such as von Kármán's differential equation, required approximations to simplify the integration. These assumptions limited analyses until the usefulness of the computer in solving these types of problems with numerical techniques was identified. Alexander [22] presented a solution to von Kármán's differential equation in computer form in 1972. Since then several general numerical methods have been developed which can be applied to a wide range of problems. The most common are the finite difference method, the boundary element method, and the finite element method. Of these, the finite element method is the most widely used in the analysis of metal working processes.

The theory of the finite element method is well documented. References that cover the topic in detail include: Bathe [23], Burnett [24], Cook *et al.* [25], and Zienkiewicz [26]. In the first section of this chapter a brief overview of the method is given. After this some of the finite element work on the rolling process that is available in the literature is presented.

The accuracy of numerical simulation depends on both the accuracy of the modelling technique and the accuracy with which a problem is defined. The finite element method is a proven technique and, therefore, the accuracy of work will depend on the accuracy of the description of the problem. While the geometry and kinematics of the rolling problem are easily described, material properties of specific aluminium alloys, and frictional and heat transfer conditions are either not well understood or not fully researched. The remaining sections of this chapter investigate the various important aspects in the hot-rolling problem and describe how they are included in the modelling.

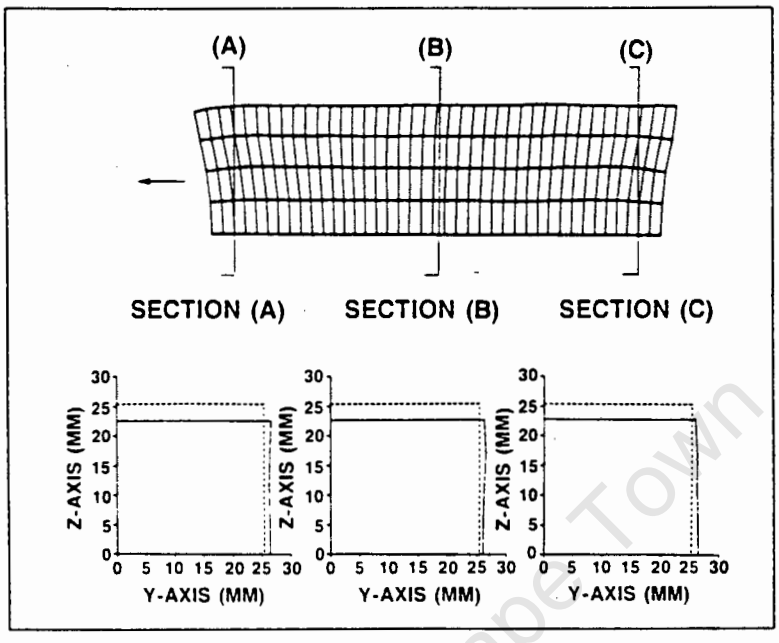

Figure 4.1: Predictions of the spread in modelling of Park and Oh [39]

4.3 Geometry of the ingot

Generally the rolling problems are analysed in two dimensions. This is done by assuming plane strain conditions in the lateral direction (direction 33 in Figure 4.2). However, the edge profiles being studied here are a result of non-uniform strains in this direction and consequently full three-dimensional modeling is required to study the changes in these profiles. A major problem with three-dimensional analyses is the large amount of computer time that is required, and because of this, two-dimensional analyses were performed initially to study the effect of various variables and to gain familiarity with the problem.

The length of the ingot that need be modelled was considered to be such that the steady state of rolling could be observed in the middle section. After several trial analyses, this was found to be approximately two times the initial height of the ingot.

To reduce the size of the problem the ingot is considered to be symmetrical through two planes which are marked with the dashed lines in Figure 4.2. The one being the vertical centre plane extending in the rolling direction and the other being the horizontal centre plane. The two-dimensional model, which is assumed to be plane strain in the lateral direction, thus consists of half the ingot vertically and a reduced length horizontally. The three-dimensional model consists of half the ingot laterally, half the ingot vertically, and a reduced length — the section that has been modelled is shaded in the diagram. Suitable

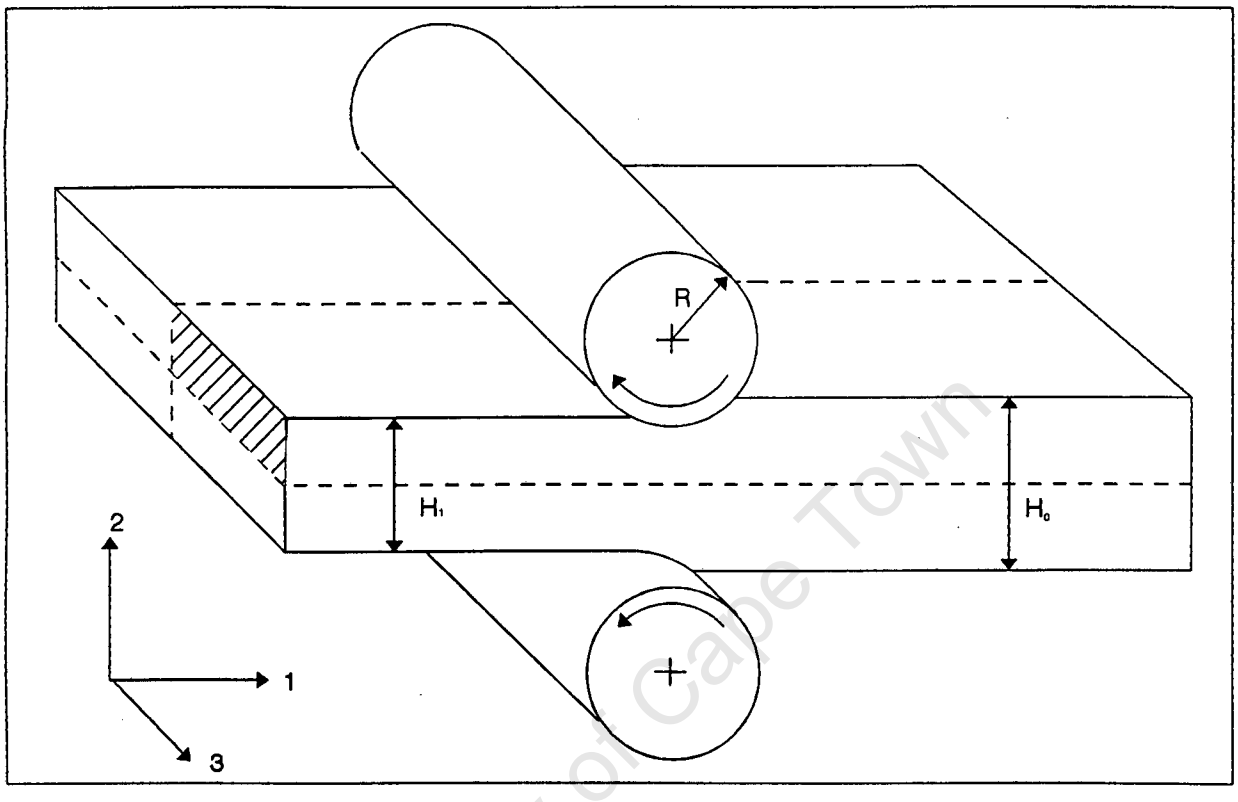

Figure 4.2: Sketch of the rolling problem

boundary conditions for the planes of symmetry are imposed.

4.4 Constitutive relations for modelling the Al-alloy

The alloy used in the process is coded AA5182, AA indicating the standard coding system for aluminium alloys as set out by the Aluminium Association in the U.S.A., and 5182 designating the specific alloy. Properties of AA5182 are given in Table 4.4. Due to the large scale deformation in the rolling process, the plasticity definition is the most important criteria when modelling the problem. The definition of the yield value for the alloy is given below in terms of temperature, plastic strain and strain rates [41].
Uniaxial yield stress (MPa), σ_y (Valid for AA5182 between 300°C and 550°C) :

$$\sigma_y = 83.05\epsilon^k \ln\left[x + \sqrt{(x^2+1)}\right] \tag{4.2}$$

where,

$$x = \left[\frac{\dot{\epsilon}}{4 \times 10^{10}} \exp\left(\frac{18500}{T}\right)\right]^{0.2}$$

$$k = 0.109\left(1 - \tanh[7.325\left(\frac{T}{873}\right) - 4.74]\right)$$

ϵ = Maximum of : true plastic strain, 0.008

$\dot{\epsilon}$ = Maximum of : strain rate ($\sec^{-1}$), $\left[\frac{\exp(\frac{18500}{T})}{4 \times 10^{10}}\right]^{0.2}$

T = Absolute Temperature, K

Main alloying materials	
Magnesium	4.5%
Manganese	0.35%
Physical properties	
Density	2650 g/m^3
Modulus of elasticity	71 GPa
Poisson's ratio	0.33
Melting range	575 - 640°C
Thermal conductivity (at 25°C)	121 W/m°C

Table 4.1: Properties of aluminium alloy AA5182

By inspecting the equations above, the effects of the three variables can be determined.

1. Increases in temperature soften the alloy (lower its yield stress value). At 300°C the yield stress, σ_y, is equal to 132 MPa; while at 550°C, σ_y equals 49 MPa ($\epsilon^{pl} = 0$, and $\dot{\epsilon} = 0$).

2. The material hardens as it undergoes plastic deformation. This effect is commonly called work-hardening. The plot of σ_y versus ϵ^{pl} in Figure 4.3 ($\dot{\epsilon} = 0$) shows this trend as well as its prominence at the lower temperatures in the range.

3. At higher strain rates the yield stress of the alloy increases. This is shown in the plot of σ_y versus $\dot{\epsilon}$ in Figure 4.4 ($\epsilon^{pl} = 0$).

These three effects must all be included in the numerical modelling, and the way this was done for each effect is described in the following sections.

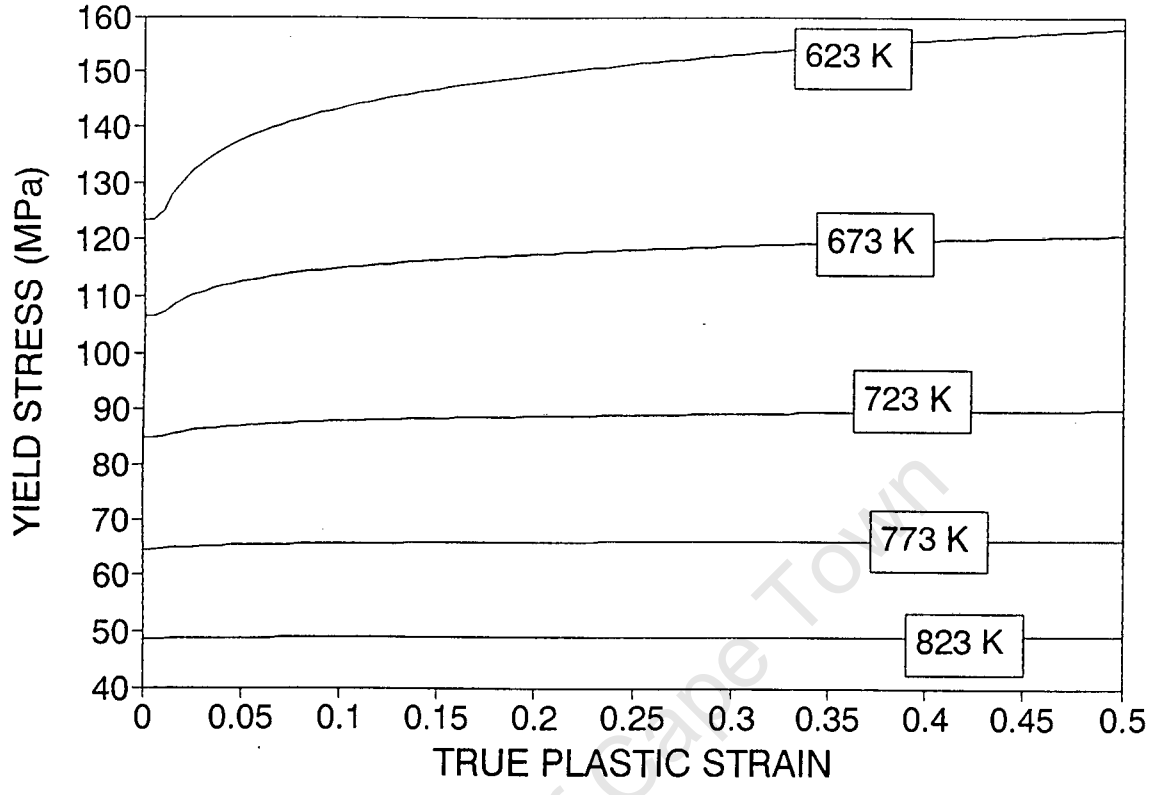

Figure 4.3: Yield stress of AA5182 versus amount of plastic strain

4.4.1 Identification of the yield point with the von Mises yield criterion

To understand how the aluminium alloy undergoes plastic deformation, it is useful to look at the structure of the metal. Microscopically, the metal consists of grains in which atoms are packed together in an ordered or crystalline manner. The orientation of the packing is different in the grains. There are different types of crystalline structures which metals assume; for aluminium the structure consists of face-centred cubic units (f.c.c.).

In the crystalline structures there are planes along which slip occurs most easily. The plastic deformation of metals occurs through slipping in those grains which are orientated with their slip planes in the direction of maximum shear.

Two mechanical models are used widely to describe the yielding of metals, the Tresca and the von Mises yield criteria. Of these, the von Mises criterion has been shown to be the most accurate.

According to the von Mises yield criterion, yield occurs when the root mean shear stress reaches a certain constant:

$$\left[\frac{(\sigma_1-\sigma_2)^2(\sigma_2-\sigma_3)^2(\sigma_3-\sigma_1)^2}{3}\right]^{1/2} = C \tag{4.3}$$

Where the uniaxial tension test is used to obtain yield criteria data, σ_1, can be taken as the uniaxial yield stress, σ_y. In the other directions the stresses are zero and therefore the root mean shear stress is:

$$\left[\frac{2\sigma_y^2}{3}\right]^{1/2} = \sqrt{2/3}\,\sigma_y = C$$

Where the simple shear test is used in which yielding occurs when the normal stresses are $\pm k$, then $\sigma_1 = k$, $\sigma_2 = 0$, $\sigma_3 = -k$. Then the root mean shear stress is:

$$\left[\frac{6k^2}{3}\right]^{1/2} = \sqrt{2}k = C$$

The yield criteria are often also given in the following form:

$$(\sigma_1-\sigma_2)^2 + (\sigma_2-\sigma_3)^2 + (\sigma_3-\sigma_1)^2 = 2\sigma_y^2 = 6k^2 \tag{4.4}$$

One of the material models in the ABAQUS program was specially developed for modeling the plastic response of metals. This uses the von Mises yield surface model with associated plastic flow. The yield surface is defined by giving the value of the uniaxial yield stress as a function of uniaxial plastic strain and temperature. For the rolling problem the hardening of alloy is best represented by isotropic hardening in which the yield surface changes size uniformly in all directions (the yield stress increases in all stress directions as plastic straining occurs). This material model therefore takes temperature and work-hardening effects into account directly.

4.4.2 Strain-rate dependency

The effect of strain rate on the yield stress is included by using the following model in which the two parameters D and p need be defined:

$$\dot{\bar{\epsilon}}^{pl} = D\left(\frac{\bar{\sigma}}{\sigma_0} - 1\right)^p \qquad \text{for } \bar{\sigma} \geq \sigma_0$$

where, $\sigma_0\left(\epsilon^{pl}, T\right)$ is the static yield stress
$\bar{\sigma}$ is the equivalent stress
$\dot{\bar{\epsilon}}^{pl}$ is the uniaxial equivalent plastic strain rate

To implement this, values for the two parameters were chosen to give the closest approximation to the yield stress data (at specific temperatures) given by Equation 4.2. A comparison of the yield values given by this model, with the chosen values of D and p, and the original data is shown at three temperatures in Figure 4.4. The approximation by the ABAQUS model differs at most by 8.4%.

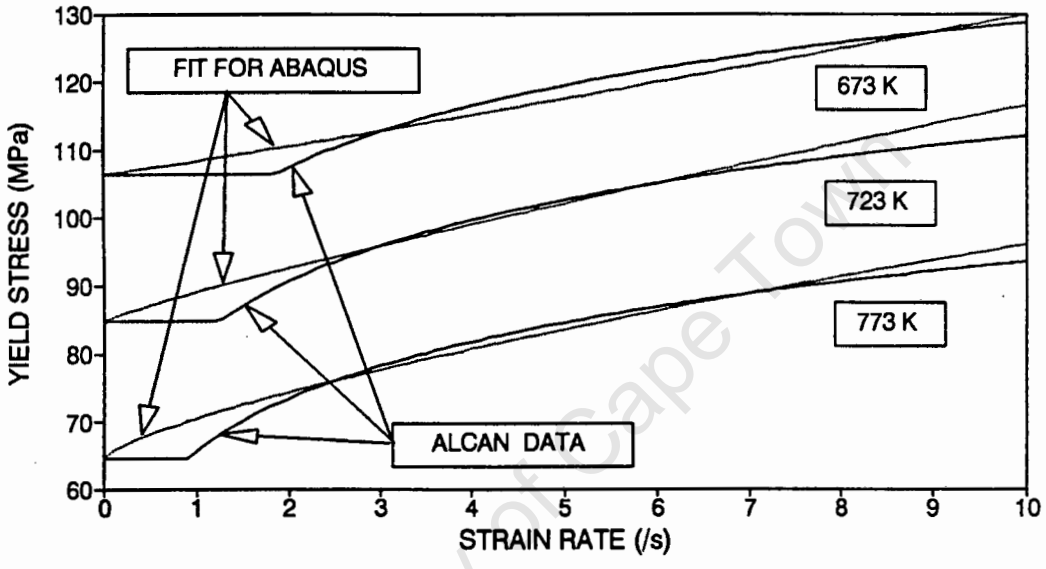

Figure 4.4: Comparison of yield stresses predicted by ABAQUS model and the original data.

4.5 Thermal effects in the hot-rolling process

The temperature of the ingot as well as the temperature profile through the ingot are important factors when analysing the hot-rolling problem. This is because the yield strengths of materials depend on temperature. The strong dependence of the yield strength of AA5182 on temperature can be seen in Figure 4.4; the effect of temperature on the work hardening can also be seen. At the higher temperatures the response of the material is almost perfectly plastic while at $\pm$ 350°C definite work hardening effects can be seen.

In the hot-rolling problem the ingot generally starts with a uniform temperature profile. In the process being studied here, the billet is initially 505°C. Then, during the process, various mechanisms put heat into and take heat out of the ingot. Heat gain results from the energy produced by dissipation of plastic work and also from the friction in the

roll gap. Meanwhile heat is lost to the work rolls and tables, as well as to the general environment.

Various thermal effects and methods of analysing them are discussed in this section.

4.5.1 Heat flows inside the ingot

When considering the rolling problem there are heat flows inside the ingot as well as heat flows in and out of the ingot. In the ingot the heat flows from high-temperature to low-temperature regions. This type of heat transfer is called conduction and is described by the second order differential equation:

$$\frac{\delta}{\delta x}\left(k\frac{\delta T}{\delta x}\right)+\frac{\delta}{\delta y}\left(k\frac{\delta T}{\delta y}\right)+\frac{\delta}{\delta z}\left(k\frac{\delta T}{\delta z}\right)+\dot{q}=\rho c\frac{\delta T}{\delta \tau}$$

where, k : thermal conductivity, W/m°C
c : specific heat capacity, J/kg°C
$\dot{q}$: energy generated per unit volume, W/m^3
τ : time, s

The following values were used for the constants. The thermal conduction coefficient of AA5182 is known to be $k = 121$ W/m°C at 25°C and, although the conduction of pure aluminium is known to rise as a function of temperature [42], this value was taken as constant, as no specific information on the temperature dependency was available. No value for the specific heat capacity of AA5182 was identified, so after comparing values of similar alloys; that of AA5083 was chosen, $c = 970$ J/kg°C. The density of AA5182, $\rho = 2650$ kg/m^3 has been given previously. The only heat generated inside the ingot is due to plastic work being done. The amount of energy producing heat was taken as 0.9 times the total energy dissipated, a value typical for this type of problem [43].

4.5.2 Heat losses to the environment

There are three different heat flow mechanisms; conduction, convection and radiation. Conduction has been discussed above. The other two are important when considering heat losses from the billet into the surrounding environment.

Convection occurs when heat flows from a body to a fluid (gaseous or liquid). The heat is really flowing by conduction into the layer of fluid surrounding the body and then into the fluid surrounding that. The difference from the conduction above is that the fluid can move; and so the amount of heat transfer depends also on the velocity of the fluid. Heat flows can be described as:

$$q = hA(T - T_\infty)$$

where,
- T : temperature of the body
- T_∞ : temperature of the environment
- A : surface area of the body
- h : convection heat transfer coefficient, $W/m^2\,°C$ (Usually found experimentally for specific conditions.)

For the ingot moving at approximately 1 ms^{-1} in its initial passes, the convection heat transfer has been estimated as $h = 10$ $W/m^{2o}C$.

The mechanism of radiation heat transfer between two bodies is electromagnetic radiation. Here the net heat flow is proportional to the difference between the fourth power of the absolute temperatures. For a body enclosed by a much larger surface, the heat flow is:

$$q = \epsilon\sigma A\left(T_b^4 - T_s^4\right)$$

where,
- ϵ : emissivity of surface
- σ : Stefan-Boltzman constant, 5.669×10^{-8} W/m^2K^4
- A : surface area, m^2
- T_b : temperature of body, K
- T_s : temperature of surrounding surface, K

4.5.3 Heat transfer to the work-rolls

During the rolling process the work-rolls are cooled by spraying. An estimate of the average work-roll temperature during the initial passes is 242°C. (Entry side temperature ± 124°C and exit side temperature ± 310°C [44]). So, even though the work rolls are in contact with the surfaces of the ingot for only short periods, significant cooling of the ingot is expected here.

The transfer of heat between two surfaces occurs through three different mechanisms. These can best be described by using Figure 4.5 which shows a magnified section of contact between two surfaces. Firstly, heat flows through the areas of solid-to-solid contact by conduction. Secondly, heat flows through entrapped fluids, also by conduction. Thirdly, heat transfer occurs as radiation directly between the two bodies.

Unfortunately an understanding of how the heat flows does not lead directly to a quantitative means of predicting heat flows. For the contact area between hot aluminium alloy and the steel work-rolls, the dominant mechanism is heat conduction through the solid-to-solid contact areas where the coefficient of conduction, k, is in the region of 100 $W/m^2\,°C$. The entrapped fluid is either lubricant or air, for which coefficients are in the region of

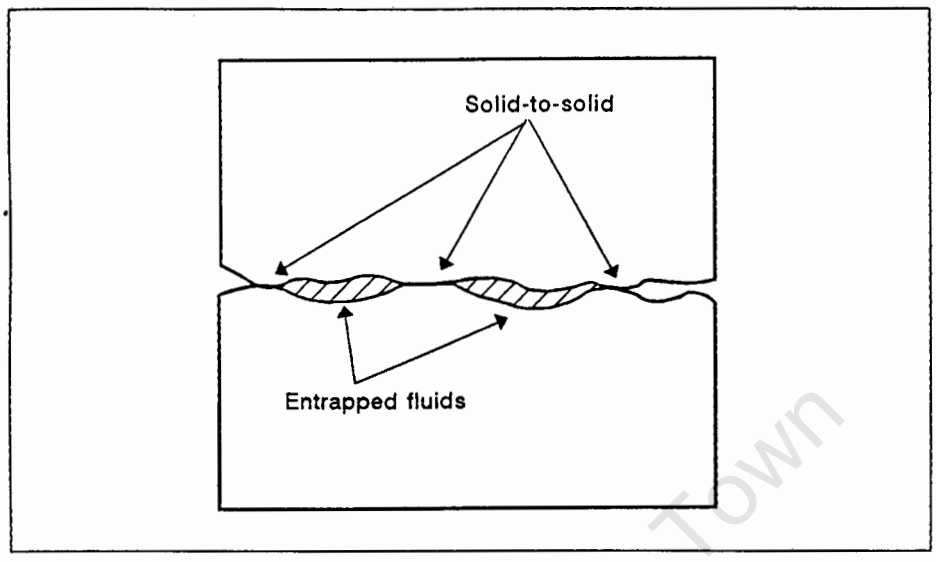

Figure 4.5: Microscopic view of two bodies in contact

0.5 W/m^2 °C and 0.025 W/m^2 °C respectively. The radiation heat flows are also negligible in comparison (see calculated values of heat flow in Table 4.3).

The view of heat conduction given above does not, however, provide a means of predicting magnitudes of heat transfer, as the areas of solid-to-solid contact are not known. It does however lead to the conclusion [42] that an increase in the contact pressure will cause an increase in the heat transfer as the solid-to-solid contact areas increase. The increases in the area depending on the amount of local plastic deformation that occurs.

Experimental work by Semiatin *et al.* [45] shows this increase in interface heat transfer with pressure. Their results indicate an increase in heat transfer by approximately an order of magnitude with an increase from nominal pressure to those used in bulk forming processes. They also show, however, that above a certain pressure it remains constant.

With the varying contact pressures in the roll gap the coefficient of heat transfer would need to be described as a function of pressure to predict the heat transfer in the roll gap. Unfortunately sufficient data is not available and a rough approximation has been made from the data in Table 4.2.

4.5.4 Heat generation due to friction in the roll-gap

In an interface in which the surfaces are sliding relative each other, energy is released as heat at the following rate:

$$\dot{q} = \mu V p$$

Source	Description	Coefficient ($W/m^2\,°C$)
Pietrzyk *et al.* [46]	Warm-rolling of aluminium at 150°C to 200°C with work-rolls at 20°C	30000
Pietrzyk *et al.* [47]	Cold-rolling of aluminium strip	4000
Semiatin *et al.* [45]	Ring compression tests, steel die at 195°C and AA2040 ring at 425°C	
	slow test	7500 → 10000
	fast test	15000 → 20000

Table 4.2: Heat transfer coefficients

where, μ : coefficient of friction
V : 'relative velocity between the two surfaces, $m.s^{-1}$
p : pressure between the two surfaces, MPa

For the process being investigated here a value has been estimated for the amount of heat generated on one surface as it passes through the roll-gap. The following assumptions have been made:

- The Coulomb coefficient of friction, $\mu = 0.3$.
- The maximum possible relative velocity between the work-rolls and the ingot is 0.05 $m.s^{-1}$, which would give an average value for V of 0.025 $m.s^{-1}$.
- The maximum normal pressure in the roll-gap is 160 MPa. This value was taken from results of plane strain analyses that had already been performed.
- The length of contact between the work-rolls and the ingot is 0.1 m.

With these assumptions the amount of energy generated per square metre of surface is 120 kJ per pass.

4.5.5 Relative magnitudes of heating and cooling mechanisms

To get a feeling for which mechanisms were most important in the rolling system some rough calculations were performed. The calculations and results of analyses performed are given in Appendix A. To compare the mechanisms, the following conditions, typical of the first five passes, were assumed. The total time for a pass is 9 seconds, and the time of contact between a point on the ingot surface and the work-roll is 0.1 seconds.

Mechanism	Coefficient	Heat loss per area (kJ/m^2)
Convection	$h = 10\ W/m^2\,°C$	43.02
Conduction to work-rolls	$k = 10000\ W/m^2\,°C$	263.00
Radiation to environment	$\epsilon = 0.09$	16.45
Radiation to work-roll	$\epsilon_{al} = 0.09$; $\epsilon_{WR} = 0.066$	0.07

Table 4.3: Comparison of heat loss mechanisms

The most important heat loss mechanism is the conduction of heat to the work-rolls in the roll gap. To compare this effect with the heat generated by the dissipation of plastic work energy, it was necessary to look at the temperature profile and heat flows in the ingot.

A simple one-dimensional finite element model of heat flows in ingot was used. The results of this were compared with the calculated solution of the temperature profile in a surface cooled semi-infinite sheet and were found to be in agreement. This model was then used to predict the temperature profile produced by heat losses to the work-rolls. The temperature profile at the exit from the roll gap and the profile after 8.9 seconds of heat transfer are shown (with the temperature profile due to plastic work heating) in Figure 4.6.

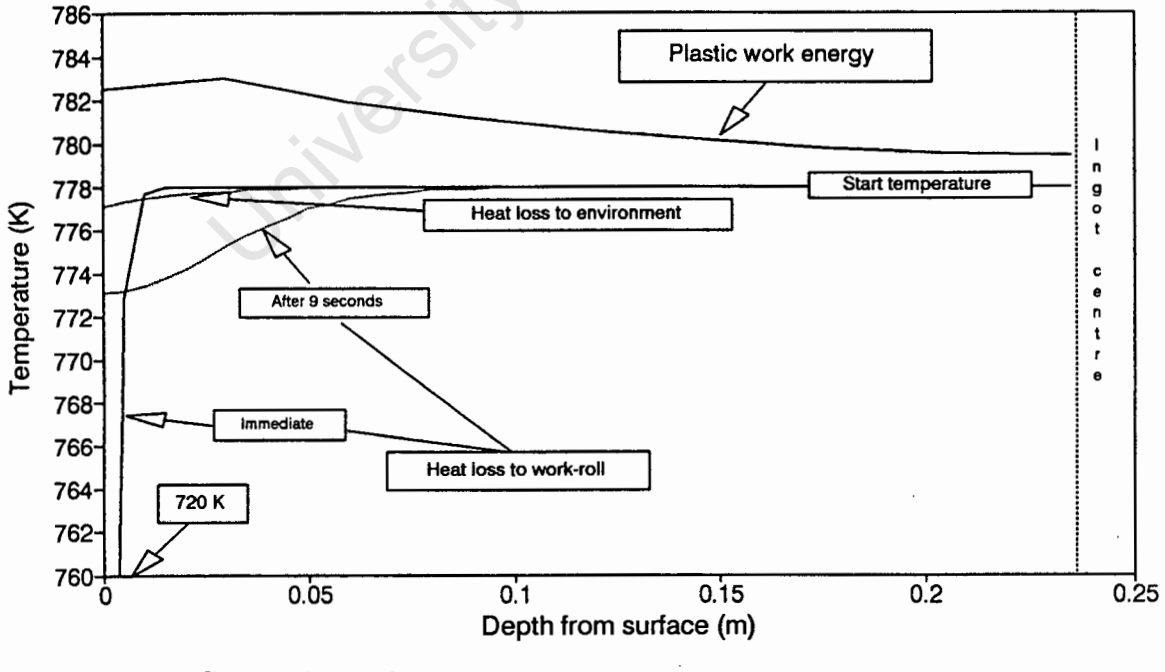

Figure 4.6: Comparison of temperature profiles through the depth of the ingot

4.6 Friction conditions in the contact area

The driving force in the rolling system is the friction between the work-rolls and the ingot. Coulomb's Law, in which the sliding frictional stress, f, is proportional to the normal pressure, p, is frequently used to model friction. Coulomb considered friction to be mainly due to the interaction between rough surfaces where the asperities on each surface slide over each other. The friction would then depend on the average angle of the asperities,
θ, and the constant of proportionality, μ, is therefore equal to $\tan(\theta)$.

$$f = \mu p$$

Today friction is understood to act differently. According to Tabor [48], three basic elements are involved in the friction of unlubricated solids:

1. The area of true contact between the sliding surfaces.
2. The type of strength of bond that is formed at the interface where contact occurs.
3. The way in which the material in and around the contacting regions is sheared and ruptured during sliding.

The coefficient of friction depends on many factors such as the materials involved, the relative speed at which the two surfaces slide over one another, and the presence of lubricants. Lim and Lenard [49] give a review of work on friction and give a complete list of the factors.
Experimental studies of friction in rolling have shown that a constant coefficient of friction does not describe the relationship between frictional and normal stresses throughout the roll-gap [49,50,51]. However, there is no explanation of how the coefficient of friction is related to the varying factors in the roll-gap.
Several different ways of modelling friction have been used in analyses of the rolling problem. The standard Coulomb Law with a constant coefficient has been used by many researchers [29,52,35]. Another popular method, especially for hot-rolling problems where high friction stresses occur, uses a friction factor, m, to give the frictional stress:

$$f = mk$$

where, k : the yield stress in pure shear, equal to $\sigma_y/\sqrt{3}$

This method has been implemented by Oh and Kobayashi [53], Liu *et al.* [40], and Barata Marques and Martin [54].

A model put forward by Chen and Kobayashi [55] has also been implemented by others [30,32,33]. The model, as used by Hwu and Lenard [32], is:

$$F = -f\left[\frac{2}{\pi}\tan^{-1}\left(\frac{\bar{V}_r}{a}\right)\right]\frac{\bar{V}_r}{|\bar{V}_r|}$$

where, f : the friction stress given by μp
$\bar{V}_r$: the relative velocity between the roll and the material
a : a constant

There have also been some alterations made to these standard models. Aanestad [56], Lau *et al.* [33], and Johnson [57] have implemented the Coulomb model with the coefficient dependent on the relative velocities of the two surfaces. Richelsen [58] used the model proposed by Wanheim and Bay which includes a transition between Coulomb friction and the constant friction shear stress limit ($k = \sigma_y/\sqrt{3}$).

In ABAQUS the standard friction model is the Coulomb model with an optional limit on the shear stress. It is implemented with both a stiffness method and a Lagrange multiplier method for sticking friction; the user being able to make a choice between the two.

Both implementations have been tried in rolling analyses and the stiffness method is now being used as difficulties occurred with the Lagrange multiplier method.

4.7 Roll flattening

In thin strip rolling the work-rolls exert large pressures and are deformed to a considerable extent. Thus, when modelling these processes the roll flattening is usually taken into account by using Hitchcock's theory (explanations of this theory are given in many books on metalworking [13,14,15,59]). Due to the size of the problem it is not reasonable to model the work-rolls with finite elements as well.

In the problem being investigated here, however, the slab is thick and the hot aluminium alloy being rolled is soft relative to the work-rolls. Therefore, in this research work the work-rolls have been modelled as rigid cylinders and the effect of the roll flattening has been ignored.

Chapter 5

Results

For the investigation of the edge profile, the finite element modeling required much development. For each of the aspects mentioned in § 4 many analyses were required before the effect was correctly modelled. For the initial stages of development the results reported here will be limited to the discussion of the important and interesting features. Much of the development work required an inspection of results, usually contour plots of stress, strain and plastic strain, to identify unexpected features. Then it was necessary to discover the reason behind them; and, if it was a problem in the modeling technique, make the necessary adjustments.

It has been mentioned previously that work started with two-dimensional plane strain analysis because of the significant saving in time. The results of these analyses have, however, much more worth than simply being a development stage. Practically all the existing rolling theory is based on plane stain assumptions and the results will be useful for investigating the theory. For this reason the effects are first looked at in the two-dimensional analyses and then the variation of these effects in the lateral direction is noted.

When looking at the actual edge profiles that are predicted by the three-dimensional modeling, it is possible to compare more quantitative results. These results are useful for checking the effects of approximation in the modeling, but there are not many results available in the literature with which to compare the final results. Analyses were performed which used the parameters of the tests done by Wright and Sheppard [6] in order that some verification could be made. Unfortunately there are some details which are not given clearly and extra analyses were required to cover a range of assumptions.

The final section of work reported on in this chapter is the modelling of the formation of the edge profile with a model consisting of only a section of the ingot. In this work simple models were analysed in attempts to incorporate specific effects which were thought to contribute to the development of the profile.

5.1 Development of the model

5.1.1 Quasi-static analyses

The first type of two-dimensional analyses which was tried, is performed quasi-statically in the following way. The work-roll is fixed at its centre and has a prescribed rotation over the time of the analysis that is the same as the real rotation. This rotation occurs as a ramp function and is thus equivalent to a constant radial velocity. The ingot is initially pushed into the roll-gap by prescribing displacements of nodes at the back of the ingot. This step is necessary as otherwise the ingot would be unrestrained in the rolling directions and numerical problems would occur. Once the ingot has been pushed a sufficient distance into the roll gap a new step is started with no prescribed displacement on the ingot. The analysis continues with the friction between the work-rolls and the ingot being the driving force. When the ingot is about to leave the work-rolls the front nodes are given a prescribed displacement to 'pull' the ingot out. This is again necessary to avoid numerical problems.

During the first and third stages of this process the relative velocity between the work-rolls and the ingot depends on the prescribed conditions. This is not representative of the real situation in which the relative velocities would be determined by the conditions in the roll gap. For this reason the modeling of the end sections is not realistic.

Although this study is looking specifically at conditions which occur during the steady state rolling away from the ends, it was preferable to model the entire process correctly. Furthermore, with this method it was necessary to stop the analysis after each step and read the displacements so that the prescribed displacements could be calculated.

For these two reasons an 'automatic' method that could cope with multiple passes was developed. This method consists of a rotating rigid roller, a discretised ingot and a weak spring to restrain any rigid body modes whilst the ingot is not in contact with the rollers. The various stages in the analyses are described below.

Prior to contact (Figure 5.1a)

Prior to contact with the rolls, the ingot is unrestrained horizontally in the finite element model. To provide this restraint a 'soft' spring is attached to one of the central nodes. The stiffness of the spring was chosen such that after a pass through the rolls (when it was extended by more than the length of the ingot) the force applied to a node would not be large enough to cause any plastic deformation. Then, to get the ingot into contact with the rolls, a horizontal body force is applied as a user controlled loading.[1] The loading at this stage cannot be much larger than the spring force, because large forces create

[1]The ABAQUS program has interfaces on to which code, written by the user, can be attached. One of these interfaces allows body loads to be described by the user.

convergence problems when contact does occur.

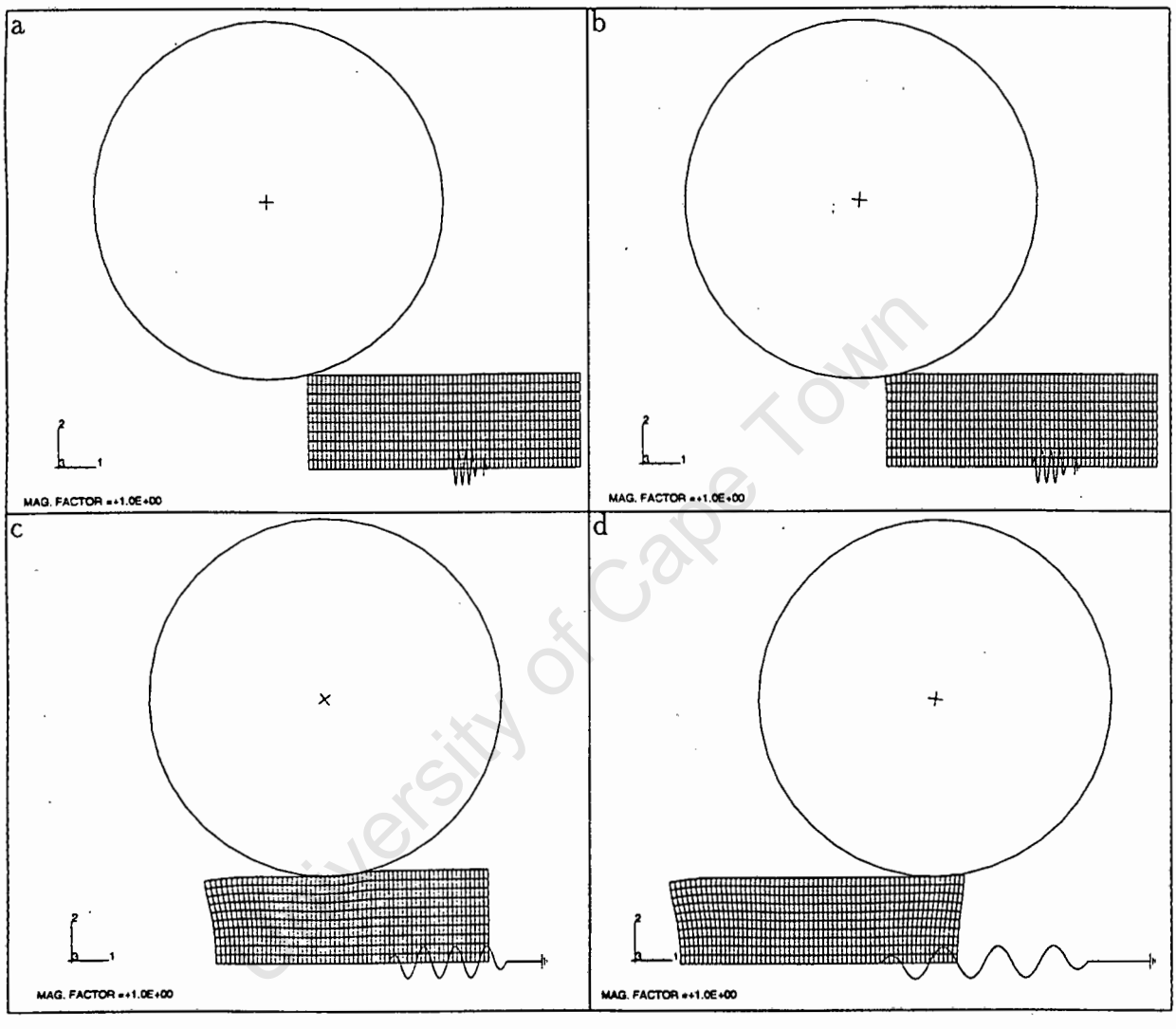

Figure 5.1: Stages in quasi-static analysis

Entry into rolls (Figure 5.1b)

Whilst the first node is in contact with the rolls, the loading is increased as a function of the horizontal distance which the front node has moved into the rolls. It increases up to the force which will balance the spring force once the ingot leaves the rolls.

Middle section of the roll pass (Figure 5.1c)

Once the rolls have a grip on the ingot no further loading is necessary. The ingot is then pushed/pulled through the rolls by the frictional forces between them. The user controlled loading is simply left at the load level which would balance the spring force at exit from the rolls. (The small forces involved do not have a significant or even noticeable effect on the results.)

Exit from the rolls (Figure 5.1d)

It was discovered that a body force, greater than that required to balance the spring force, was necessary to ensure that the ingot exits from the rolls. This force is not large, being equivalent to a horizontal gravitational field of 0.4g. It is applied when the last corner node enters the rolls and is kept constant until the ingot leaves the rolls.

After exit

Initially attempts were made to decrease the body force immediately after exit from the rolls. This would have been to the force required to position the ingot, against the spring force, for the following pass next to the rolls. However, no satisfactory method of checking for exit from the rolls could be determined as the displacements coming into the user element module after the predictor stage are sometimes excessive and this led to the force being reduced at the wrong stage. Eventually it was decided to leave the extra force on and to let the ingot come to equilibrium against the spring some distance away from the rolls. Then, in the next analysis-step during which the rolls are moved down for the next roll-pass, the ingot body force is adjusted to provide the correct position. This method was found acceptable as no plastic work was done whilst the ingot came into equilibrium in its new position with the spring force.

This technique worked well and was used to perform up to six roll passes in one run. However, fine tuning the technique did take significant effort. Firstly, a complete knowledge and understanding of the data being provided by the software's interface is required. Then, as mentioned earlier, the establishment of initial contact must be carefully controlled, because if the predictions for the increment in which contact take place are too large, problems arise with the plasticity algorithm.

When the three-dimensional modelling was first started, the method was easily adapted for this.

5.1.2 Dynamic Analyses

The two main types of dynamic finite element analysis were discussed in § 4.1. Both the implicit and explicit methods were used during the development stages. The explicit

method was found to be the most efficient tool, especially when three-dimensional analyses are performed.[2]

The method of analysis is simpler when performing dynamic modelling for two reasons. The one is that there is no problem with unrestrained rigid body modes of deformation. The other is that the inertial force terms in the equations make the establishment of contact easier.

Originally analyses were performed with the ingot being given a starting velocity of one metre per second, which is the same as that in the real case. The work-roll also has a prescribed angular velocity which results in the correct rolling speed. Then in one step the ingot establishes contact with the work-rolls, is rolled, and leaves the roll gap. The step is stopped when the ingot has moved a sufficient distance away from the work-rolls to have the work-rolls repositioned for the next pass. This is followed by a step during which the ingot velocity is reversed and the work-rolls are prescribed into their next position.

This process is then repeated as often as is required. One problem with this method was that the reversal of the ingot velocity required either an applied force or acceleration over a finite time. This time is a significant proportion of the overall analysis time, because plasticity problems arose if it was set too short. To avoid the extra 'turn-around' time a new method was tried.

This method, which was used for the majority of the three dimensional analyses, leaves the ingot relatively stationery while the work-rolls move in the model. Now as the work rolls are never deformed it is possible to use more than one rigid surface to model a set of work-rolls in which each surface is already positioned for a pass. Then as one roller leaves the ingot the next roller starts off and each roll pass requires only one analysis step. The initial configuration of the work-rolls and the ingot for a twelve pass analysis are shown in Figure 5.2.

A comparison of the results of analyses performed with both methods showed the deformation and plastic strains to be identical. This is to be expected as no matter which body is moving globally, the relative velocity between the ingot and the work-rolls is the same in each case.

For the dynamic analyses the process was accelerated by artificially increasing the critical time step, which was given in Equation 4.1. This is done by exaggerating the density, ρ, by a factor. The critical time step is then increased accordingly. The alternate method of accelerating the analyses by increasing the velocities was not considered as this would affect the strain rates; and the material properties are known to be strain rate dependent.

The amount by which densities can be increased is most easily determined by performing analyses with different densities and identifying the density at which inertial forces start to have an effect on the results. Properties which are dependent on density must also be adjusted. In this investigation the only property that was density dependent was the

[2]ABAQUS/Explicit v 5.1. became available for this work in May 1992.

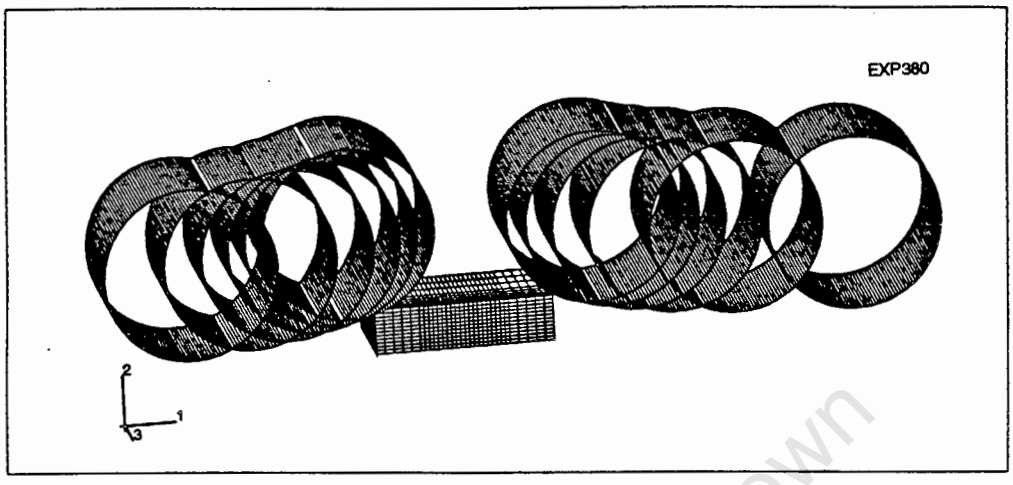

Figure 5.2: Configuration of work-rolls and ingot for an analysis of twelve roll passes

specific heat capacity of the alloy and this is simply divided by the density factor.

5.2 Comparison of results predicted by the quasi-static implicit and dynamic explicit methods

The quasi-static method was used in the initial modelling work. This was done as, with the ABAQUS code, it is possible to perform coupled stress and heat transfer analyses when the implicit method is used. In later work, however, the explicit method was used as significantly quicker analyses were expected.

Parameter	Quasi-static	Explicit
Length	1.0 m	1.0 m
– no. elements	60	60
Height	0.235 m	0.235 m
– no. elements	10	10
Friction coefficient	0.4	0.4
Rolling speed	1.0 $m.s^{-1}$	1.0 $m.s^{-1}$
Density factor	–	100
Run time	16340 s	5100 s

Table 5.1: Parameters used in comparison of the implicit and explicit methods

To compare the two methods a two-dimensional analysis was performed with each. The

various parameters of the analysis are given above in Table 5.1. It was found that the explicit analysis could produce the same results in approximately one third of the time. A comparison of the plastic equivalent strains plotted on the deformed shape is given in Figure 5.3 for each method. The one significant difference between the results of the two is the deformation that occurs at the leading end. The shape predicted by the explicit analysis does not have as pronounced a 'crocodile jaw' shape. It is believed that this is due to the inertial effects involved when the ingot initially impacts with the work-rolls; and these effects would not be reproduced with the quasi-static implicit analysis.

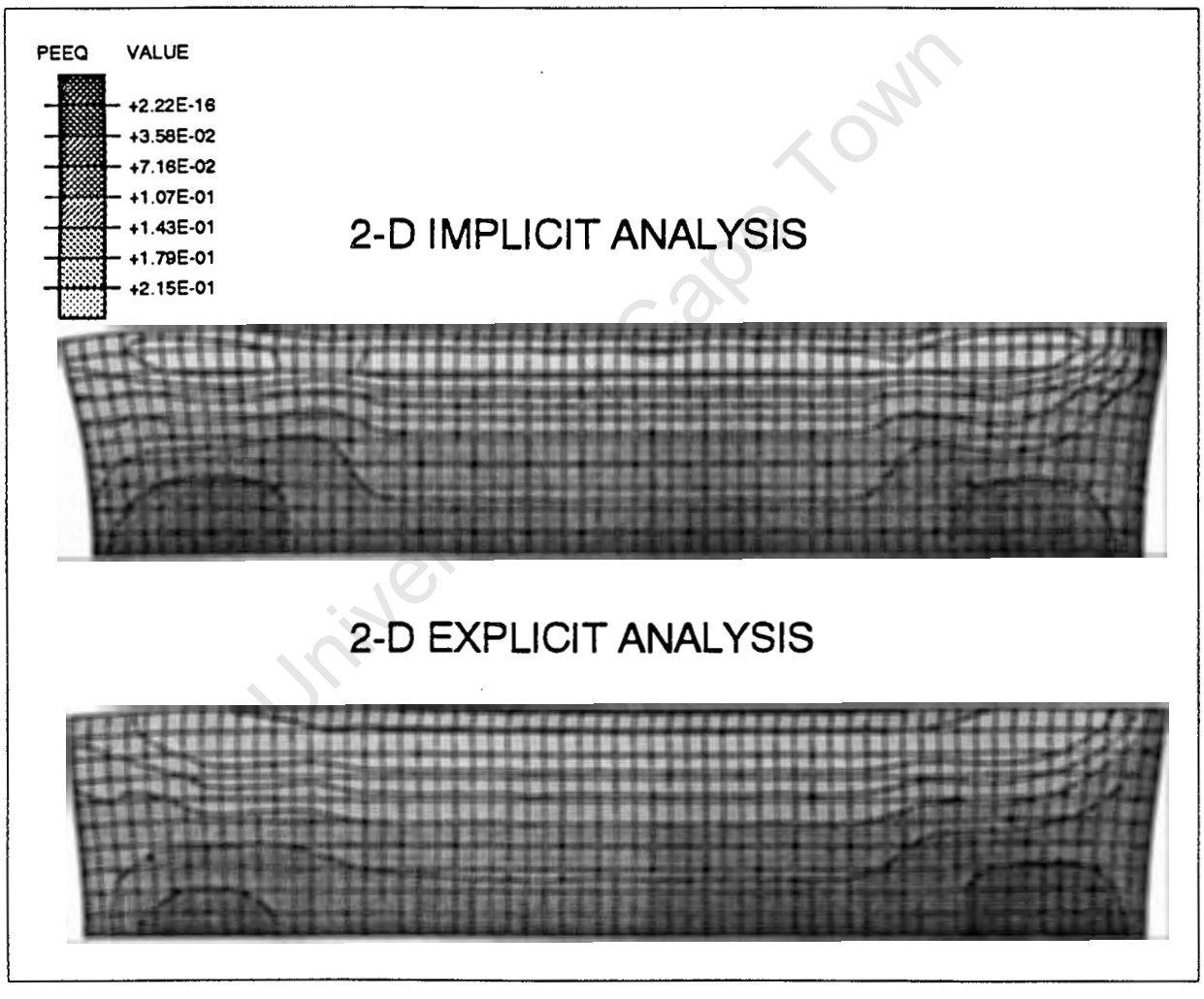

Figure 5.3: Plastic equivalent strains predicted by the quasi-static and explicit dynamic methods

With three-dimensional modelling the system of equations is a great deal larger due to

both the greater number of elements required, and the extra degree of freedom involved. Therefore for these models the time savings with the explicit method will be even greater.

5.3 Description of the stress state in the roll-gap

The major loading is the work-roll load being transmitted vertically through the ingot. At the work-rolls the highest vertical stresses go up to and above 160 MPa near the entry side of the roll-gap. Then, through the height of the ingot, the area of material carrying the load increases and the stresses correspondingly decrease. The vertical stresses are shown on a contour plot in Figure 5.4, and the horizontal stresses in Figure 5.5. At the axis of symmetry an arching of the vertical load can be seen.

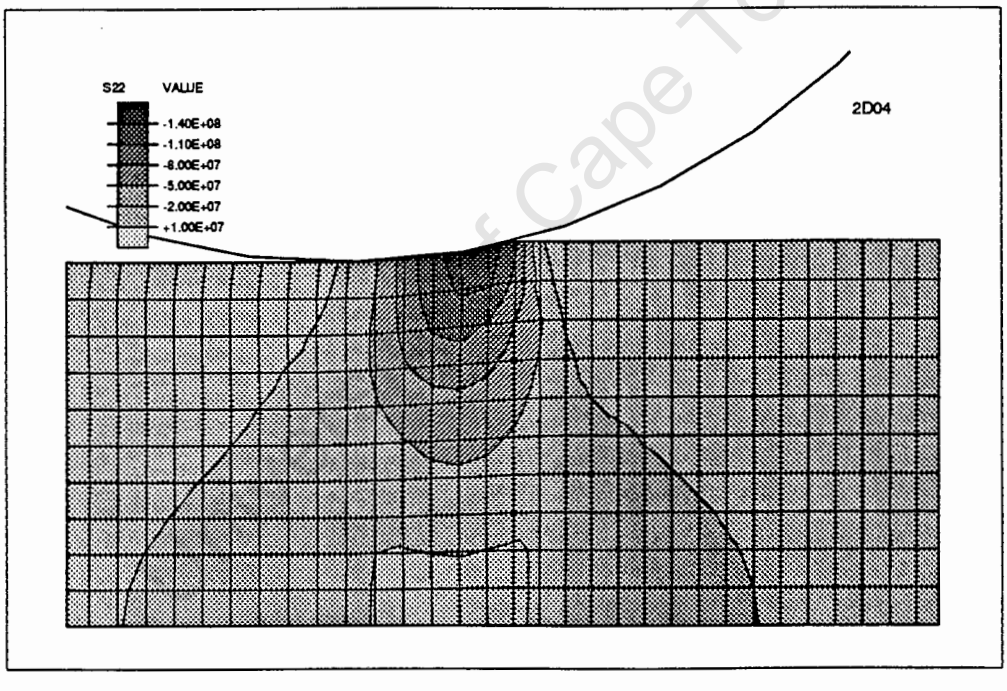

Figure 5.4: Contour plot of vertical stresses between the work-rolls

An interesting feature which is associated with this arching effect is the presence of tensile stresses in the rolling direction at the axis of symmetry. The possibility of this effect occurring in slab rolling was mentioned in the review of a slip-line field solution for slab rolling in § 2.2.

Figure 5.6 is a contour plot of the shear stresses. The material about to enter the work-rolls has a positive shear stress, then as it moves through the roll-gap the shear decreases

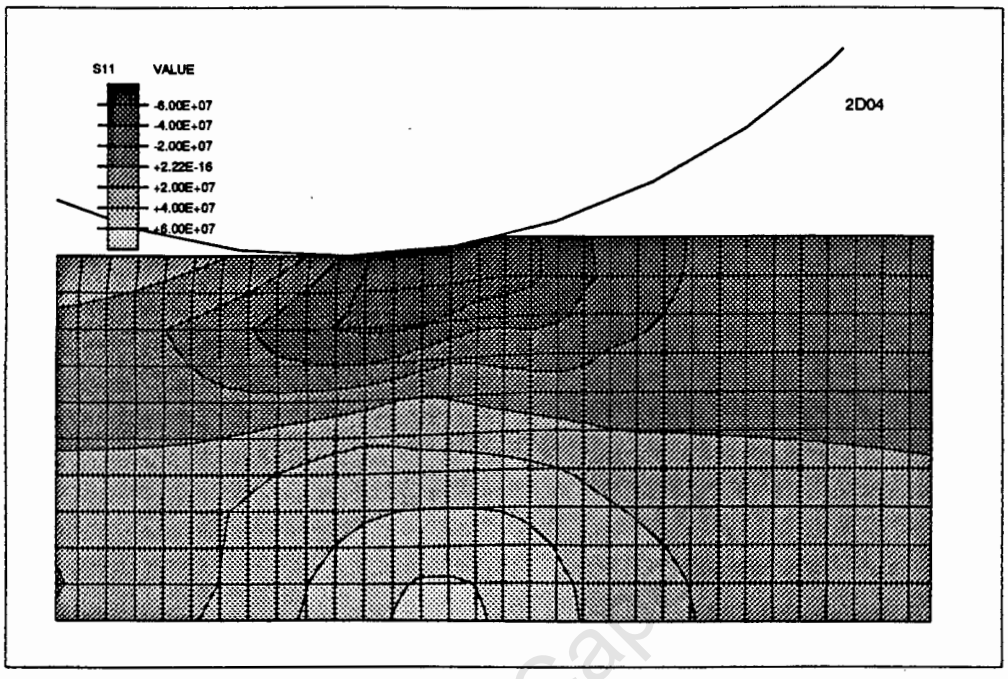

Figure 5.5: Contour plot of the stresses in the horizontal direction between the work-rolls

and eventually becomes negative. It should be noted here that in many rolling processes with higher coefficients of friction there would be another region of material at the surface with a positive shear stress to the exit side of the work-rolls. This region occurs when the friction forces in the roll-gap switch over from pulling the material into the roll-gap to restraining its exit past the neutral point. The presence of this neutral point will be discussed further in § 5.5.4.

Variations in the lateral direction

The pattern of stresses is generally the same through the lateral direction of the ingot. The middle section of the ingot, away from the edges, has plane strain conditions and is therefore the same as the two-dimensional analyses. The area closer to the edges is not restrained laterally to the same degree and therefore the magnitudes of the compressive stresses are lower. Although the change occurs over the entire width of the ingot, it is only of a significant amount in the region two thirds of the distance from the vertical axis of symmetry to the edge. The maximum vertical stress under the work-rolls is 160 MPa in the centre, this drops to 140 MPa within 100 mm of the edge and then to 100 MPa at the edge.

The stresses in the lateral direction have a similar pattern to the stresses in the rolling

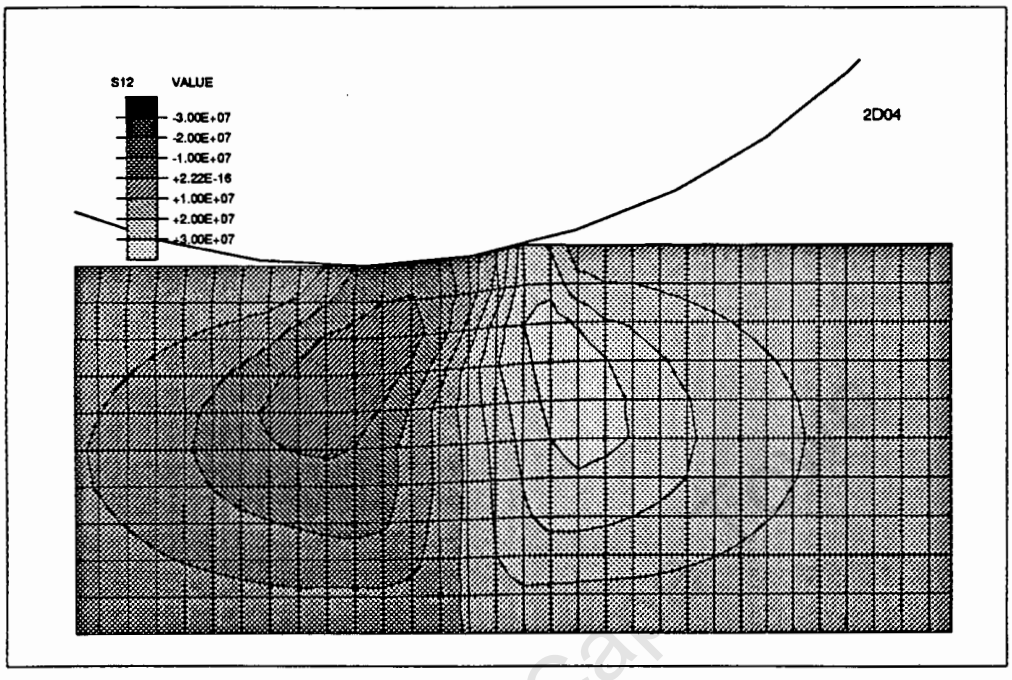

Figure 5.6: Contour plot of shear stresses in the roll-gap

direction. They also have the same type of variation from the vertical axis of symmetry to the edges. The axial stresses are compressive in the surface region of the roll-gap and tensile near the horizontal axis of symmetry.

The shear stresses which occur in planes extending in the lateral direction must be zero at the vertical axis of symmetry. Towards the edge the maximum shear stresses in these planes have values in the region of 10 MPa.

5.4 Plastic strains at the end of a pass

When the ingot leaves the work-rolls, the material away from the ends has uniform plastic strains in the (11) and (22) directions, i.e. the material has been homogeneously compressed in the vertical direction and spread in the horizontal direction. This is to be expected if the region of yielding material between the work-rolls is considered. On either side of the yielding material is a block of elastic material which is virtually rigid in comparison with the yielding material. The yielding material can therefore expand horizontally as it is loaded, but the amount it expands must be equal throughout the height of the ingot.

The plastic shear strains, however, are not homogeneous through the ingot. This is be-

cause, although the width of the yielding material must grow by equal amounts throughout the height, variations may occur within the zone of yielding material. The result of this is that sections which were originally vertical planes end up being slightly bent. This change in shape of a section can clearly be seen in Figure 5.7 which also shows the plastic shear strains that have occurred in the ingot during the first roll pass.

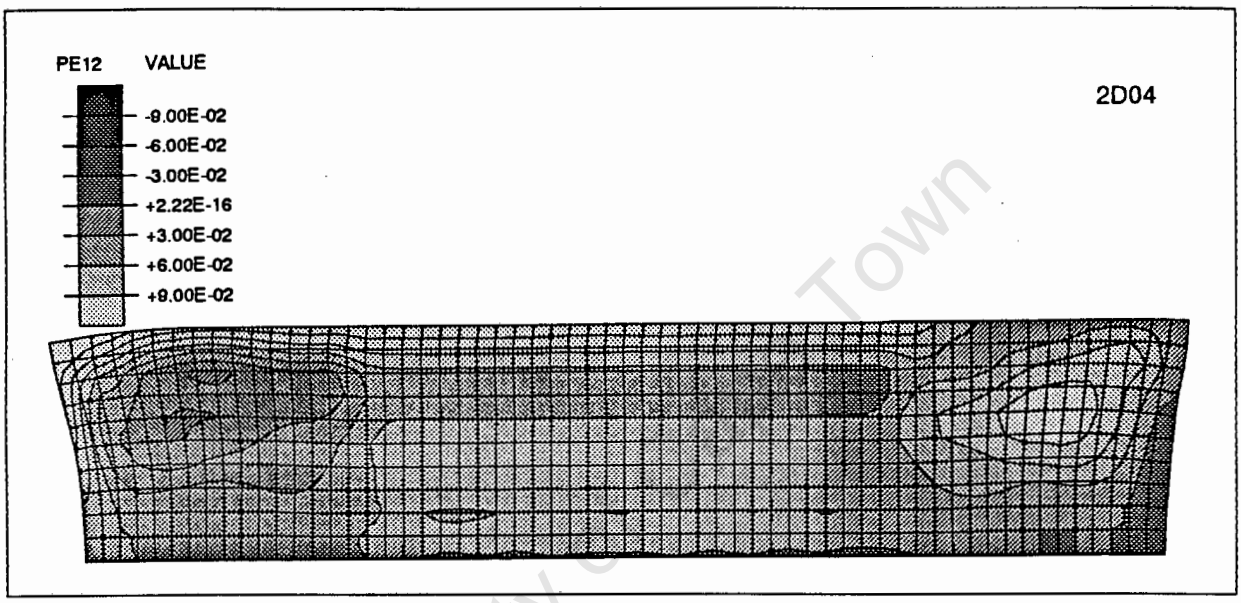

Figure 5.7: Contour plot of plastic shear strains after the first roll pass

5.5 Agreement of results with analytical predictions

The results will be looked at to see how they compare with the five points summarised at the end of § 2.1.

5.5.1 Region of highest plastic straining

A study of the contour plot of the equivalent plastic strain in Figure 5.8 shows the highest equivalent plastic strain to have occurred in a layer which is at a depth of one third of the roll gap length below the surface. Therefore the most plastic straining is as predicted, below the surface; it is not however possible to tell how the depth of the layer is affected by the size of the contact gap from these results.

Although the most plastic strain has occurred in this region the final plastic strains are not the largest here. The largest final plastic strains occur on the surface. An explanation

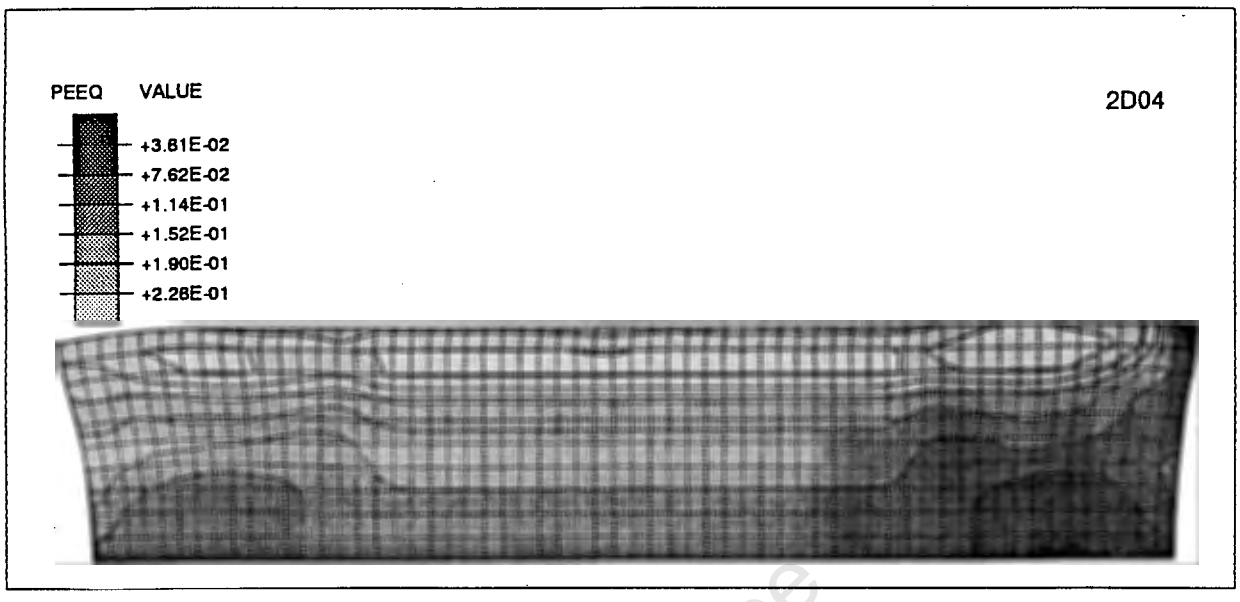

Figure 5.8: Contour plot of equivalent plastic strains after one roll-pass

for this is given below when the next point is considered.

5.5.2 Stress and strain histories

From the contact theory the stress history for a point of material in the ingot was expected to be first a positive shear, as the point enters into, then a vertical compression whilst in between, and finally a negative shear whilst exiting from the work-rolls. This definitely does occur and can easily be seen in the contour plot of the shear stresses (Figure 5.6). The material passes through the 'bulb' of positive shear stress and then the shear drops down until the 'bulb' of negative shear stress is reached.

The plastic strains also follow this pattern which explains how the most plastic straining occurs at a point where the strains are not the highest — the material is first sheared positively and then sheared back negatively. As there is no significant work-hardening at this temperature the major importance of this feature in this modelling is the increase in temperature which will be highest in this region.

The plastic strains in the vertical and rolling directions occurs monotonically with first plastic straining occurring midway between the surface and the axis of symmetry. Although different areas in a vertical plane are strained at different positions in the roll gap, the plastic strains after rolling are relatively constant throughout the ingot. This is to be expected when one considers that the region of yielding material is confined on each side

by a relatively rigid block of elastic material and therefore the total spread in the rolling direction must be constant through the depth of the ingot.[3]

5.5.3 Deformation of vertical planes

As predicted, the surface of the ingot is deformed forward relative to the material in the centre of the ingot. This can be seen by looking at a column of elements in any of the previous figures containing contour plots. However, when one looks at the elements in the layer next to the surface it can be seen that it is the material just below these elements that has been displaced forward the most. The top layer has been permanently positively sheared.

To investigate the deformation in this region it is worthwhile to look at the results of analyses which were performed with a refined mesh near the surface. Looking at the actual deformation of the mesh in Figure 5.9 it can be seen that the surface is deformed forward (negatively sheared), but a zone below this is positively sheared. This zone reaches a depth below the surface which is roughly one third of the contact gap length.

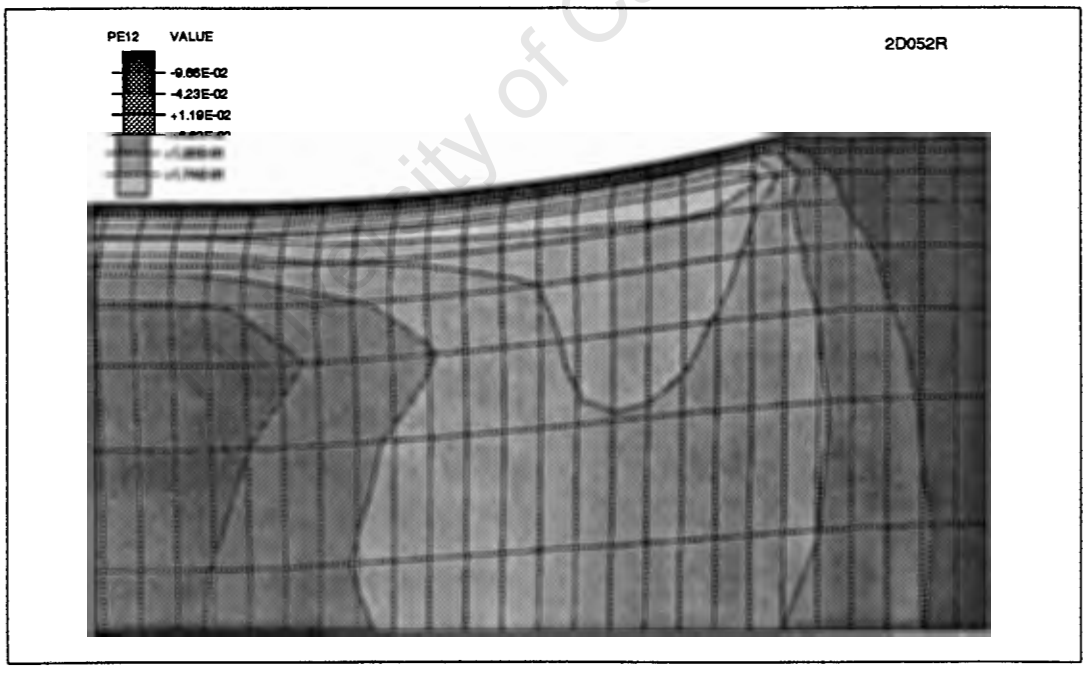

Figure 5.9: Contour plot of plastic shear strains in the roll-gap

[3]At the ends where there is no constraint on one side the 'crocodile jaw' phenomenon occurs. This phenomenon will be discussed briefly in § 5.10.

This negative shearing of the surface is to be expected due to the friction forces and will be looked at in more detail when the stress conditions in the contact gap are discussed.

The zone of permanently positively sheared material below this however, has been considered a result of the deformation pattern.

5.5.4 Stress conditions in the area of contact

An investigation of the contact conditions in the finite element analyses shows that, for the conditions of the first roll-pass, sticking conditions occur throughout the roll-gap. The possibility of this occurring in hot-rolling was mentioned in the reference by Orowan [11] discussed in § 2.2.

The normal stresses and tangential stresses (friction) in the contact area are given in Figure 5.10. The normal stresses have a hill shape with the maximum compressive stress of 160 MPa near the entry side of the contact area. A reversal of the direction of the friction occurs near the exit side, but the magnitude of these resisting forces is small.

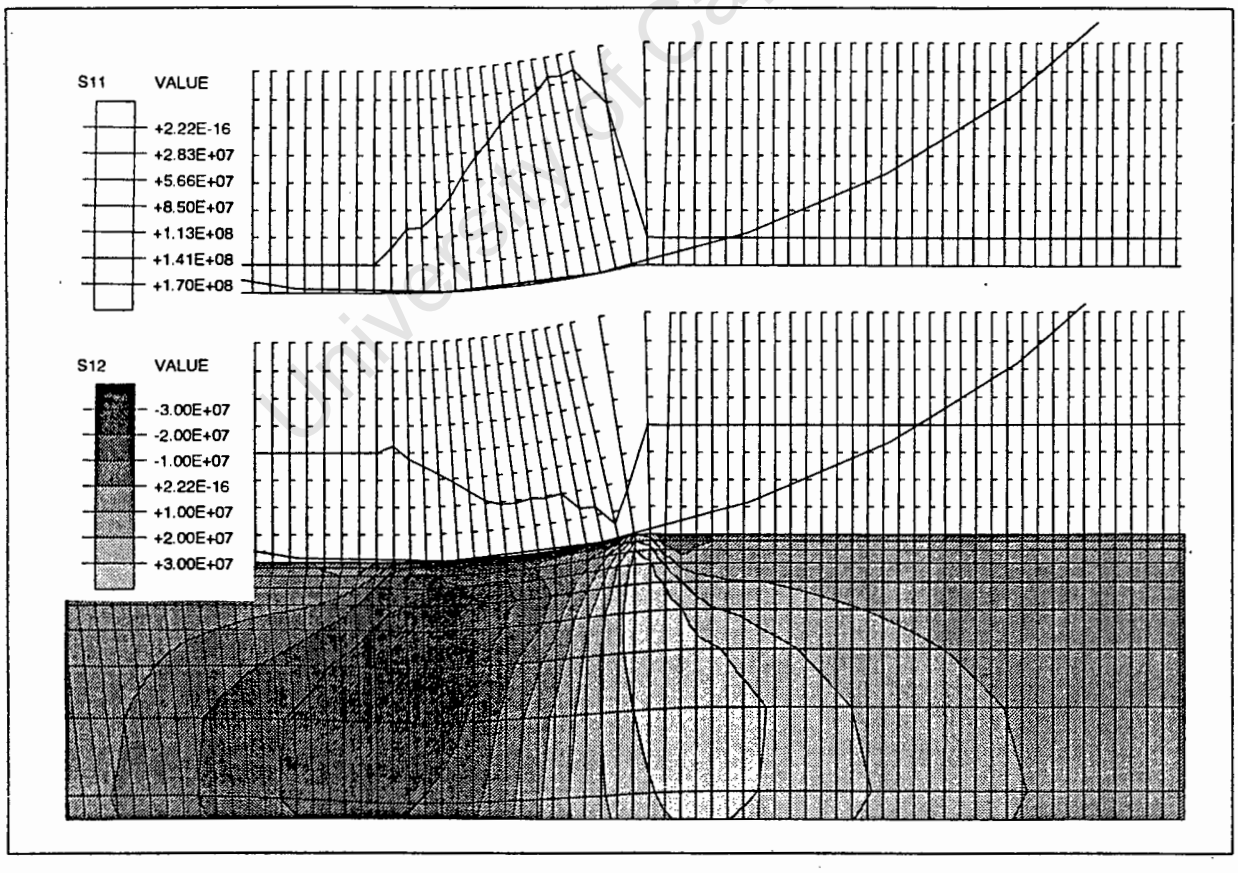

Figure 5.10: Normal stress and friction conditions in the contact area

5.6 Edge Profile

When work started with three-dimensional analyses it was possible to have a first look at the predicted edge profile. These first models were analysed with the quasi-static method and it was necessary to use a coarse mesh because of the amount of computer time required. (On the fastest computer available here, an IBM RISC SYSTEM/6000 560, an 800 element mesh consisting of 20-node reduced integration elements required more than seven hours of cpu time to complete a single pass.) Nevertheless, the edge profile produced was concave as expected.

With ABAQUS/Explicit it was possible to concentrate on the edge profile. As these analyses still take a considerable amount of time it is necessary to ensure that extra time is not being used to obtain excessive accuracy. For the explicit analyses there are two important factors which affect the length of an analysis. These are the refinement of the mesh and the factor by which the density is increased.

Density factors and mesh refinement

Both of these factors affect the length of an explicit analysis significantly. The time step depends on the density in that the critical time step is proportional to the square root of the density. Meanwhile, the mesh refinement affects the length of the analyses in two ways. The one is that the more elements there are, the more equations there are that need to be solved in each increment. This effect is not as great in explicit analyses as in implicit analyses due to the system of equations being uncoupled. The other is that, as the mesh is refined, the smallest element dimension is decreased and therefore so is the critical time step.

The main criteria used to check at which level both of these parameters could be set was the shape of the edge profile. It was found that each parameter could not be determined individually, but that when checking convergence with one, the other must be set at a reasonable level.

The first parameter that was investigated was the density. To do this a mesh of thirty elements in the rolling direction and six in both the vertical and lateral directions was used. This was chosen after considering the results of the two-dimensional analyses and the minimum number of points required to produce the edge profile. Using the work of Wright and Sheppard [6], which indicates that the profile is suitably described with a fourth order polynomial, the minimum number of elements on the edge is four. Meanwhile, the two-dimensional results showed convergence with a mesh of sixty by ten elements.

The following density factors were tried; 2500, 625, 100 and 25. It was found that between the 100 and 25 factors, the results showed a maximum difference in the profiles equivalent to ten percent of the maximum spread. The profile for each of these analyses are plotted in Figure 5.11. The last analysis required over nine hours of cpu time on the IBM 560.

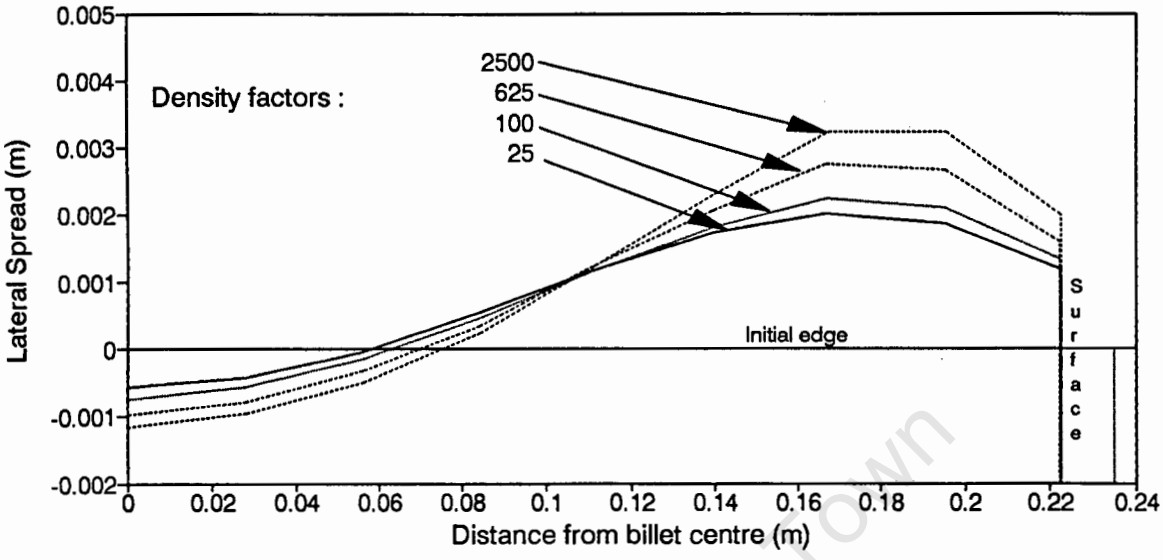

Figure 5.11: Edge profiles for analyses performed with different density factors

Next the mesh refinement was examined. Using the density factor of 25, mesh refinements of 8 by 8 by 30 and 12 by 12 by 40 were analysed. With the last analysis of these the computer cpu time had increased to over fifty-nine hours and yet there was still a difference of sixteen percent between the average spread of the last two analyses.

When this refined mesh was analysed with higher density factors, however, the change of profile was found to be negligible for a factor of 100 and less than five percent for a factor of 400.

Run code	Total no. elements	No. edge elements	Description of mesh	Density factor	cpu time hr:min	Max. spread (mm)	Ave. spread (mm)
EXP320	1872	8	30 by 8 by 6	2500	0:55	3.242	1.072
EXP321	1872	8	"	625	1:48	2.758	0.952
EXP322	1872	8	"	100	4:36	2.243	0.852
EXP323	1872	8	"	25	9:14	2.021	0.828
EXP360	2352	8	30 by 8 by 8	25	13:01	2.473	0.893
EXP361	6048	12	40 by 12 by 12	25	59:44	3.621	1.055
EXP362	6048	12	"	100	29:56	3.584	1.041
EXP363	6048	12	"	400	14:58	3.822	1.112
EXP370	3312	12	30 by 12 by 9	400	8:39	4.090	1.209
EXP371	2772	12	Refined to edge	400	6:07	3.999	1.113
EXP372	2772	12	"	400	8:30	3.918	1.151
EXP373	5742	18	"	400	34:50	4.214	1.167

Table 5.2: Details of three dimensional analyses

Once a density factor of 400 had been shown to be reasonable, the refinement could be considered further. As discussed in § 5.3, and § 5.5.4 the variation in the lateral direction of stresses and strains occurs mainly near the edges. The material in the centre is subjected

to the plane strain conditions assumed in most of the theory on rolling. Greater changes in the stresses and strains also occur in the material near the top and bottom surfaces. Because of these two observations the mesh was next refined locally in the region of the edges, with the spacing of the nodes being biased towards both the edge and the top surface.

The profile is then found to converge, the average spread for a mesh of 2772 elements is within two percent of a mesh with 5742 elements. The average spread is 1.17 mm and the maximum spread is 4.2 mm which occurs 28 mm from the surface. The centre of the billet spreads negatively, i.e. moves inward, by 1.6 mm. The change in profile with increased mesh refinement can be seen in Figure 5.12; the run codes used are those in Table 5.2 in which details of the analyses are given.

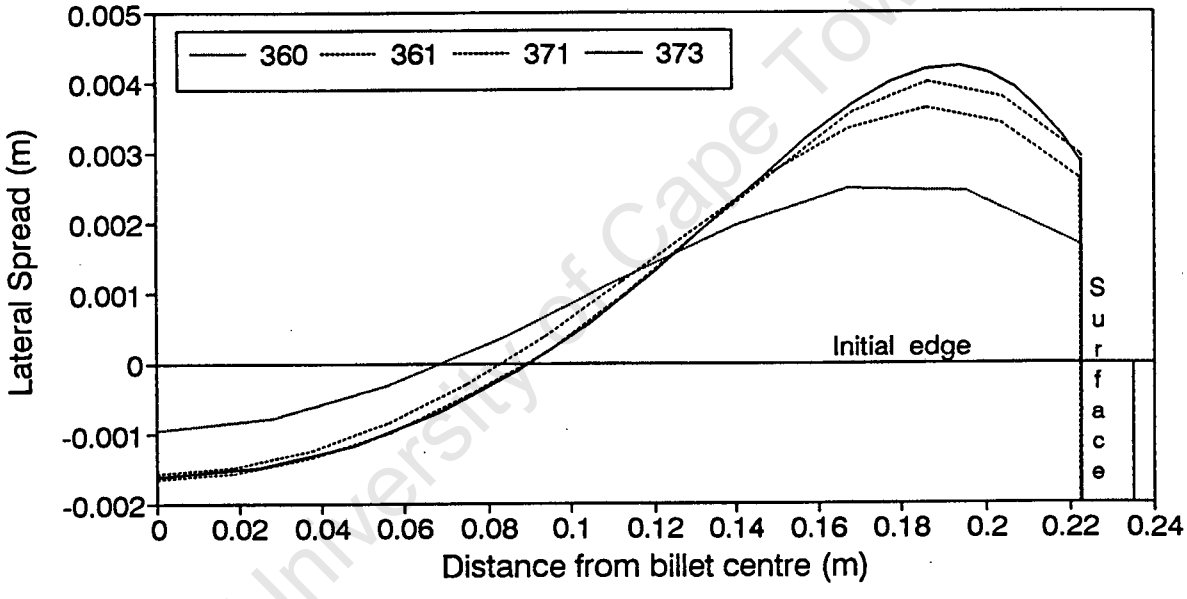

Figure 5.12: Edge profiles for analyses performed with different mesh refinements

These results show that the numerical modelling is working correctly for the model. The accuracy of the results therefore, depends only on the accuracy of the assumptions that have been made and on the data which has been used. Unfortunately there are no physical measurements with which these results can be compared. For this reason the model was adapted to analyse one of the experiments that Wright and Sheppard had reported on.

5.6.1 Comparison of edge profiles predicted by finite element model and experimental measurements

The only available data on the edge profile is that contained in the reference of Wright and Sheppard [6]. The experiment which was chosen for comparison is the one for which details have been given in Tables 3.1 and 3.2. Unfortunately certain parameters could not be determined, the two most important of these being the rolling speed and the friction conditions. The ways in which various aspects of the experiment were modelled are given below.

Geometry

Use is made of the two planes of symmetry, with the length being restricted to 0.052 m. This is larger than the length of two times the thickness used for the original modelling because, for this case, the contact area is relatively much larger.

Material description

The alloy being used, 1S or AA1050A, was researched previously by Sheppard and Wright and a description of the mechanical properties of AA1050A are given in a reference [60]. Details are given on work-hardening, temperature and strain rate effects. As the experiments were performed at 500°C, the work-hardening is not significant. The strain-rate effects are however important and were included by finding suitable constants for the equations used by ABAQUS to include strain rate effects. The analyses are explicit analyses, and do not include heat transfer. The yield stress value was defined as 10 MPa, and the strain rate effect described by Equation 4.4, where:

D : 9.97
p : 2.73

Rolling speed

Details of the experimental work are given in the reference [5]. The maximum speed of the work rolls is given as 28 rev.min.$^{-1}$ which is equal to a rolling speed of 0.37 m.s^{-1}. Then two strain-rate values are given as 1 s^{-1} and 2 s^{-1}, but the meaning of these rates is not explained. If Sim's formula for strain rates in rolling is used, the two rates are equivalent to rolling speeds of 0.46 m.s^{-1} and 0.9 m.s^{-1}; both well above the maximum rolling speed given. For the profile results given, there is also no mention of whether the fast or slow rate was used. For the modelling, the maximum roller speed was used.

Friction conditions

In the experimental work two different types of contact conditions were used. In the first the rolls were de-greased with alcohol and acetone and in the second they were lubricated with Mobil Prosol 44A rolling oil. Again details on which of these were used, are not given. For this reason analyses were performed with a range of coefficients of friction.

Predicted profiles

Initially it was hoped that the profiles could be compared by fitting a fourth order polynomial to the finite element results and then comparing these with the polynomial fitted by Wright and Sheppard. However, if the data in Table 3.2 is plotted, the profile produced does not fit the graphical data given, possibly due to the constants having been round off. For this reason their graphically plotted results given below in Figure 5.13 were used. It can be seen that the profile is in between the concave and convex type. This is to be expected as the value for the profile criteria of Wright and Sheppard is, $\sqrt{R\delta}/H_0 = 0.71$, which is close to the transition value of 0.82.

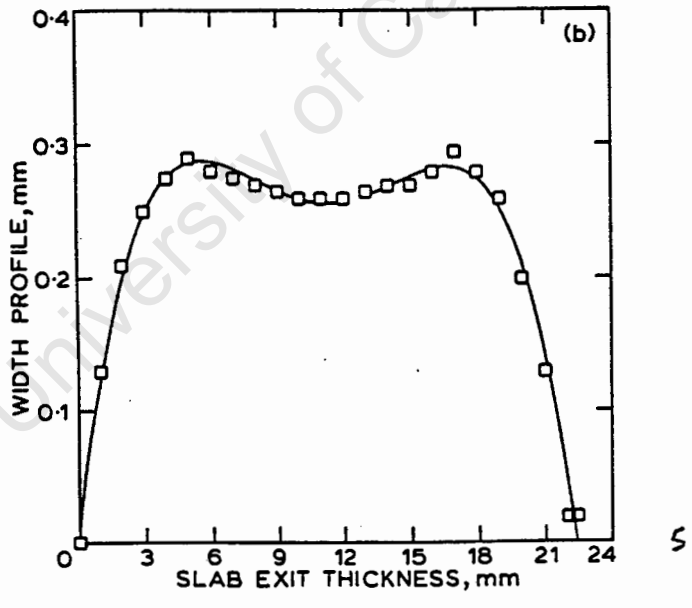

Figure 5.13: Edge profile measured by Wright and Sheppard [6]

The results of the finite element analyses predict a range of profiles. The results of analyses in which different coefficients of friction have been used are given in Figure 5.14. For the low friction cases significant spread of the rolling surface has occurred. For the friction coefficient, $\mu = 0.2$, the spread of the surface is 0.465 mm which is not much less than the maximum spread of 0.480 mm. For a friction coefficient more representative of

unlubricated conditions, $\mu = 1.0$, the surface spread is less than half the maximum spread, i.e. the spread of the surface decreases to a much greater extent than the maximum spread.

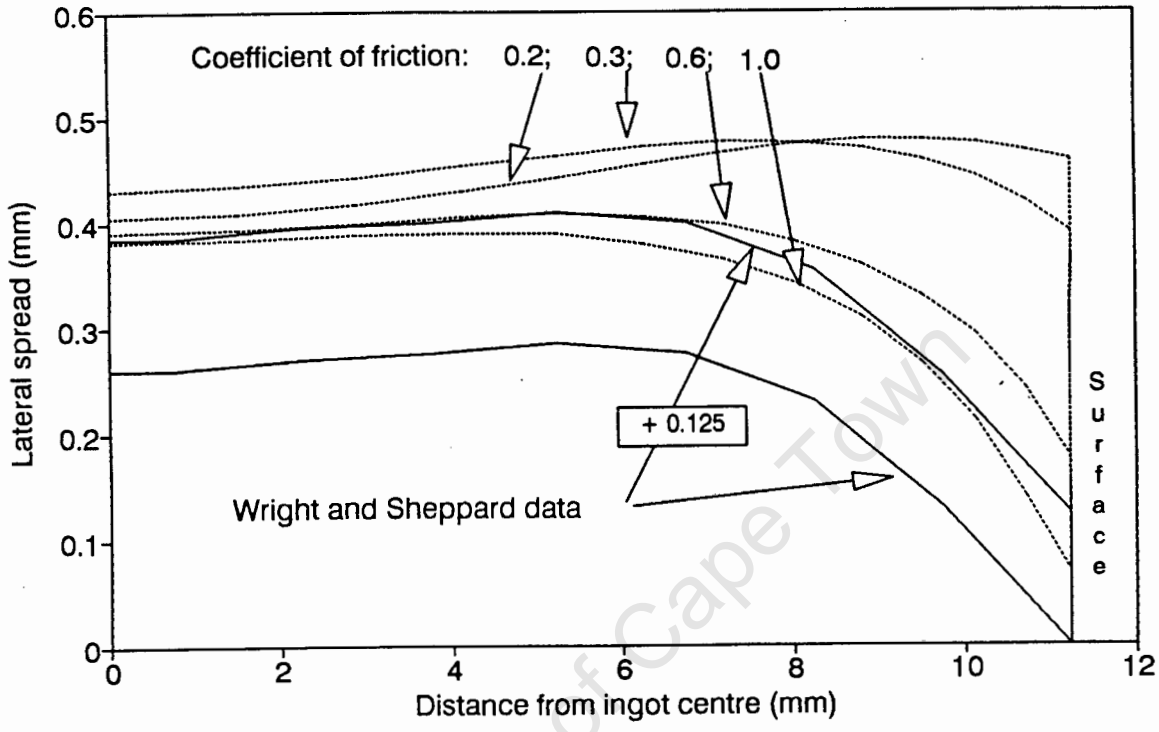

Figure 5.14: Edge profile for analyses performed with different coefficients of friction

The data given by Wright and Sheppard uses the corner of the edge as the origin for their measurements of spread. The spread is then given relative to this corner point, but no details of the actual spread are given. In order to compare the numerical results with the experimental work the corner points have simply been shifted. When this is done the shape predicted for the analyses with coefficients of $\mu = 0.6$ and $\mu = 1.0$ are very similar to the experimental results. The differences as a percentage of the overall spread between the profiles shown in Figure 5.14 are less than ten percent.

5.7 Concave edge profile — the reasons for its development

Once the accuracy of the numerical modelling had been verified, the results could be used to investigate the mechanics which lead to a concave profile.

5.7.1 Zone of yielding material

The zone of yielding material is outlined in Figure 5.15. The blocks of elastic material on either side can be considered rigid relative to the yielding material, and therefore constrain the edges of the yielding zone in all directions except the rolling direction. Due to this the following two observations can be made:

1. As the material is compressed in the roll-gap, it will spread in the rolling direction, and the total elongation of this material after passing through the yielding zone must be equal throughout the depth of the ingot.[4]

2. The resultant of the horizontal forces acting on either of the two rigid blocks is zero.

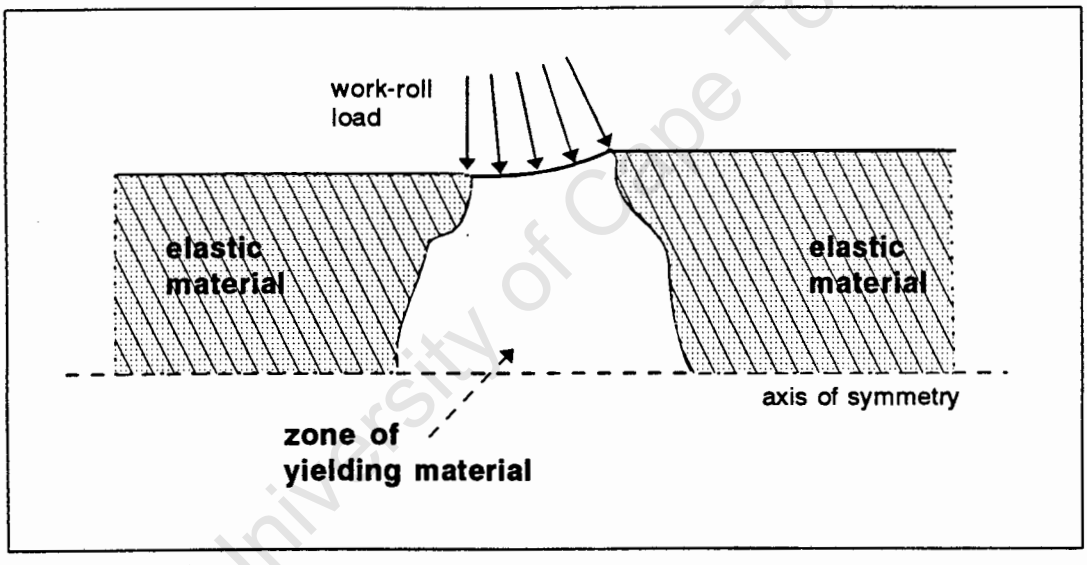

Figure 5.15: Zone of yielding material between relatively rigid elastic blocks

The major loading, the normal stresses in the contact area, are also shown in the diagram, Due to this loading there are high vertical stresses at the top of the yielding zone; and as these compress the material vertically, the material is inclined to spread in the horizontal directions due to the Poisson effect.

Moving from the surface toward the axis of symmetry the vertical stresses decrease as they are being carried by a larger area. The result of this is that the material is not being forced to elongate to the same degree in the yielding zone that it was at the surface.

[4]The plastic strains are not exactly equal through the depth because elastic strains do also exist. There are slightly lower plastic strains in the rolling direction (these result in the residual tensile stress at the surfaces), but the difference in magnitude is less than five percent.

Considering point 1 above, however, the amount that the material elongates is equal throughout the zone; and therefore some other mechanism must be causing the elongation in the region of the axis of symmetry. This mechanism is the 'stretching' of the material in the rolling direction, which is due to the material being pulled apart by the forces required to give horizontal equilibrium in the rigid block. Considering the diagram in Figure 5.16, the material pushes against the rigid blocks in the surface region and is pulled outward by the blocks at the axis of symmetry. The material at the axis of symmetry is therefore placed in tension in the rolling direction.

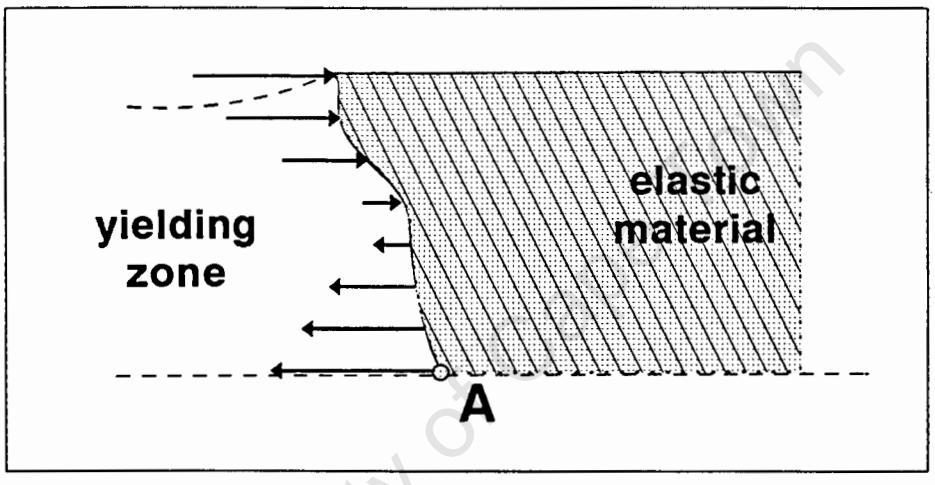

Figure 5.16: Horizontal equilibrium of a rigid elastic blocks

The arching effect that has been mentioned previously, fits in with this description of the mechanics. The tensile force in the central tie which keeps the double arch together in the diagram in Figure 5.17 is the equivalent of the tensile stress at the axis of symmetry. The reason that the front side of the arch carries more vertical load is that at the contact area part of the normal stress at the entry side has a forward horizontal component. Due to this a larger vertical force is required at the axis of symmetry to balance the moment of these horizontal forces (consider moments about point A in Figure 5.16).

5.7.2 Lateral spread

The previous discussion ignored the lateral direction. Deformation in this direction is restricted to a large extent by the rigid block on the entry side of the roll-gap and is therefore considerably smaller than in the vertical and rolling directions. The lateral deformation that does occur can, however, be understood in the context of the mechanics explained in the previous section.

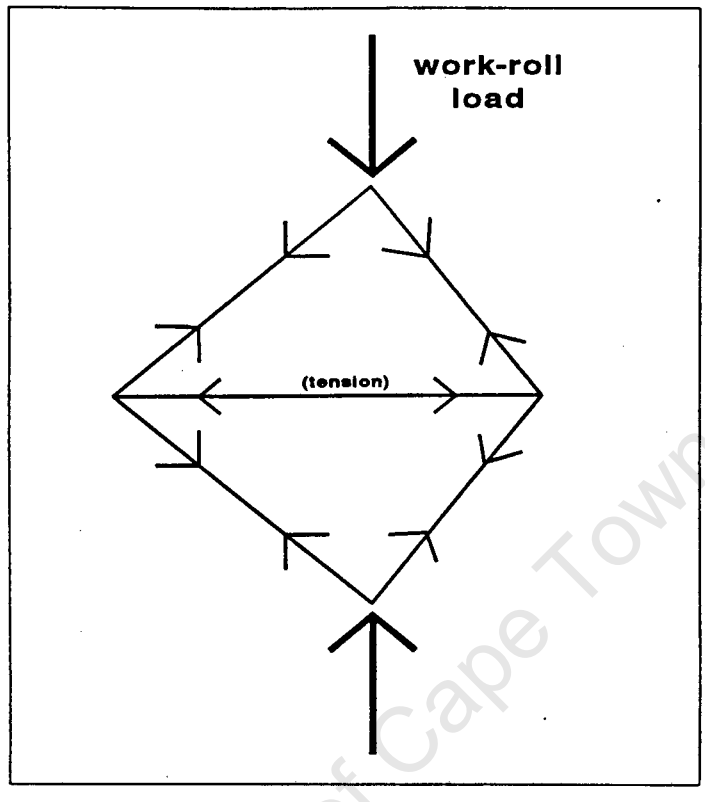

Figure 5.17: Simplification of arching in the roll-gap

At the surface the material in the roll-gap is being compressed vertically and, because of the Poisson effect, should spread horizontally. This does occur; near the surface the material does spread outward in the lateral direction. In the region of the axis of symmetry, however, the material is being stretched in the rolling direction. Thus, considering the Poisson effect, the material should contract in the vertical and lateral directions. Again this does occur — there is actual negative spread at the axis of symmetry.

The explanation of the stress patterns in the rolling problem given in § 5.7.1 thus provides a valid rationale for the formation of the concave profile. One area of the profile, however, has not yet been covered. The maximum spread occurs slightly inward from the surface, and not at the surface. The major reason for this was shown in the results presented in § 5.6.1 to be the friction in the lateral direction.

5.7.3 Friction in the lateral direction

The spread of the material laterally is constrained by the elastic material in front of and behind the roll-gap, and by the work-rolls at the surfaces. The amount that the work-rolls restrain the material depends on the frictional conditions between them. The results

shown graphically in Figure 5.14 indicates the importance of the friction in restraining spread at the surface. The surface spread drops from 97 % of the maximum spread when a Coulomb coefficient of friction, $\mu = 0.2$ is used, to 18 % when $\mu = 1.0$.

5.7.4 Contribution of other aspects to the profile shape

The profile shape is mainly determined by the mechanics of deformation that were discussed in § 5.7.1 and the friction conditions in the contact area. Certain aspects will have an effect on the state of stress and therefore the effect of these is investigated here. The aspects covered are strain rates, temperature profiles, and work hardening.

Strain rates

An indication of the strain rates that occur through the depth of the ingot are given in Figure 5.18. The highest strain rates occur close to the surface.

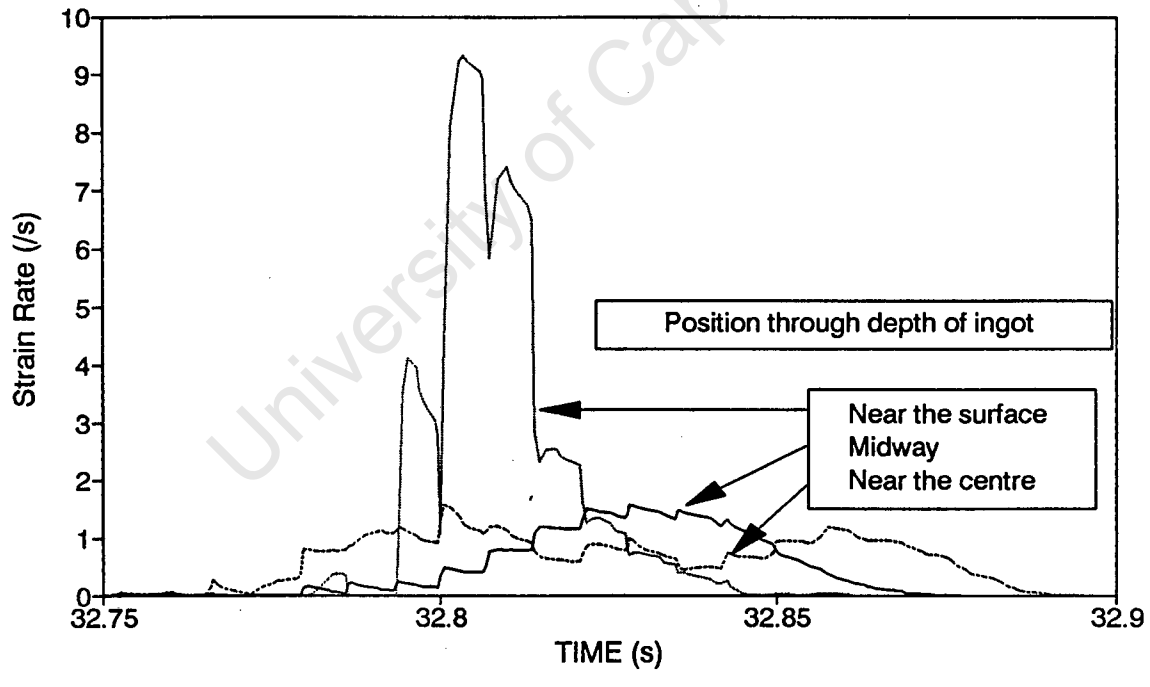

Figure 5.18: History of the strain rates at different heights in the ingot

The result of the variation in strain rates would be that the material will yield at a higher stress here and less spread would be expected. This was shown to be the case with two analyses which used the parameters for the experimental work of Sheppard and Wright [5].

For the analysis run without strain rate effects, the average spread was 0.3255 mm while that for the analysis with strain rate effects was 0.3396 mm, i.e. the average spread decreased very slightly when the strain-rate effects were omitted. The surface spread, however, changed from 0.0693 mm to 0.1528 mm, which is a more than doubling of the surface spread. The profiles for each of these analyses are shown in Figure 5.19.

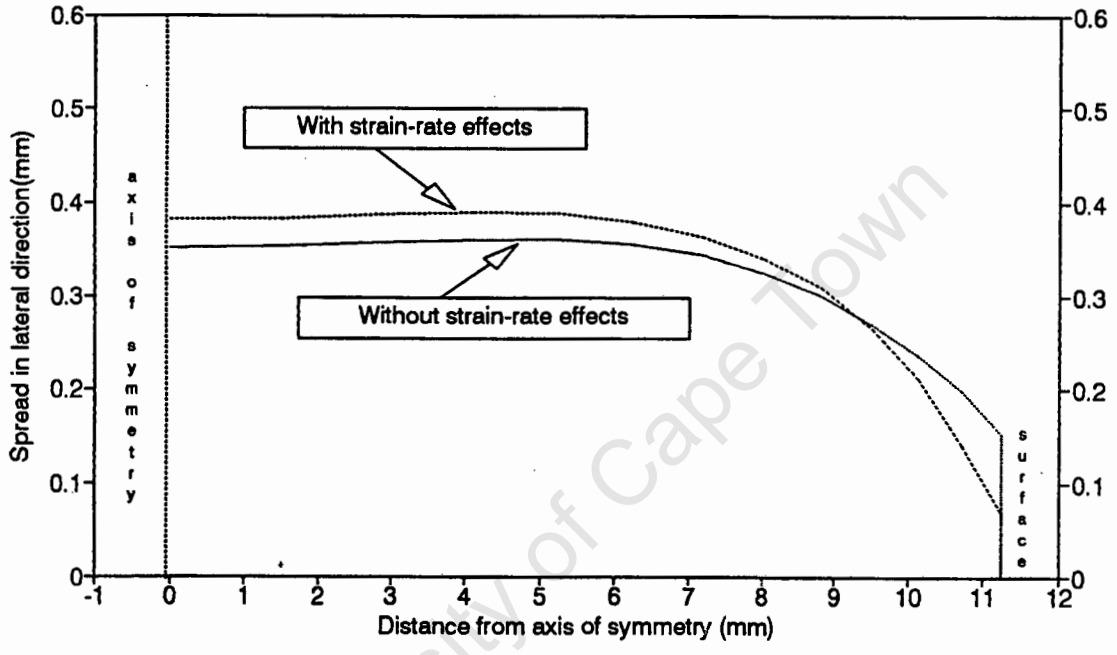

Figure 5.19: Edge profiles for analyses performed with and without strain-rate effects

Temperature profile

In § 4.3 the effects of various mechanisms on the temperature profile was shown. Material on the surface is cooled substantially as it passes through the roll-gap, and then afterwards its temperature rises once again as heat flows from the interior. Inside the ingot heat is being produced as plastic work is done and the maximum temperatures are found in zones near the surfaces. In this zone the temperatures rise by approximately four degrees Centigrade in the first roll pass. The only analyses performed which include heat losses were two-dimensional plane strain analyses. The substantial cooling and associated rise in the yield stress of the material which occurs at the surface is expected to reduce the spread of the material at the surface.

The three-dimensional analyses did, however, include the heating effects due to the dissipation of plastic work energy. The results of these show an unexpected trend — the spread is less for analyses where the heating effect is included. The results of two analyses

performed with and without the heating effect are given in Figure 5.20 for the first two roll-passes. The region in which the spread is reduced is the region in which the most heat is produced; the temperatures are shown in Figure 5.21 which contains a contour plot of the temperatures in a cross-section through the quarter ingot after one roll-pass.

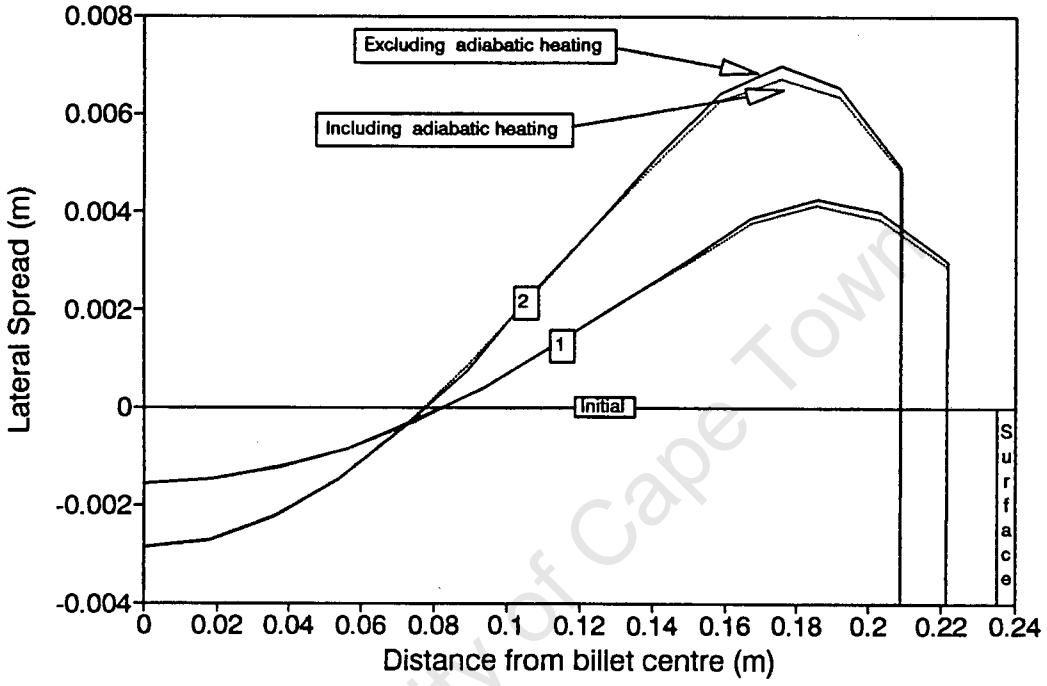

Figure 5.20: Edge profiles for the first two roll-passes of analyses with and with out the heating effect of plastic work

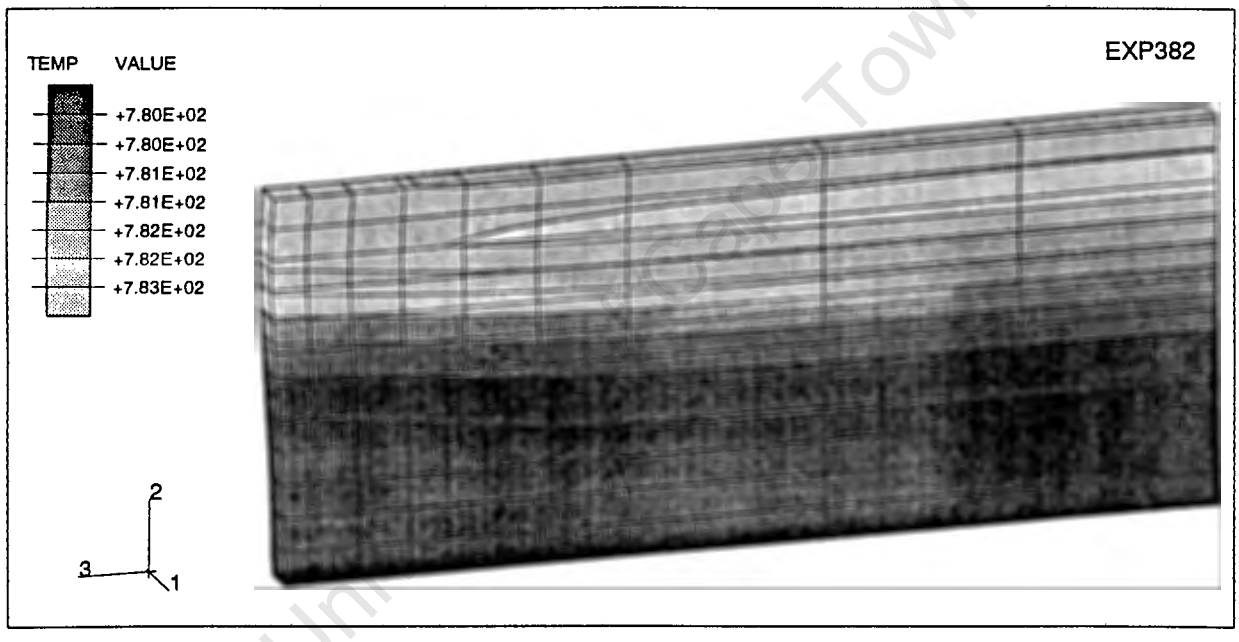

Figure 5.21: Temperature profile after one roll-pass due to heating by plastic work

5.8 Analysis of multiple pass rolling

The industrial process consists of 21 passes through the work-rolls. The first nine passes of this schedule were analysed to investigate how the profile changes. The analyses were performed using the explicit dynamic analysis method with the same mesh as was used to model the experimental work in § 5.6.1. The profiles for the half-edge are shown for the odd-numbered passes in Figure 5.22.

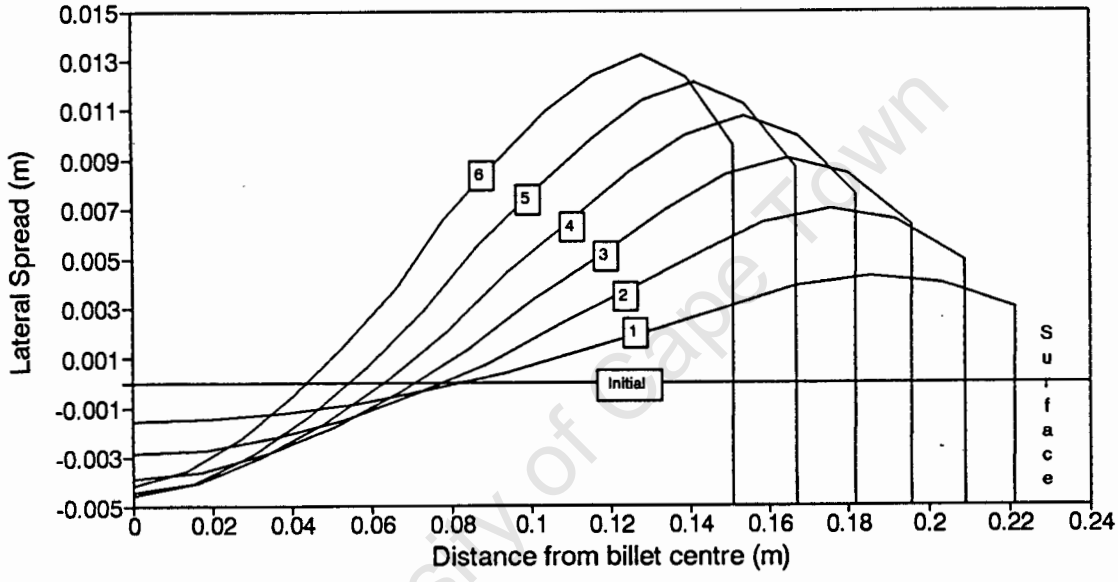

Figure 5.22: Edge profiles for first five odd-numbered roll-passes

To study these results various parameters of the profile have been included in Table 5.3. Also given is the value of the geometric relationship given in Equation 3.1 to identify the transition point.

From the data in the table the following observations can be made:

1. The average spread increases by a relatively constant amount in each pass; this amount is in the region of one millimetre per pass.

2. The spread at the peak point increases during each pass, but the amount by which it spreads per pass decreases as the value of the geometric relationship drops.

Pass number	Reduction δ (mm)	Thickness H (mm)	Transition point $\sqrt{R\delta}/H$	Lateral spread (mm)		
				Average	Maximum	Minimum
1	26.61	470.0	0.332	1.315	4.256	-1.542
2	25.10	443.4	0.342	2.179	7.000	-2.864
3	26.49	418.3	0.372	2.943	9.038	-3.855
4	27.97	391.8	0.400	3.741	10.70	-4.437
5	29.96	363.8	0.455	4.561	12.08	-4.581
6	31.98	333.9	0.513	5.491	13.22	-4.172
7	31.48	301.9	0.562	6.500	14.33	-3.501
8	29.85	270.4	0.612	7.487	15.15	-2.500
9	30.98	240.6	0.700	8.480	15.99	-1.335

Table 5.3: Parameters and results for the first nine roll passes of the industrial rolling schedule

3. At the centre negative spread occurs during the first five roll-passes, after this it starts to spread outward. The value of the geometric relationship when this occurs is:

$$0.455 \leq \sqrt{R\delta}/H \leq 0.513$$

4. The spread at the centre becomes the maximum spread per pass when:

$$0.513 \leq \sqrt{R\delta}/H \leq 0.562$$

Wright and Sheppard [6] found the geometric relationship to indicate the transition point in the edge profile when it was equal to 0.82. Observations 3 and 4 above, however, could be taken as limits for the transition point. The shape must be concave if the centre spreads negatively; and it must be convex if the maximum spread occurs at the centre. These results therefore indicate that the transition point occurs for a value of the geometric relationship between 0.455 and 0.562.

5.9 Simplified modelling of the edge profile

Once the rolling process had been successfully modelled and an understanding of the deformation obtained, an attempt was made to produce a simplified model of the material in the roll-gap. The object of producing this model was to have some quick means of investigating the effects of various variables on the edge profile.

A cross-section through the ingot was considered. As all the significant lateral effects occur in the outside quarter of the ingot, only this part of the cross-section need be included. When in the roll-gap this section does not have zero stress or strain conditions in the direction perpendicular to this surface and it is therefore not possible to use a two-dimensional model with plane stress or strain conditions. Plane strain conditions would be representative of the forging operation in which the thickness of the billet is reduced evenly; and in which a convex edge profile is produced.

The concave profile is a result of the different conditions near the surface and in the centre. Material in the surface region of the roll-gap spreads outward as the material is compressed vertically. Meanwhile material in the centre moves inward laterally as it is stretched in the rolling direction. These features are a result of the following two conditions:

1. The drop from high vertical compressive stress at the surfaces to lower compressive stress at the ingot centre.

2. The change of stresses in both the lateral and rolling directions from compressive at the surface to tensile at the ingot centre.

The first condition is a result of the vertical work-load being transmitted through an increasing area towards the centre of the ingot. To include this in a simple model would require either sufficient length in the rolling direction, or some type of boundary condition on the edge of the section to reproduce the effect of the spreading out of the load.

The second condition depends on the constraint of the relatively rigid elastic material on either side of the roll-gap. As the material pushes these blocks outward at the surfaces, they pull the material apart in the centre. To reproduce this effect the following feature was implemented. The displacements in the rolling direction of nodes on the two faces of the cross-section were constrained such that the difference between the displacements of opposite nodes are equal throughout. This forces the region in the centre to elongate by the same amount as the material near the surface. The first modelling work included this feature, but the profile predicted was convex.

The most suitable method found of including the arching effect was to simply increase the thickness of the model at the ingot centre. The mesh shown in Figure 5.23 was that used to model this effect. With the larger base on the model, the vertical stresses are reduced here and the concave profile is predicted. The plot in Figure 5.24 shows the displaced mesh of this model in which the top half of the concave profile can be seen clearly. The magnitude of the lateral spread is however excessive, with the maximum spread being 12.1 mm at the surface.

In the real case the lateral spread is reduced by the following two features:

1. The restraint of lateral spread at the surface of the roll-gap due to friction between the material and the work-rolls.

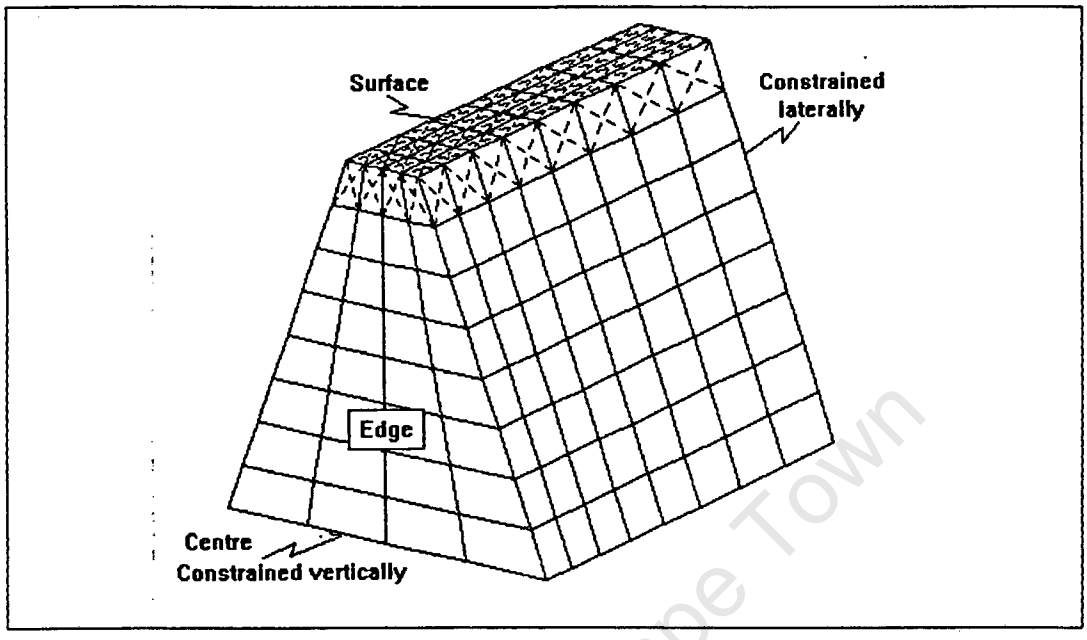

Figure 5.23: Original mesh used for the simplified model of the top half of the ingot edge

2. The restraint of lateral spread in the yielding material by the relatively rigid elastic material in front of and behind the roll-gap.

The frictional constraint was implemented by performing the loading with a rigid surface. The frictional conditions could then be included in the contact area. The deformed shape of this model can be seen in Figure 5.25 where a coefficient of friction of 0.3 has been used. Here the surface spread has been reduced significantly. As is to be expected, the amount that the surface spreads depends on the level of friction. A high coefficient of friction will reduce the spread to a greater extent.

The restraint of the material on the sides of the cross-section is more complex. On the entry side of the yielding zone the material can be considered totally restrained by the elastic material. However, as the cross-section passes through the roll gap these conditions will change. One method of providing this restraint would be to include more of the ingot in the model, but this would increase the size of the model and defeat the object of trying to analyse the profile quickly. Other methods were tried, such as constraining the cross-section on the side which enters the roll-gap last, but no satisfactory solution was found.

Although the simplified modelling did not accurately reproduce the edge profile, the profile predicted was found to be suitable enough to check trends caused by changes in three variables.

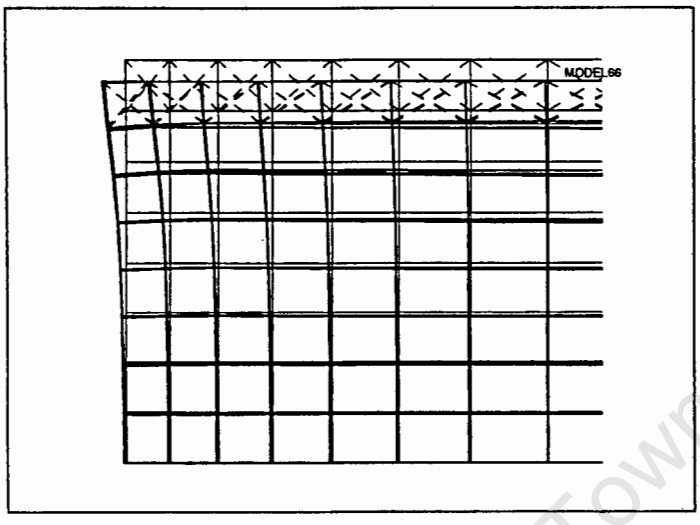

Figure 5.24: Deformed shape of model showing the top half of the edge profile

Strain rate dependency of the material

The effect of strain rate dependency on the edge profile was checked in the full three-dimensional modelling of the experimental results, see § 5.7.4. This showed that the spread was reduced in the regions near the surfaces where the highest strain rates have occurred. These profiles were, however, of the transition point type.

When the dependency of the yield stress on the strain rate was included in the simplified model, the effect was that expected. The spread near the surface was reduced. The magnitude of the change was small in comparison to the overall spread; near the surface the spread was reduced by 0.3 mm while at the centre it increased by 0.1 mm.

Temperature dependency of the material

The aluminium alloy softens as its temperature rises, therefore when the plastic work heating was included in the full analyses the lateral spread in the warmest regions was expected to increase by the most. The results given in § 5.7.4 however, indicated the opposite.

The simplified model was, therefore, also used to investigate this effect. Here, however, the spread did increase where expected, though very slightly. The spread near the surface increased by 0.02 mm, while at the centre it decreased by even less.

This led to the discovery of why the unexpected results had occurred in the full analyses. The data used to describe the temperature dependency also includes the work hardening effect. When the data had been removed to investigate the effect of the temperature the

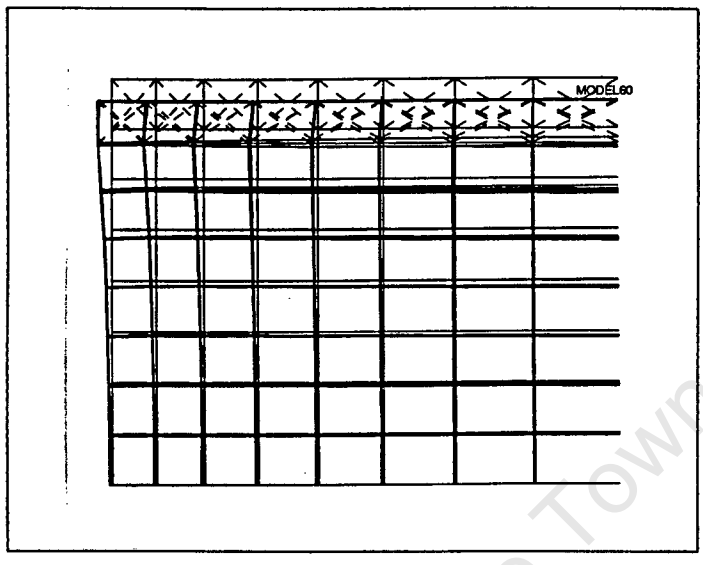

Figure 5.25: Deformed shape of model with friction included at the surface

work hardening had been ignored as it is so small at this temperature (see the data for material at 500°C [773 K] in Figure 4.3). However, the work hardening effect is actually more important than that of the heating due to the dissipation of plastic work energy.

Work hardening

To check whether the work hardening of the material was responsible for the reduction in spread, the effect was included in the simplified model. The results showed that this was the case; the spread near the surface was reduced by 0.04 mm which is more than its increase due to the increase in temperature.

5.10 Discussion of the crocodile jaw phenomenon

Although the work of this thesis looks into the profile that occurs on the edge of the ingots, the understanding of the mechanics in the ingot has provided an explanation for why the ends of the ingot develop the 'crocodile jaw' profile. A plot of the deformed shape of one end of the ingot in Figure 5.26 shows this phenomenon as it has been produced in the finite element modelling. This profile which involves spreading several orders of magnitude greater than that at the edges, does create problems during the rolling process. In the industrial process being studied here, it is necessary to stop the rolling at some stage in the rolling schedule to crop the ends, and then to crop them once more at the end of the schedule.

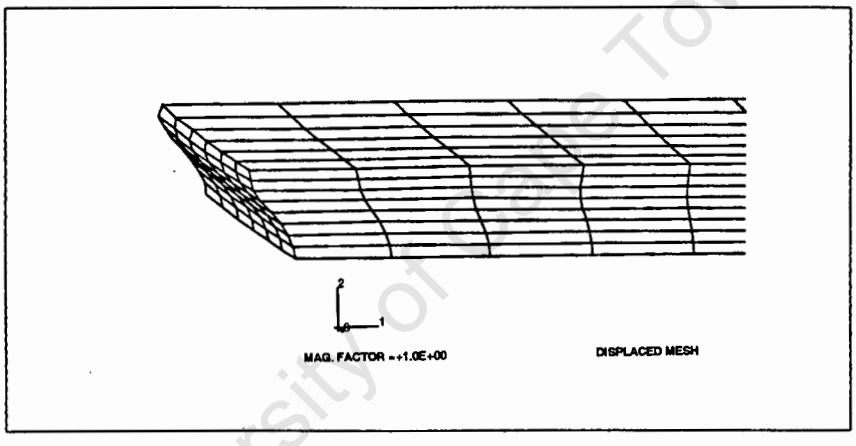

Figure 5.26: Top half of the 'crocodile jaw' shape that develops at the ends of the ingot

In the first roll-pass of the analyses the start of the typical 'alligator' or 'crocodile jaw' shape can be seen at the front and back ends of the ingot. This shape develops because the material in the central region at the ends is not deformed as much as the material above and below. The material at the centre does not elongate, whilst the outside material is forced to. The areas which are not deformed can be seen in the contour plot of the equivalent plastic strains (Figure 5.8); they are the two dark, roughly semi-circular regions on the plot.

The reason for these two regions not being deformed to the same extent is that near the ends the material is not constrained on both sides by the blocks of relatively rigid elastic material. Therefore when the work-roll load compresses the material vertically it is free to spread in the lateral direction. In the region near the axis of symmetry the material is not pulled apart, as it is in the central regions, and therefore does not elongate.

5.11 Analyses including heat losses to the work-rolls

Although analyses which solve the coupled stress and heat transfer problem do require considerable time, some work was performed for the plane strain case. To include the heat loss to the work-rolls the roller was defined as a cylinder of nodes. These nodes were constrained such that they produced a rigid cylinder and elements which model both the contact and the heat transfer conditions were defined along the nodes.

The analyses included only the generation of heat due to the dissipation of plastic work energy and the heat loss to the work-rolls. The thermal properties used for the calculations in § 4.5 were also used for these analyses.

The temperature profile through the ingot half-thickness is given in Figure 5.27 for a section firstly, as it leaves the roll-gap and secondly, after 8.9 seconds of heat transfer at which stage it is about to re-enter the roll-gap.

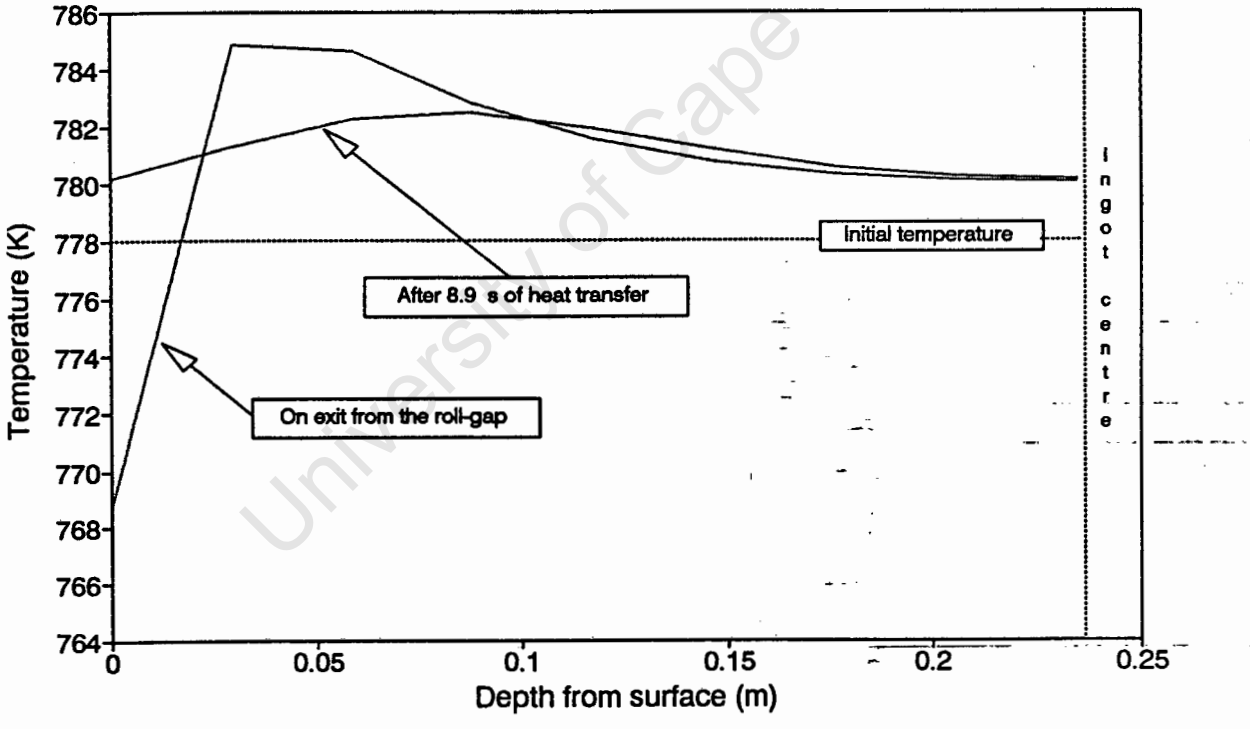

Figure 5.27: Finite element prediction of the temperature profile through the ingot

The profiles are as expected; the large cooling of the surface disappears before the next roll-pass as heat flows out of the central region. The temperature at the surface is not as low as that predicted in § 4.5, but this is most likely due to the relatively coarse mesh which has been used.

Chapter 6

Conclusions and scope for future work

The initial objective of this thesis was to develop a technique of simulating the hot-rolling process. This could then be used both to investigate the mechanisms which lead to a concave edge profile, and to study the effects of changes in the rolling parameters. With this knowledge it is then possible to investigate methods of reducing the edge waste of the final product.

Numerical simulations of the hot-rolling process have been developed in which the edge profile is correctly reproduced. The profile predicted by the modelling has been validated by performing analyses of one of the experiments reported by Wright and Sheppard [6]. The profile measurements given in their reference are reproduced by the numerical model when a suitable coefficient is chosen for the friction conditions between the ingot and the work-rolls.

These methods of simulation were also used to investigate the deformation mechanisms inside the ingot. The reason for the development of a concave edge profile was discovered.

In the roll-gap the work-load arches through the ingot; and for roll passes with small reductions a stress pattern occurs which leads to the concave edge profile. In this pattern the stresses of highest magnitude at the surface are compressive stresses in the vertical direction, while in the centre of the ingot they are orientated in the rolling direction and are tensile. Thus deformation occurs by vertical compression near the surfaces and by stretching in the rolling direction at the centre. At the edges the material is not constrained laterally; and due to the Poisson effect the material spreads outward near the surfaces and moves inward at the centre.

Certain parameters were varied in the analyses to check their effects on the edge profile. A simplified model of the material in the roll-gap was also produced. This model did not reproduce the edge profile accurately because the complicated and varying boundary

conditions could not be simulated well enough. However, the profile was of the correct shape.

The type of edge profile, concave or convex, depends on the amount of reduction occurring per pass. Other variables do, however, affect the shape of the profile. Of those investigated in this thesis, the friction between the work-rolls and the ingot has the greatest effect. The lateral spread of the surface for the case investigated was halved when the coefficient of friction was changed from 0.3 to 0.6. Other variables investigated were the strain rate dependency, work hardening, and heating due to plastic work in the aluminium alloy. The effects of these were slight:

- The highest strain rates occur near the surfaces, and as the material is hardened at high strain rates this leads to a decrease in spread in these regions.
- The highest plastic equivalent strains occur in zones just below the surfaces, and as the material hardens here the spread is decreased.
- The highest heating due to plastic work also occurs in the zones just below the surfaces. However, while the yield stress is increased by work hardening, it is decreased by temperature rises. Thus heating leads to increased spread in the regions below the surfaces; this effect is smaller then that due to work hardening during the first roll-pass.

6.1 Scope for future work

There are two areas in which the work of this thesis can be extended. The first is to improve the accuracy of the numerical simulation, and the second is to use these findings to identify ways of optimising the industrial rolling process.

6.1.1 Improving the accuracy of the numerical simulation

During the development of the numerical modelling in this thesis, two aspects were identified in which improvements can be made. These are the way in which the friction is modelled between the work-rolls and the ingot, and the inclusion of temperature changes due to cooling.

The Coulomb model of friction used in this work sets the limit of the frictional forces equal to the normal force times the coefficient, μ. By using different values of μ in analyses the shape of the profile has been shown to be highly dependent on the friction conditions. However, the references given in § 4.6 indicate that friction is also dependent on other effects such as the relative velocity between the surfaces. Different methods of modelling

friction have been presented and it would be worthwhile to investigate the changes that occur when these are implemented.

For the three-dimensional work the temperature dependency of the aluminium alloy's yield stress was included. Due to time constraints, the only variations in temperatures were those due to the dissipation of plastic work energy. However, two-dimensional analyses which solved the coupled stress and heat transfer problem showed that the surface is cooled significantly underneath the work-rolls. This is expected to reduce the surface spread and therefore affect the edge profile shape. For this reason it would also be worthwhile to include the cooling effects in the modelling work. The use of coupled analyses, however, requires significantly more time than the stress analyses performed here. A method which would not require coupled analyses has been considered. This consists of initially building up a knowledge base of the temperature profile and its history by performing heat transfer analyses. This knowledge could then be used either to develop a routine which adjusts the temperatures in the analysis, or to directly enter the temperatures into the analysis.

6.1.2 Methods of reducing edge waste in the industrial rolling process

The possibility of reducing the edge waste of the final product was the original motivation for this research. Two ways in which this may be accomplished are envisaged.

Identification of an optimum initial edge profile

The work in this thesis assumed an initial edge profile which is flat. In industry, however, different profiles are used. The numerical simulation developed here could be used to investigate differing starting profiles and to identify an optimum initial edge profile.

Identification of an optimum schedule for the industrial rolling process

During the industrial rolling schedules the value of the reduction as a percentage of the ingot height varies. These differences in the rolling geometry result in varying changes in the edge profile during each pass. It has already been suggested by Wright and Sheppard [6] that the edge profile might be controlled by specific planning of the schedule of reductions; and they put forward their geometric relationship in Equation 3.1 as a means of doing this.

The work presented in this thesis offers an explanation of how the concave edge profile develops. With this understanding it is possible to predict the type of edge shape from the stress state indicated in the roll-gap by plane strain finite element analyses. The inward movement of the material at the centre is due to the predominant mechanism of

elongation being the 'stretching' in the rolling direction. With reductions producing a convex profile the predominant mechanism will be compression in the vertical direction. A simple way of checking which of these mechanisms is predominant in the plane strain analyses would be to inspect the out of plane stresses at the centre of the ingot. These would be positive when the 'stretching' mechanism is predominant and negative when the vertical compressive mechanism is predominant.

It should therefore be possible to use the relatively faster two-dimensional analyses to plan improved schedules of reductions.

The prediction of the magnitudes of spread in the profile will still however require full three-dimensional analyses.

Bibliography

[1] Chitkara N.R. and Johnson W. Some experimental results concerning spread in the rolling of lead. *Journal of Basic Engineering, ASME*, 88(2):489–499, June 1966.

[2] El-Kalay A.K.E.H.A. and Sparling L.G.M. Factors affecting friction and their effect upon load, torque, and spread in hot flat rolling. *Journal of the Iron and Steel Institute*, 206(2):152–163, February 1968.

[3] Helmi A. and Alexander J.M. Geometric factors affecting spread in hot flat rolling of steel. *Journal of the Iron and Steel Institute*, 206(11):1110–1117, November 1968.

[4] Beese J.G. Ratio of lateral strain to thickness strain during hot rolling of steel slabs. *Journal of the Iron and Steel Institute*, 210(6):433–436, June 1972.

[5] Sheppard T. and Wright D.S. Parameters affecting lateral deformation in slabbing mills. *Metals Technology*, 8(2):46–57, February 1981.

[6] Wright D.S. and Sheppard T. Edge profile during initial passes of aluminium slab rolling. *Metals Technology*, 8(5):180–189, May 1981.

[7] Johnson K.L. *Contact Mechanics*. Cambridge University Press, Cambridge, 1989.

[8] Mandel J.[1]. Résistance au roulement d'un cylindre indéformable sur un massif parfaitement plastique. In *Le Frottement & l'Usure*, page 25, GAMI, Paris, 1967.

[9] Bentall R.H. and Johnson K.L. Slip in the rolling contact of two dissimilar elastic rollers. *International Journal of Mechanical Sciences*, 9(6):389–404, 1967.

[10] Hartley P., Sturgess C.E.N., Liu C., and Rowe G.W. Experimental and theoretical studies of workpiece deformation, stress, and strain during flat rolling. *International Materials Reviews*, 34(1):19–34, 1989.

[11] Orowan E. The calculation of roll pressure in hot and cold flat rolling. *Proceedings, The Institute of Mechanical Engineers*, 150:140–167, 1943.

[12] Alexander J.M. *Proceedings, The Institution of Mechanical Engineers*, 169:1021–1028, 1955.

[1]Copies of these works were not obtained. Details presented in this thesis were those cited in other references. These references are documented with the work that is presented.

[13] Hosford W.F. *Metal Forming: Mechanics and Metallurgy.* Prentice-Hall, Englewood Cliffs, N.J., 1983.

[14] Rowe G. W. *Elements of Metalworking Theory.* Edward Arnold (Publishers) Ltd., Bath, Great Britain, 1979.

[15] Harris J.N. *Mechanical Working of Metals. International Series on Materials Science and Technology*, Pergamon Press, Oxford, 1983.

[16] Hencky H.[1]. *Zeit. fur angew. Math. u. Mech.*, 3:241, 1923.

[17] Chao H.D.[1]. Fundamentals of plastic deformation and principles of rolling. 81–82, 1979.

[18] Chen Fuh-Kuo and Kobayashi Shiro. Three-dimensional analysis of metal flow in shape rolling. In *Computer Modeling and Simulation of Manufacturing Processes, MD-vol. 20, PED-vol. 48*, pages 249–263, The Materials Division and The Production Engineering Division, ASME, November 1990.

[19] Lahoti G.D., Akgerman N., Oh S.I., and Altan T.[1]. Computer-aided analysis of metal flow and stresses in plate rolling. *J. of Mech. Working. Tech.*, 4:105–119, 1980.

[20] Harty B.D. *Hulamin and Alcoa 5182 Rolling Ingot.* Internal Memorandum, Hulett Aluminium Limited, March 1991.

[21] Brooks P. J. S.[1]. Alcan Research and Development Report, (Banbury), BP-ER 48/70.

[22] Alexander J.M. On the theory of rolling. *Proc R Soc*, A326:533–563, 1972.

[23] Bathe Klaus-Jürgen. *Finite Element Procedures in Engineering Analysis.* Prentice-Hall, Englewood Cliffs, New Jersey, 1982.

[24] Burnett D.S. *Finite Element Analysis.* Addison-Wesley, Reading, Massachusetts, 1987.

[25] Cook R.D., Malkus D.S., and Plesha M.E. *Concepts and Applications of Finite Element Analysis.* John Wiley & Sons, Singapore, third edition, 1989.

[26] Zienkiewicz O.C. *The Finite Element Method.* Mc Graw-Hill, London, third edition, 1977.

[27] Zienkiewicz O.C., Jain P.C., and Oñate E. Flow of solids during forming and extrusion: some aspects of numerical solutions. *International Journal of Solids and Structures*, 14(1):515–38, 1978.

[28] Lindgren Lars-Erik and Edberg J. Explicit versus implicit finite element formulation in simulation of rolling. *Journal of Materials Processing Technology*, 24:85–94, 1990.

[29] Kanazawa K. and Marcal P.V. Finite element analysis of the steel rolling process. In Armen H. and Jr. R.F. Jones, editors, *Applications of Numerical Methods to Forming Processes, AMD-vol. 28*, pages 81–83, The Applied Mechanics Division, ASME, December 1978.

[30] Li Guo-Ji and Kobayashi S. Rigid-plastic finite-element analysis of plane strain rolling. *Journal of Engineering for Industry*, 104(1):55–64, February 1982.

[31] Liu C., Hartley P., Sturgess C.E.N., and Rowe G.W. Simulation of the cold rolling of strip using an elastic-plastic finite element technique. *International Journal of Mechanical Sciences*, 27(11/12):829–839, 1985.

[32] Hwu Yhu-Jen and Lenard J.G. A finite element study of flat rolling. *Journal of Engineering Materials and Technology*, 110(1):22–27, January 1988.

[33] Lau A.C.W., Shivpuri R., and Chou P.C. An explicit time integration elastic-plastic finite-element algorithm for analysis of high speed rolling. *International Journal of Mechanical Sciences*, 31(7):483–497, 1989.

[34] Li Guo-Ji and Kobayashi S. Spread analysis by the rigid-plastic finite-element method. In J.M. Alexander J.F.T. Pittman, R.D. Wood and O.C. Zienkiewicz, editors, *Numerical Methods in Industrial Forming Processes*, pages 777–786, Swansea, 1982.

[35] Mori K. and Osakada K. Simulation of three-dimensional deformation in rolling by the finite-element method. *International Journal of Mechanical Sciences*, 26(9/10):515–525, 1984.

[36] Karabin M.E. and Smelser R.E. A quasi-three-dimensional analysis of the deformation processing of sheets with applications. *International Journal of Mechanical Sciences*, 32(5):375–389, 1990.

[37] Kiefer B.V.[1]. Three-dimensional finite element prediction of material flow and strain distribution in rolled rectangular billets. In *Proceedings, The 1st International Conference on Technology of Plasticity*, pages 1116–1125, Tokyo, 1984.

[38] Liu C., Hartley P., Sturgess C.E.N., and Rowe G.W. Finite-element modelling of deformation and spread in slab rolling. *International Journal of Mechanical Sciences*, 29(4):271–283, 1987.

[39] Park J.J. and Oh S.I. Application of three dimensional finite element analysis to shape rolling processes. *Journal of Engineering for Industry, ASME*, 112:36–46, February 1990.

[40] Liu C., Hartley P., Sturgess C.E.N., and Rowe G.W. Analysis of stress and strain distributions in slab rolling using an elastic-plastic finite-element method. *International Journal for Numerical Methods in Engineering*, 25(1):55–66, January 1988.

[41] Hulett Aluminium Ltd. Private communication. April 1992.

[42] Holman J.P. *Heat Transfer*. McGraw-Hill Book Company, Singapore, sixth edition, 1986.

[43] Tseng A.A., Tong S.X., Maslen S.H., and Mills J.J. Thermal behaviour of aluminium rolling. *Journal of Heat Transfer, ASME*, 112(2):301–308, May 1990.

[44] Hulett Aluminium Ltd. Private communication. May 1992.

[45] Semiatin S.L., Collings E.W., Wood V.E., and Altan T. Determination of the interface heat transfer coefficient for non-isothermal bulk-forming processes. *Journal of Engineering for Industry, ASME*, 109(1):4–57, February 1987.

[46] Pietrzyk M. and Lenard John G. The effect of the temperature rise of the roll on the simulation of the flat rolling process. *Journal of Materials Processing Technology*, 22:177–191, 1990.

[47] Pietrzyk M. and Lenard John G. Deformation heating during cold rolling of aluminium strips. *Journal of Engineering Materials and Technology, ASME*, 113:69–74, January 1991.

[48] Tabor D. Friction—The present state of our understanding. *ASME, Journal of Lubrication Technology*, 103:169–179, April 1981.

[49] Lim Lai-Seng and Lenard J.G. Study of friction in cold strip rolling. *Journal of Engineering Materials and Technology*, 106(2):139–146, April 1984.

[50] Sparling L.G.M. Load and torque determination for hot flat rolling with variable frictional conditions. *Metals Technology*, 4(6):301–306, June 1977.

[51] Theocaris P.S., Stassinakis C.A., and Mamalis A.G. Roll-pressure distribution and coefficient of friction in hot rolling by caustics. *International Journal of Mechanical Sciences*, 25(11):833–844, 1983.

[52] Atreya Arvind and Lenard John G. A study of cold strip rolling. *Journal of Engineering Materials and Technology*, 101(2):129–134, April 1979.

[53] Oh S.I. and Kobayashi Shiro. An approximate method for a three-dimensional analysis of rolling. *International Journal of Mechanical Sciences*, 17:293–305, 1975.

[54] Barata Marques Manuel J.M. and Martins Paulo A.F. A solution to plane strain rolling by the weighted residuals method. *International Journal of Mechanical Sciences*, 32(10):817–827, 1990.

[55] Chen C.C. and Kobayashi S.[1]. Rigid-plastic finite element analysis of ring compression. *Applications of Numerical Methods to Forming Processes, AMD*, 28:163–173, 1978.

[56] Aanestad A. Simulation of cold rolling. *Materials Science and Technology*, 2:533–563, June 1986.

[57] Johnson Robert E. Shape forming and lateral spread in sheet rolling. *International Journal of Mechanical Sciences*, 33(6):449–469, 1991.

[58] Richelsen Ann Bettina. Viscoplastic analysis of plane-strain rolling using different friction models. *International Journal of Mechanical Sciences*, 33(9):761–774, 1991.

[59] Avitzur Betzalel. *Handbook of Metal-Forming Processes.* John Wiley & Sons, New York, 1983.

[60] Sheppard T. and Wright D.S. Determination of flow stress: Part 1 constitutive equation for aluminium alloys at elevated temperatures. *Metals Technology*, 6(6):215–223, June 1979.

Appendix A

Heat transfer in hot-rolling

The first section of this appendix contains the calculations of the magnitudes of the various heat-loss mechanisms which are present in the hot-rolling process. All calculations are for the total heat transfer for a square metre of the surface over the time of the first roll pass.

The second section contains describes the way the finite element method was used to predict the effects of various aspects on the temperature profile.

A.1 Calculation of the different heat-loss mechanisms

The following values were used in the calculations:

Parameters	**Value**	
Time for one roll-pass, t	9	s
Roll speed	1	$m.s^{-1}$
Length of the contact gap	0.1	m
Time spent in the contact gap, t_{CG}	0.1	s
Ingot temperature, T_{ing}	778	K
Average work-roll temperature, T_{WR}	515	K
Average factory temperature, T_{env}	300	K
Thermal properties	**Value**	
Coefficient of thermal conduction, k	121	W/m°C
Specific heat capacity, c	970	J/kg°C
Density, ρ	2650	kg/m^3
Heat transfer coefficient	10000	W/m^2°C
Convection heat transfer coefficient, h_c	10	W/m^2°C

Convection to the environment

Convection of heat from a body is given by:

$$q = h_c A(T - T_\infty)$$

where,
- T : temperature of the body, °C
- T_∞ : temperature of the environment, °C
- A : surface area of the body, m^2
- h_c : convection heat transfer coefficient, $W/m^2\,°C$ (Usually found experimentally for specific conditions.)

For the first pass of the rolling schedule, the energy lost is:

$$\begin{aligned} qt &= hA(T_{ing} - T_{env})t \\ &= (10)(1)(505 - 27)(9) \\ &= 43.02 \times 10^3\ J/m^2 \end{aligned}$$

Radiation to the environment

Heat loss from a body to an enclosing surface is given by:

$$q = \epsilon \sigma A \left(T_b^4 - T_s^4\right)$$

where,
- ϵ : emissivity of surface
- σ : Stefan-Boltzman constant, $5.669 \times 10^{-8}\ W/m^2K^4$
- A : surface area, m^2
- T_b : temperature of body, K
- T_s : temperature of surrounding surface, K

For the first pass in the rolling schedule, the energy lost is:

$$\begin{aligned} qt &= \epsilon \sigma A \left(T_{ing}^4 - T_{env}^4\right) t \\ &= (0.09)(5.669 \times 10^{-8})(1)(778^4 - 300^4)(9) \\ &= 16.45 \times 10^3\ J/m^2 \end{aligned}$$

Conduction to the work-rolls

The conduction of heat between two bodies is given by:

$$q = hA(T_1 - T_2)$$

where, h : coefficient of heat transfer between the bodies, $W/m^2/,°C$
A : area of contact, m^2
T : temperatures of the bodies, °C

The heat loss to the work-rolls via conduction during the time of contact is:

$$\begin{aligned} q\,t_{CG} &= hA(T_{ing} - TWR)\,t_{CG} \\ &= 10000(1)(505 - 242)(0.1) \\ &= 263 \times 10^3\,J/m^2 \end{aligned}$$

Radiation to the work-rolls

The net heat transfer between two bodies is given by:

$$q_{net} = \frac{\sigma(T_1^4 - T_2^4)}{\frac{1-\epsilon_1}{\epsilon_1 A_1} + \frac{1}{A_1 F_{12}} + \frac{1-\epsilon_2}{\epsilon_2 A_2}}$$

where, ϵ : emissivity of the surfaces
F_{12} : a shape factor
σ : Stefan-Boltzman constant, $5.669 \times 10^{-8}\ W/m^2K^4$
A : areas of the surfaces, m^2
T : temperatures of the bodies, K

As most of the heat transfer will occur when the work-roll is in contact with the ingot the shape factor has been taken as 1.
The heat loss to the work-rolls via radiation during the time of contact is therefore:

$$\begin{aligned} q_{net}\,t_{CG} &= \frac{\sigma(T_{ing}^4 - T_{WR}^4)}{\frac{1-\epsilon_{ing}}{\epsilon_{ing}A} + \frac{1}{A} + \frac{1-\epsilon_{WR}}{\epsilon_{WR}A}}\,t_{CG} \\ &= \frac{(5.669 \times 10^{-8})(778^4 - 515^4)}{\frac{1-0.09}{0.09} + 1 + \frac{1-0.066}{0.066}}(0.1) \\ &= 66.42\,J/m^2 \end{aligned}$$

A.2 Finite element modelling of heat transfer through the thickness of the ingot

To model the heat transfer the ingot was considered an infinite sheet, heat flow is then one-dimensional. The analytical solution for the temperature profile through the thickness of an infinite sheet is the following series:

$$\frac{T - T_1}{T_i - T_1} = \frac{4}{\pi} \sum_{n=1}^{\infty} \frac{1}{n} e^{-[n\pi/2L]^2 \alpha \tau} \sin \frac{n\pi x}{2L} \qquad n = 1,3,5,...$$

where, T_i : initial temperature
T_1 : temperature at the edge
T : temperature at distance x through the sheet and at time τ

A one-dimensional finite element model was set up to model heat flow in an infinite sheet which is cooled at the surfaces. This was verified with the series solution. Then the model was used to predict the temperature profiles which occur when the following cooling mechanisms are applied:

- Heat transfer to the work-rolls with $h = 10000$ W/m^2°C. The work-rolls are in contact for 0.1 seconds and then heat transfer is allowed to continue for a further 8.9 seconds.
- Convection heat loss to the environment with $h = 10$ W/m^2°C for 9.0 seconds.

The predicted profiles were given in Figure 4.6.

Appendix B

Courses completed in partial fulfillment of the M. Sc. degree

Course		Date	Credits
AMA321F	Numerical Analysis & Scientific Computation	1991	3
CAM500Z	Applied Mechanics A	1991	3
CAM501Z	Applied Mechanics B	1991	3
CAM503Z	Finite Element Analysis	1991	4
CAM504Z	Engineering Software Design and Development	1991	3
CIV504S	Structural Dynamics	1991	3
CIV539F	Deep Excavations	1991	3

Course Credits: 22
Thesis Credits: 20
Total: 42

Minimum credit requirement for the M.Sc. degree: 40 credits